AQUIND Limited

AQUIND INTERCONNECTOR

Environmental Statement – Volume 3 – Appendix 6.2 Modelling Technical Report - Low Resolution

The Planning Act 2008

The Infrastructure Planning (Applications: Prescribed Forms and Procedure) Regulations 2009 – Regulation 5(2)(a)

The Infrastructure Planning (Environmental Impact Assessment) Regulations 2017

Document Ref: 6.3.6.2

PINS Ref.: EN020022

AQUIND Limited

AQUIND INTERCONNECTOR

Environmental Statement – Volume 3 – Appendix 6.2 Modelling Technical Report - Low Resolution

PINS REF.: EN020022

DOCUMENT: 6.3.6.2

DATE: 14 NOVEMBER 2019

Units 5 & 10
Stephenson House,
Horsley Business Centre
Horsley,
Northumberland,
NE15 0NY
England, UK

DOCUMENT

Document	**6.3.6.2 Environmental Statement – Volume 3 – Appendix 6.2 Modelling Technical Report - Low Resolution**
Revision	001
Document Owner	Natural Power Consultants Ltd
Prepared By	Partrac Ltd
Date	23 October 2019
Approved By	R. Hodson
Date	30 October 2019

CONTENTS

FIGURES

EXECUTIVE SUMMARY

AQUIND Ltd has proposed to develop a new HVDC interconnector cable between the UK and France. To support the consenting of the Project a coupled hydrodynamic and wave model has been developed to help understand the potential effects related to construction, operation and decommissioning of the interconnector.

The model has been locally validated against various measured datasets (wave, water level and tidal flow), and has been shown to be accurately predicting water levels, depth averaged tidal flow magnitude, significant wave height and spectral wave approach. Hydrodynamic and wave data derived from the model has been used to inform the assessment of baseline conditions and potential impacts related to the Proposed Development.

The model has also been adapted specifically for the consideration of the fate of sediment plumes created during the disposal of dredge material following dredging activity undertaken as part of large ripple and sandwave clearance during the construction phase. This material is intended for release within the bounds of an identified marine disposal site located in the Marine Cable Corridor.

A realistic worst-case model scenario was simulated. Model outputs show that although suspended sediment concentrations are enhanced local to the point of release, the material rapidly disperses to levels in line with background suspended sediment concentrations within the wider Channel. The model also shows that due to the coarse nature of the deposits, disposal operations will likely induce a build-up of sediment on the seabed local to the area of disposal. While this deposited sediment is predicted to remain in place in the short-term, bedload transport processes will act to disperse this sediment through time.

1. MODELLING TOOLS AND DATA SOURCES

1.1.1.1. Development of the knowledge base in relation to the hydrodynamic, wave, sediment regime and physical processes has been assisted through the utilisation of several numerical modelling approaches at a range of spatial and temporal scales using the MIKE21 2D modelling package; a comprehensive modelling system for two-dimensional water modelling developed at the Danish Hydraulic Institute ('DHI').

1.1.1.2. A European, basin-scale flexible mesh hydrodynamic model with sub-kilometre resolution in the coastal zone has been developed. This model was developed to provide twenty years of hindcast metocean data for the Channel at various locations along the Marine Cable Corridor. In addition, hydrodynamics from this model was used to drive advection of plumes created during dredge disposal activities. This technical appendix reports on the configuration (set-up), parameterisation, calibration and validation of these models.

1.1.1.3. The modelling tools and data sources, and their application as part of this project are detailed in Tables 1 and 2, respectively.

Table 1 - Modelling tools and their application

Model	Software Used	Spatial Scale	Temporal Scale	Description
Hydrodynamic	MIKE21	Regional (Channel), and local (to the Proposed Development)	20 years (hindcast)	An appreciation of the wider distribution and geospatial variation of tidal flows across the site is available through development of a site-specific hydrodynamic model which has been developed using the MIKE21 modelling software. A numerical hydrodynamic model was configured using the MIKE21 hydrodynamic modelling package. Such modelling systems have been developed for complex applications within oceanographic, coastal and estuarine environments.
Wave	SWAN	Regional (Channel), and local (to the Proposed Development)	20 years (hindcast)	SWAN ('Simulating Waves Near Shore'), a phase averaged, third-generation wave model ideally suited for modelling waves in coastal regions was utilised to assess the local wave climate. Numerical modelling of waves in coastal areas is a useful means of understanding wave climatology and wave processes over greater spatial and temporal scales. Wave models typically use long-term historical wind datasets to simulate the formation of waves over a water body. They generate a spectrum of historic wave conditions, which are validated at certain times and points in space using measured wave data. As generally the period of time over which *in situ* data are available is limited and the wave climate can display a high degree of intra-annual variability, modelling studies enable short-term datasets to be extended to the long-term in order to derive wider data for sediment transport description and estimation of extreme

Model	Software Used	Spatial Scale	Temporal Scale	Description
				conditions.
Particle Tracking	MIKE21 (particle tracking module)	Regional (Channel), and local (Increased spatial resolution at the Proposed Development)	4 months (hindcast)	To investigate sediment plume processes at a regional and local scale MIKE21-PT (Particle-Tracking) modules were applied. Suspended sediment plumes are one of the process effects of dredging operations which impact the environment. Modelling this phenomenon allows the processes (advection, diffusion, settling) driving sediment dispersion to be simulated enabling an assessment of the localised and wider impacts on near and far field suspended sediment concentrations and seabed level changes associated with dredge disposal operations, to be investigated. The model scenario is a cumulative impact scenario* encompassing all dredge disposal operations at the site.
**** Note; The model scenario is described as a cumulative impact scenario as plume dispersion from all disposal operations was modelled in a single run and thus the model outputs show the cumulative effects of these operations. Note; that the disposal operations were not modelled in conjunction with other activities or considering other projects within the region.***				

Table 2 - Data sources utilised and their application

Data source	Application	Description
National Centres for Environmental Prediction ('NCEP') Climate Forecast System Reanalysis ('CFSR') **(Saha *et al.* 2010)**	Regional gridded atmospheric data	The Climate Forecast System Reanalysis ('CFSR') dataset, which extends over the time period 1979 to the present day, was designed and executed as a global, high resolution, coupled atmosphere-ocean-land surface-sea ice system. The system is widely recognised as the best available atmospheric dataset, providing the most accurate estimate of the state of these coupled domains over this temporal period. The CFSR reanalysis includes coupling of atmosphere and ocean during the generation of the 6-hour guess field, an interactive sea-ice model, and assimilation of satellite radiances by the Grid-point Statistical Interpolation ('GSI') scheme over the entire period. The CFSR global atmosphere resolution is ~38 km with 64 levels extending from the surface to 0.26 hPa. The global ocean resolution is 0.25 ° at the equator, extending to a global 0.5° beyond the tropics, with 40 levels to a depth of 4737 m. The global land surface model has four soil levels and the global sea ice model has three levels. In addition, all available conventional and satellite observations were included in the CFSR. Satellite observations were used in radiance form and were bias corrected with "spin up" runs at full resolution, considering variable CO_2 concentrations (enabling smooth transitions of the climate record despite evolutionary changes in the satellite observing system).
ERA-Interim is a global reanalysis produced by the	Spectral	ERA-Interim is a global reanalysis produced by the European Centre for Medium-Range Weather Forecasts ('ECMWF') which incorporates a model with three fully

Data source	Application	Description
European Centre for Medium-Range Weather Forecasts ('ECMWF') **(Dee *et al*. 2011)**	boundary conditions for the SWAN model grids	coupled components for the atmosphere, land surface, and ocean waves. The horizontal resolution of the wave model in ERA-Interim is 110 km; wave spectra are discretised using 24 directions and 30 frequencies from 0.0345 to 0.5473 Hz. Data are available every six hours between 1979 and the present.
TOPEX/Poseidon global inverse tidal model (TPXO 7.2 Atlantic Ocean Model). **(Egbert & Svetlana, 2002)**	Tidal boundary conditions	The TPXO 7.2 Atlantic Ocean Model is the latest version of a global model of ocean tides, which best-fits, in a least-squares sense, the Laplace Tidal Equations (Laplace *et al.*, no date) and along track averaged data from the TOPEX/Poseidon and Jason satellites (for instance: https://jason.cnes.fr/en/JASON2/index.htm)

2. SETUP OF THE COUPLED HYDRODYNAMIC & WAVE MODEL

2.1.1.1. The coupled hydrodynamic and wave model was developed to provide twenty years of hindcast metocean data for the Channel at various locations along the Marine Cable Corridor. Atmospheric data used for this project originated from the National Centres for Environmental Prediction ('NCEP') CFSR.

2.2. HYDRODYNAMIC MODEL

2.2.1.1. Flow and water level parameters were produced through a European, basin-scale flexible mesh hydrodynamic model with sub-kilometre resolution in the coastal zone. Tidal boundary conditions originated from the TPXO 7.2 Atlantic Ocean model (Egbert & Svetlana, 2002), maintained by the Oregon State University. In total, the model consisted of more than 166,000 triangular tessellations with increased resolution added to the study area, see Figure 1 and Figure 2.

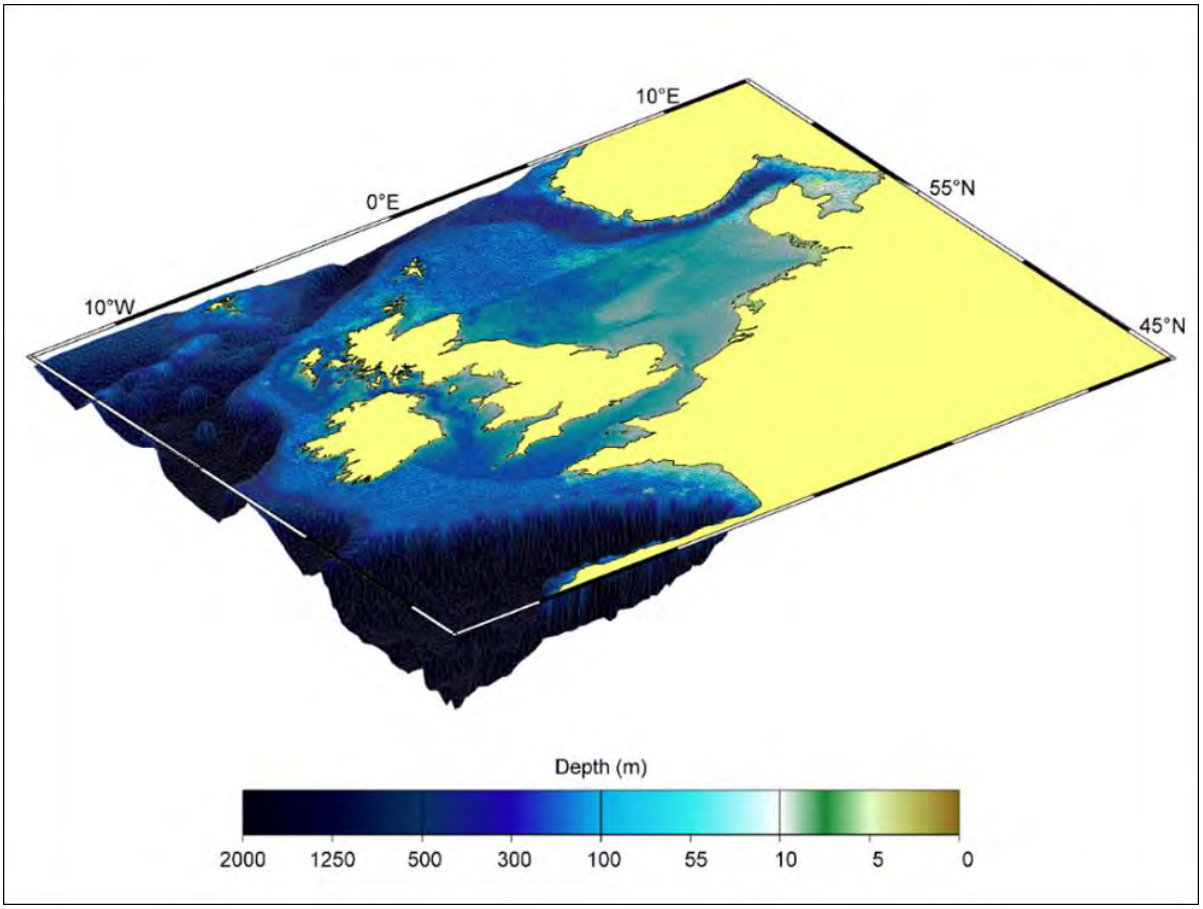

Figure 1 - Regional European MIKE21 flexible model mesh

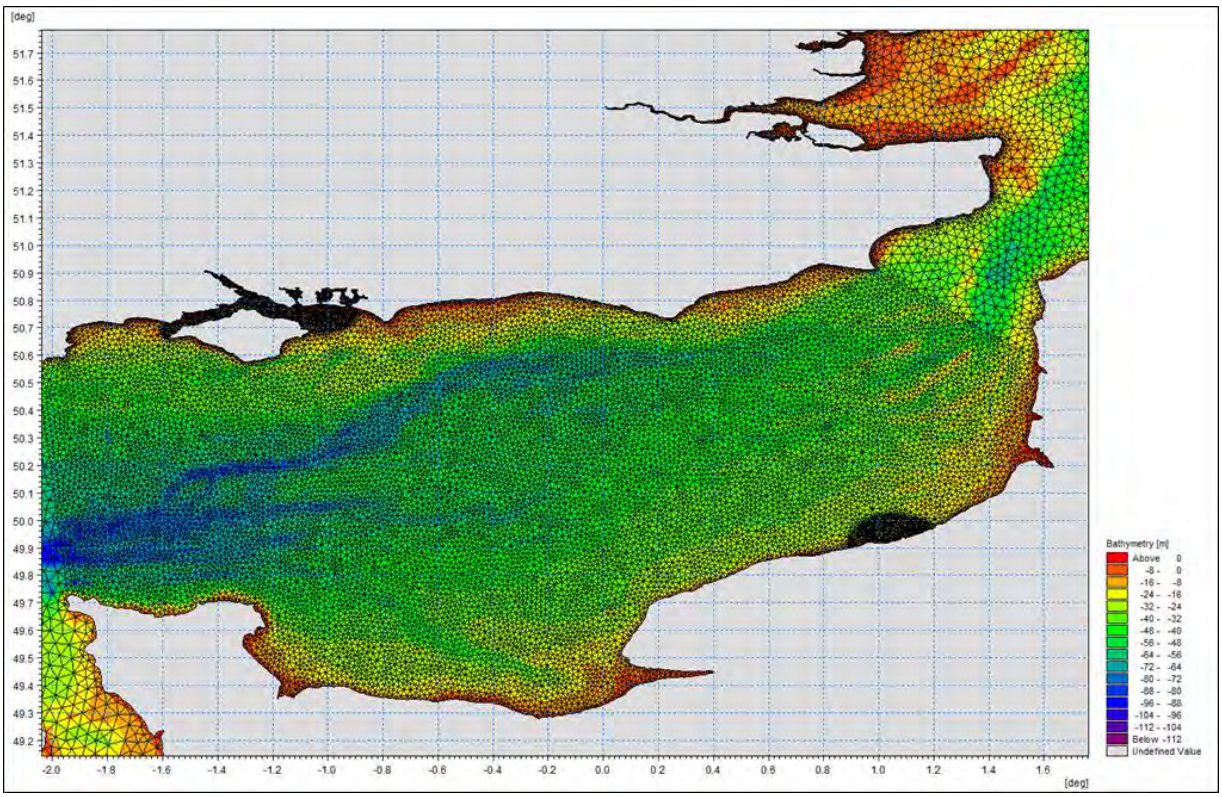

Figure 2 - Zoom in of regional MIKE21 flexible model mesh

2.3. WAVE MODEL

2.3.1.1. A bespoke SWAN wave model was deployed, with a high-resolution regional nest, to produce wave data along the Marine Cable Corridor. The wave model extents are indicated in Figure 3.

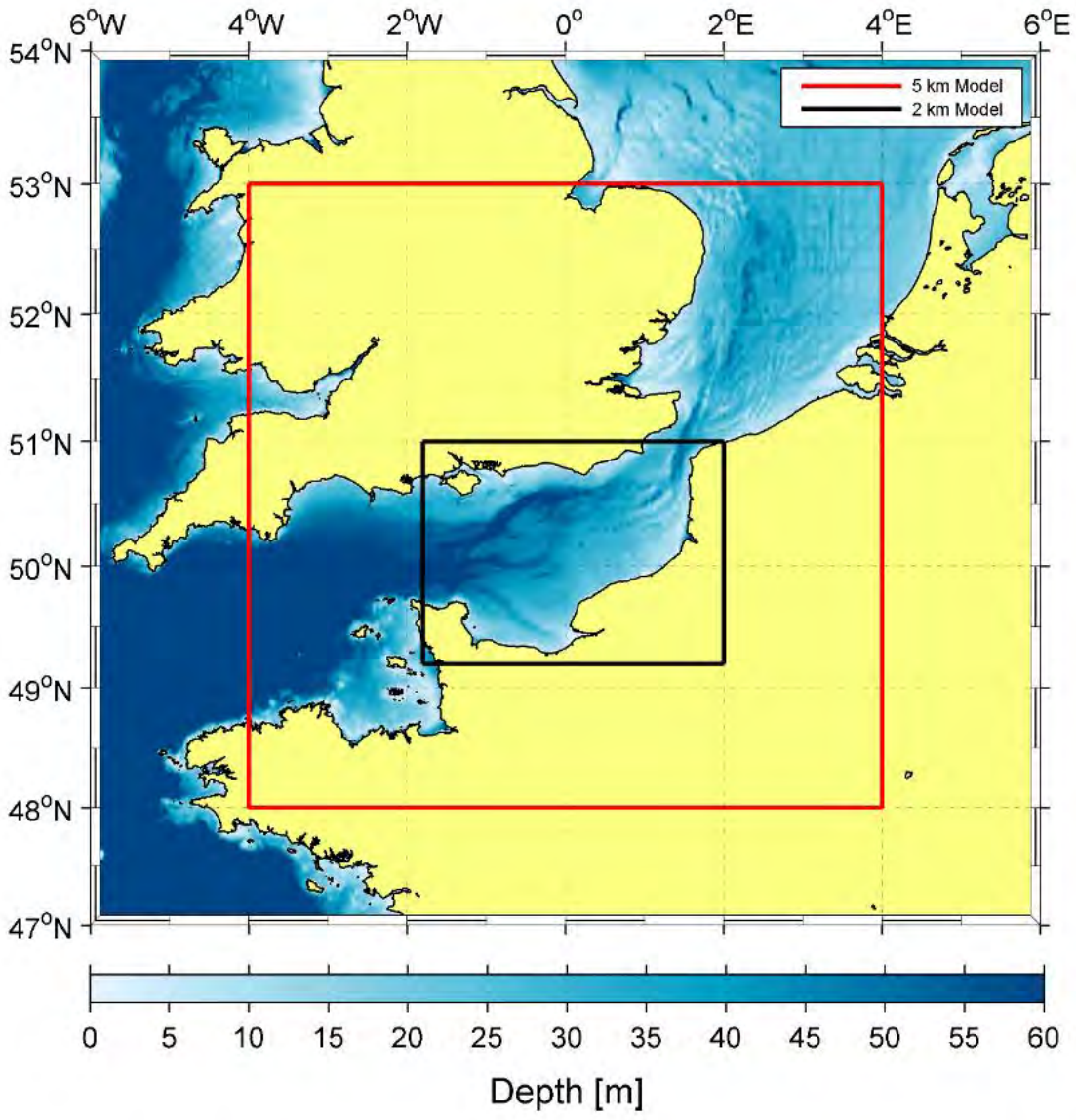

Figure 3 - SWAN wave model domains

2.3.1.2. The SWAN model accounts for the following physics:

- Wave propagation in time and space, shoaling, refraction due to current and depth, frequency shifting due to currents and non-stationary depth;
- Wave generation by wind;
- Three- and four-wave interactions;
- Whitecapping, bottom friction and depth-induced breaking;
- Wave-induced set-up;
- Transmission through and reflection (specular and diffuse) against obstacles; and

- Diffraction.

2.3.1.3. For the production run, SWAN cycle III version 40.91ABC was utilised. Spectral boundary conditions to the large model (5 km) originated from ECMWF ERA Interim data which, in turn, provided boundary conditions to the smaller model (2 km). NCEP CFSR wind fields were applied to the sea surface at hourly intervals to allow proper wave growth within the domain. Finally, tidal effects were incorporated into the wave model as time and space-varying water levels, allowing proper representation of wave processes in varying water depths.

2.3.1.4. The physics schemes and parameterisations used in the development of the SWAN model have been refined and developed by expert users. Within the model, the expression by Komen for whitecapping, and for wind, were employed (Komen & Hassleman, 1985). Triads were included and quadruplet interactions were estimated using the Discrete Interaction Approximation ('DIA') as described by Hasselmann (Hasselmann, 1985). The JOint North Sea WAve Project ('JONSWAP') bottom friction formulation was applied, and depth-limited wave breaking was modelled according to the bore-model of Battjes and Janssen (Battjes & Janssen, 1978).

2.4. BATHYMETRY AND COASTLINE

2.4.1.1. The primary source of bathymetry used in the hydrodynamic and wave models originated from the European Marine Observation and Data Network ('EMODnet', 2018), augmented locally with OceanWise Raster Charts (OceanWise, 2018). These data deliver some of the best available information on water depths around the United Kingdom ('UK'). For this project, high resolution data (i.e. with a resolution of 1 arc second, or approximately 30 m) was used, thus physical features such as trenches, ridges, sand banks and sandwaves are well represented.

2.4.1.2. The coastline was discretised using the Global Self-consistent, Hierarchical, High-resolution Geography ('GSHHG') Database (Wessel and Smith, 1996). The GSHHG is a high-resolution geography data set, amalgamated from two databases in the public domain: World Vector Shorelines (WVS, 2018) and CIA World Data Bank II (WDBII, 2018). The coastline around the Solent in the UK, and surrounding Dieppe, was further refined using Google Earth to trace around satellite imagery of the area.

2.5. MODEL CALIBRATION / VALIDATION

2.5.1.1. To support the process of numerical model calibration/validation, measured data garnered from public sources was utilised. Table 3 details the measured datasets used for model validation.

Table 3 - Measured datasets used for model calibration / validation

Type	Location	Source	Latitude	Longitude	Start Date	End Date
Wave	Hayling Island	Channel Coastal Observatory ('CCO', 2018)	50.73 °N	0.96 °W	01-Jul-2003	30-Sep-2015
Wave	Bracklesham Bay	CCO, 2018	50.72 °N	0.84 °W	01-Aug-2008	30-Sep-2015
Wave	Sandown Bay	CCO, 2018	50.64 °N	1.13 °W	01-Jul-2003	30-Sep-2015
Wave	Rustington	CCO, 2018	50.77 °N	0.49 °W	01-Jul-2003	30-Sep-2015
Water-Level	Newhaven	UK National Tide Gauge Network ('UK NTGN', 2018)	50.78 °N	0.06 °E	01-Jan-2013	01-Jan-2014
Water-Level	Portsmouth	UK NTGN, 2018	50.80 °N	1.11 °W	01-Jan-2013	01-Jan-2014
Water-Level	Dieppe	Service hydrographique et océanographique de la marine ('SHOM')	49.93 °N	1.08 °E	01-Jan-2013	01-Jan-2014
Flow	Offshore Isle of Wight	British Oceanographic Data Centre (49972)	50.52 °N	1.12 °W	08-Jul-1983	25-Jul-1983

2.5.1.2. The hydrodynamic model was initially tuned using only tidal forcing such that modelled and measured water-levels corresponded strongly at a selection of sites (e.g. the harbours of Portsmouth, Newhaven and Dieppe). Atmospheric forcing was then introduced, and the model was further calibrated until it demonstrated good skill. Finally, following the first production run, the model was re-calibrated to optimise the correlation between data produced by the model and the measured data. This final calibration required that within the model the

water levels were decreased by 2.5 % and tidal flow magnitude were reduced by 7.5 %. Please note: a 10-minute adjustment was also made to the modelled water-levels at Portsmouth for validation purposes.

2.5.1.3. Following the process of model calibration, for each measured dataset in turn, the model output at the corresponding location was compared to the data record. Simultaneous scatter plot comparisons of modelled and measured wave heights (with overlaid quantile-quantiles) are presented in Figure 4 to Figure 7 and comparisons of modelled and measured water levels are presented in Figure 8 to Figure 10. In addition, predicted tidal flow velocity magnitude and direction is presented as a time series overlain a measured dataset in Figure 11. The observed high correlation (determination) coefficients (e.g. R^2 values of 0.84 – 1.0), regression slopes marginally in excess of unity and low scatter indexes suggest excellent model fit with measured data and thus the model can be considered a strong reflection of reality.

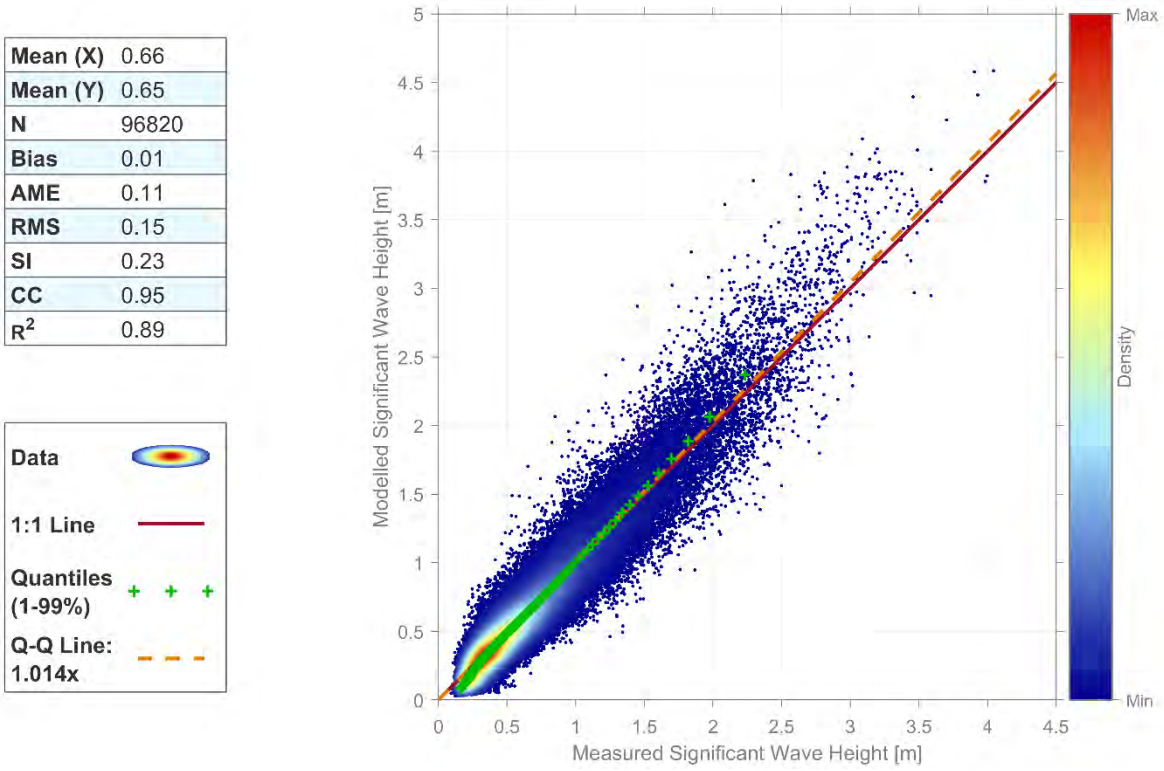

Figure 4 - Comparison of modelled and measured wave heights at Hayling Island

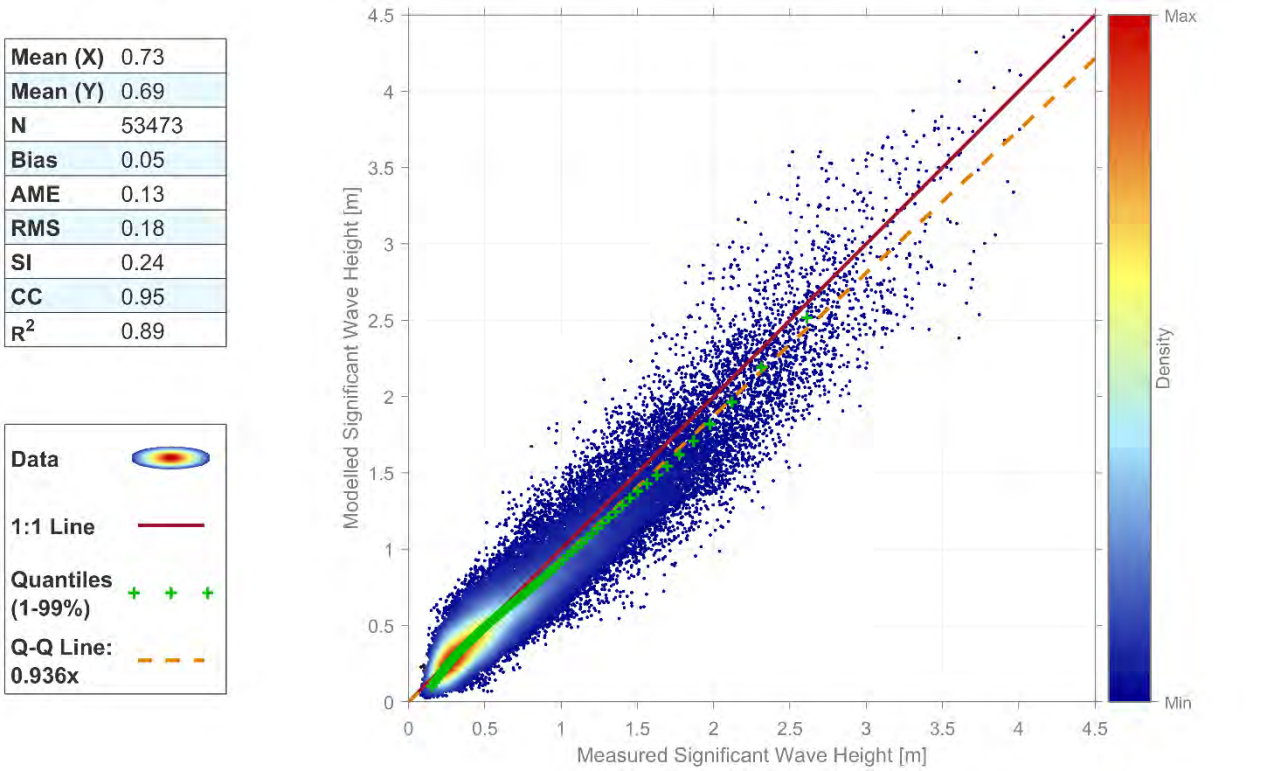

Figure 5 - Comparison of modelled and measured wave heights at Bracklesham Bay

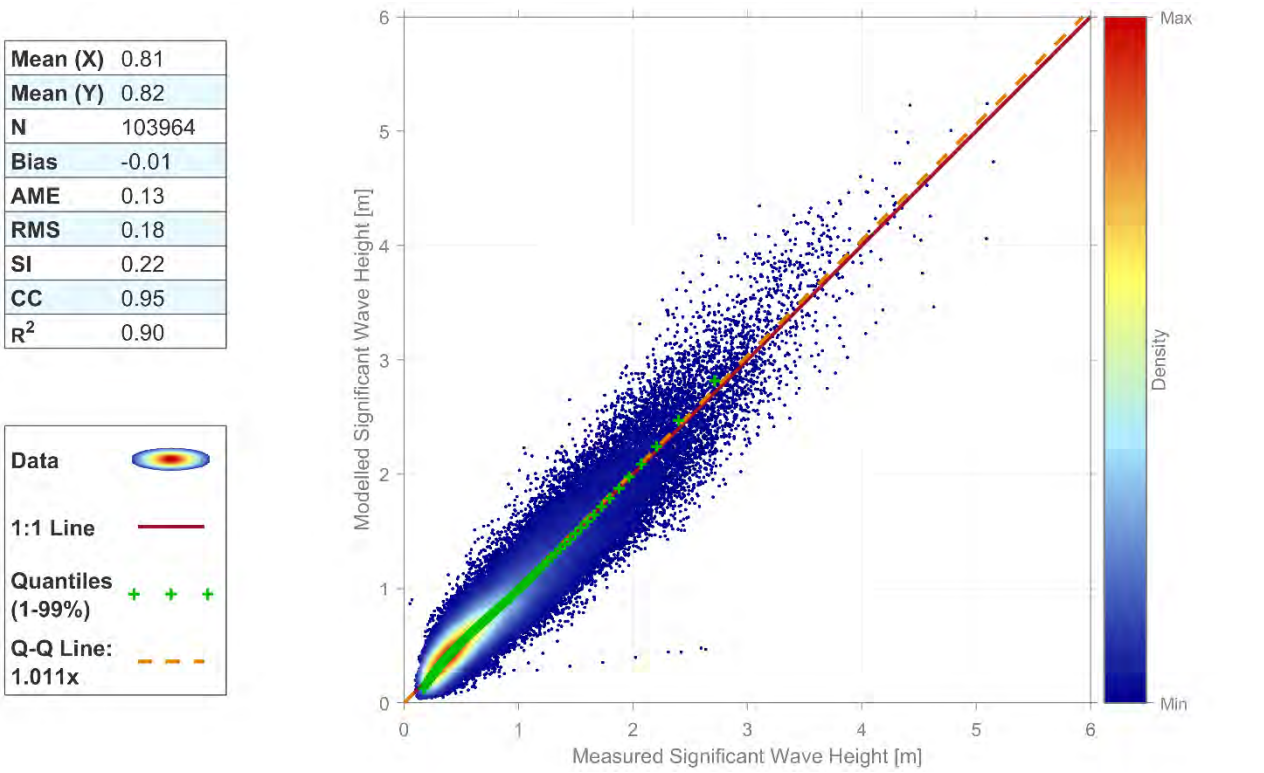

Figure 6 - Comparison of modelled and measured wave heights at Rustington

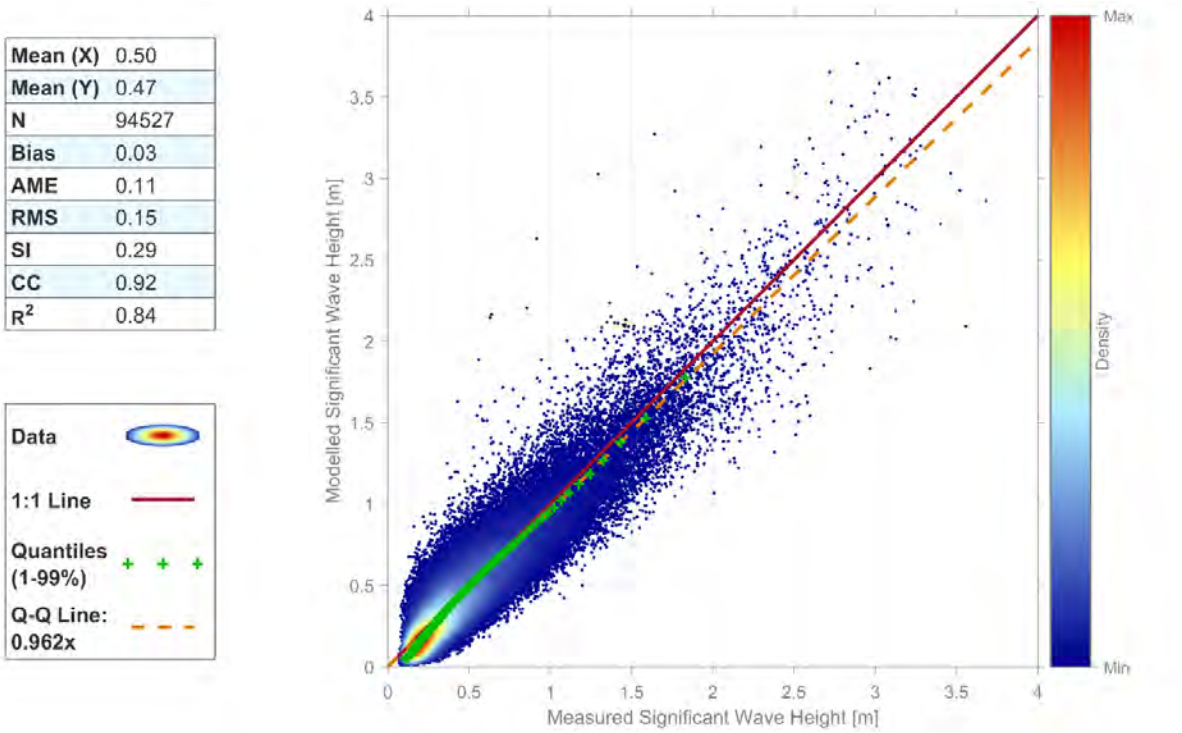

Figure 7 - Comparison of modelled and measured wave heights at Sandown Bay

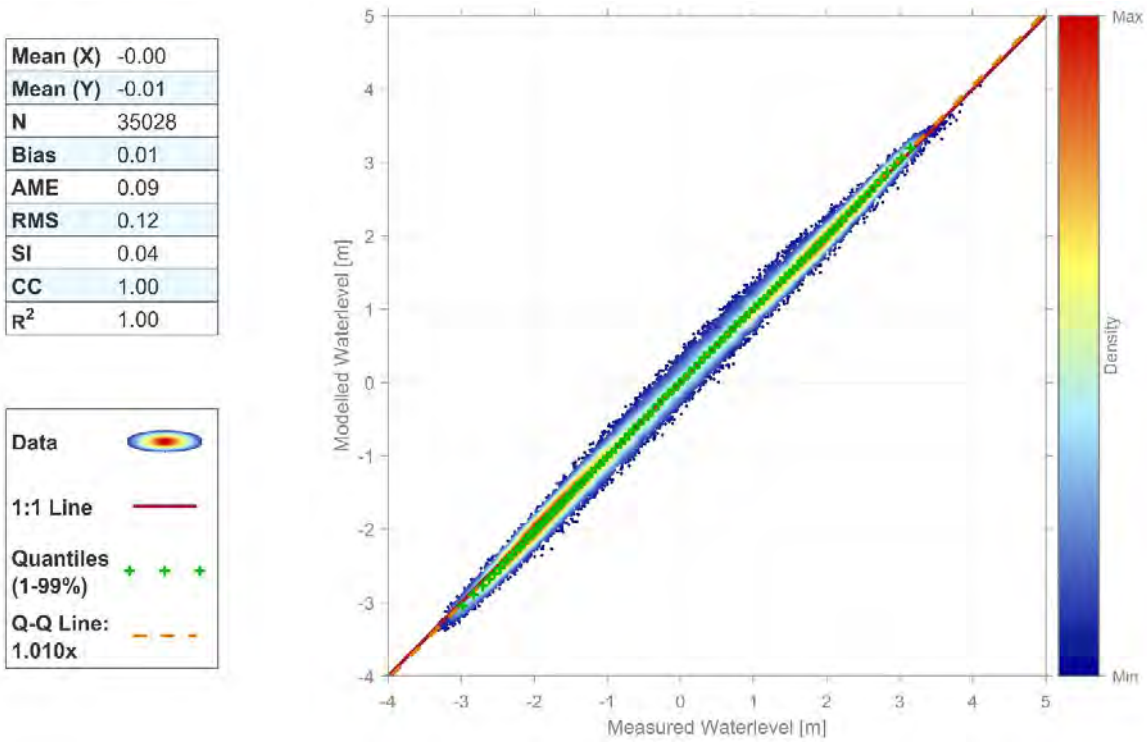

Figure 8 Comparison of modelled and measured water level at Newhaven

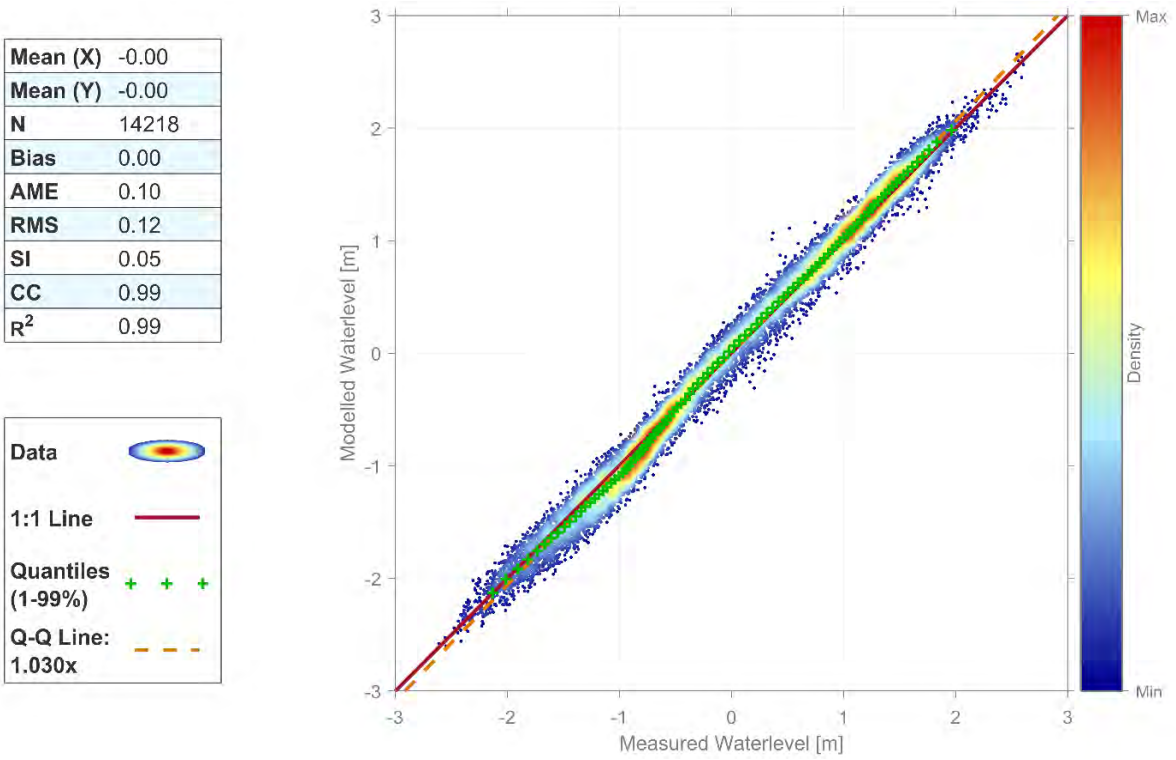

Figure 9 - Comparison of modelled and measured water level at Portsmouth

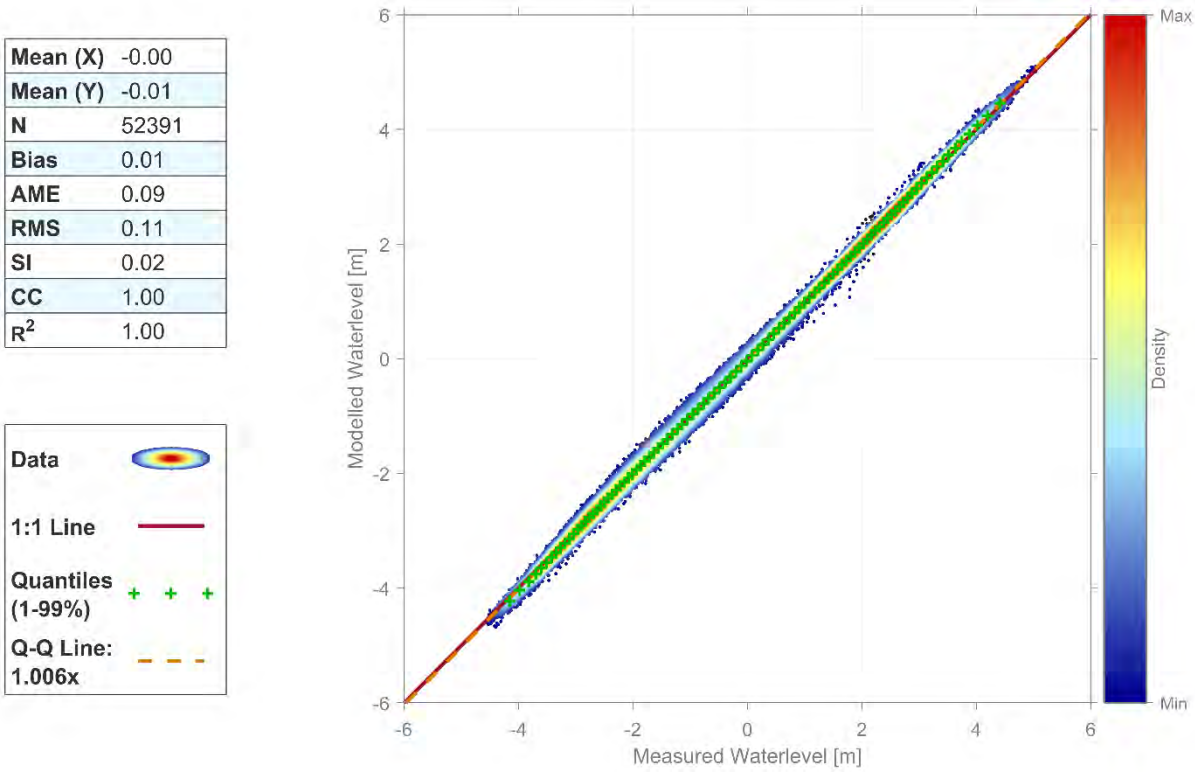

Figure 10 - Comparison of modelled and measured water level at Dieppe

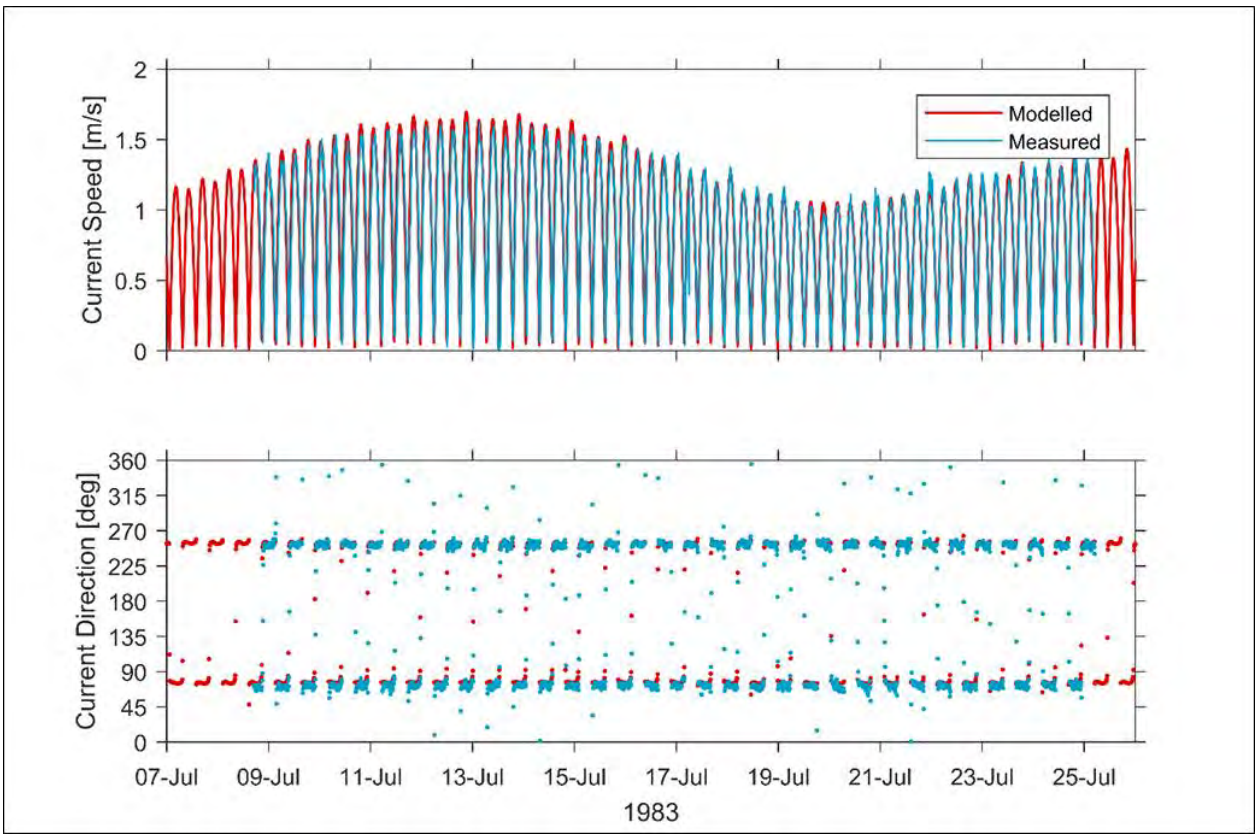

Figure 11 - Time-Series comparison of modelled and measured currents

3. HYDRODYNAMIC MODEL OUTPUTS

3.1.1.1. Depth-averaged tidal flow and water-level data were output at 10-minute intervals between 1998 and 2017 in the form of time-series. These data were derived from five locations in UK waters along the Marine Cable Corridor (Figure 12). The data generated included the following parameters:

- Significant wave height (H_s, m);
- Mean wave direction (M_{dir}, degrees from);
- Mean zero- crossing wave period (T_z, s);
- Mean energy wave period (T_e, s);
- Peak wave period (T_p, s);
- Wind speed @ 10m above Mean Sea Level ('MSL') ($u10$, ms^{-1});
- Wind direction @ 10m above MSL ($\Theta 10$, degrees from);
- Current speed (depth-average) (C_s, ms^{-1}); and
- Current direction (depth-average) (C_d, degrees towards).

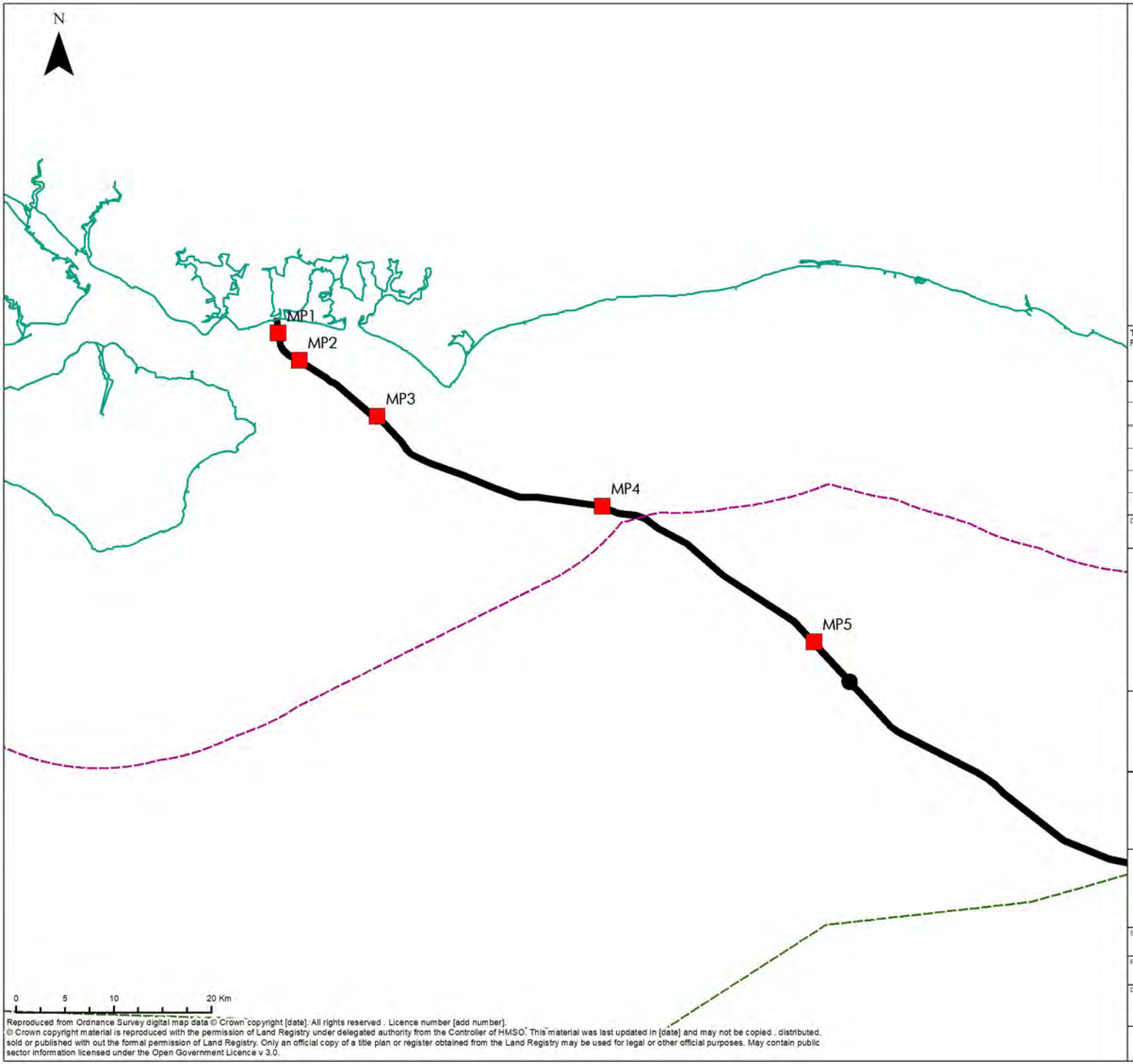

Model Inspection Point

Marine cable corridor

UK/France EEZ boundary line

UK 12 nautical mile limit

The Infrastructure Planning (Environmental Impact Assessment) Regulations 2017.

REV	DATE	BY	DESCRIPTION	CHK	APP
01	22/07/2019	JP	FIRST DRAFT	SL	

DRAWING STATUS: DRAFT

PARTRAC

www.partrac.com

CLIENT: AQUIND

PROJECT: AQUIND Interconnector

TITLE: Figure 12 Hydrodynamic Model Inspection Point Locations

SCALE AT A4	CHECKED		APPROVED
1:568,978	[SL]		[]
PROJECT NO: EN020022	DESIGNED: [JP]	DRAWN: [JP]	DATE: 07.06.2019

DRAWING NO: EN020022-ES APPENDIX-6.1-8 | REV NO: 01

Reproduced from Ordnance Survey digital map data © Crown copyright [date]. All rights reserved . Licence number [add number].
© Crown copyright material is reproduced with the permission of Land Registry under delegated authority from the Controller of HMSO. This material was last updated in [date] and may not be copied , distributed, sold or published with out the formal permission of Land Registry. Only an official copy of a title plan or register obtained from the Land Registry may be used for legal or other official purposes. May contain public sector information licensed under the Open Government Licence v 3.0.

© WSP UK Ltd

3.2. DATA ANALYSIS

3.2.1.1. To inform the assessment of baseline conditions and potential impacts associated with the Proposed Development, data retrieved from each model inspection point has been analysed. These analyses are presented in Figure 13 - Figure 65. The interpretation of these data (which is presented variously as graphs, diagrams and tables) is provided in Chapter 6 (Physical Processes) of the Environmental Statement ('ES') Volume 1 (document reference 6.1.6). Thus, it is recommended that the following section is read in conjunction with Section 6.5 of the Physical Processes chapter.

Water Levels

3.2.1.2. The temporal variation in water levels over a period of one year at each model inspection point is presented as a time series in Figure 13 to Figure 17.

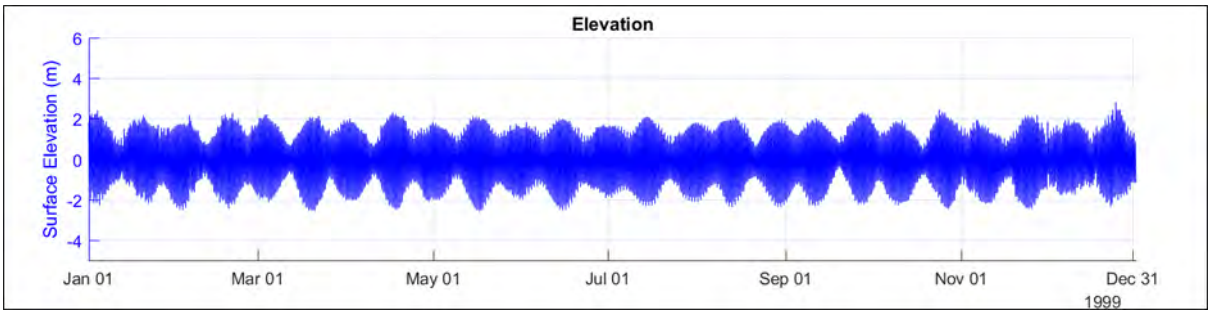

Figure 13 - Time series water level data for model inspection point 1

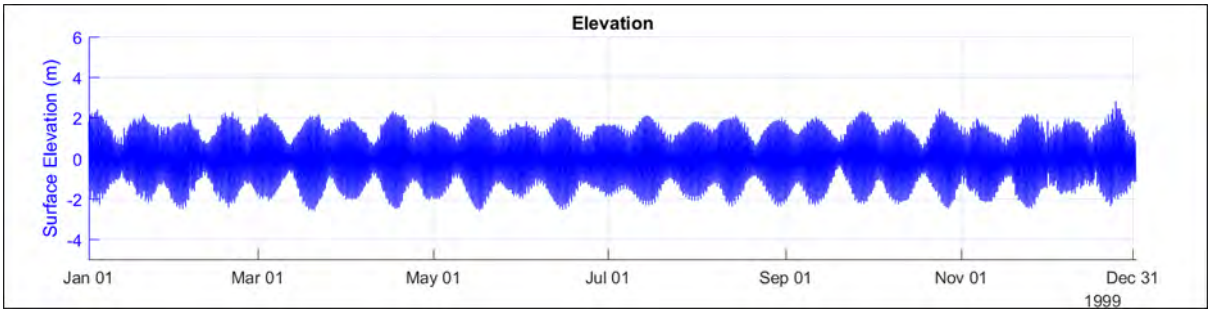

Figure 14 - Time series water level data for model inspection point 2

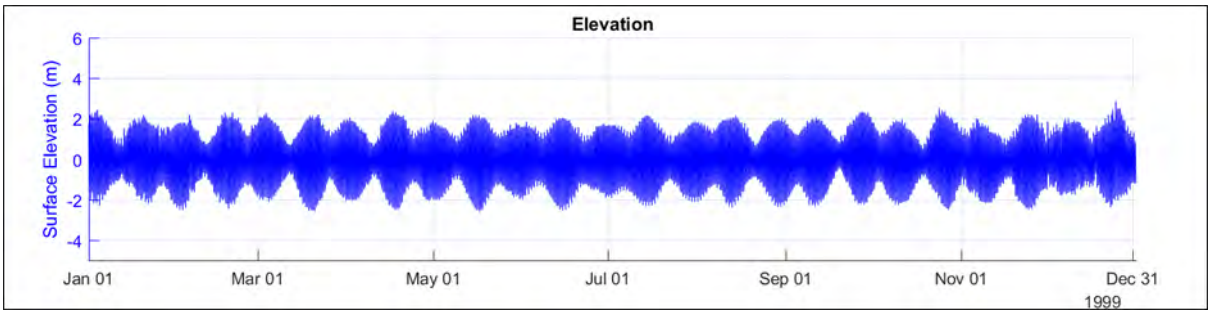

Figure 15 - Time series water level data for model inspection point 3

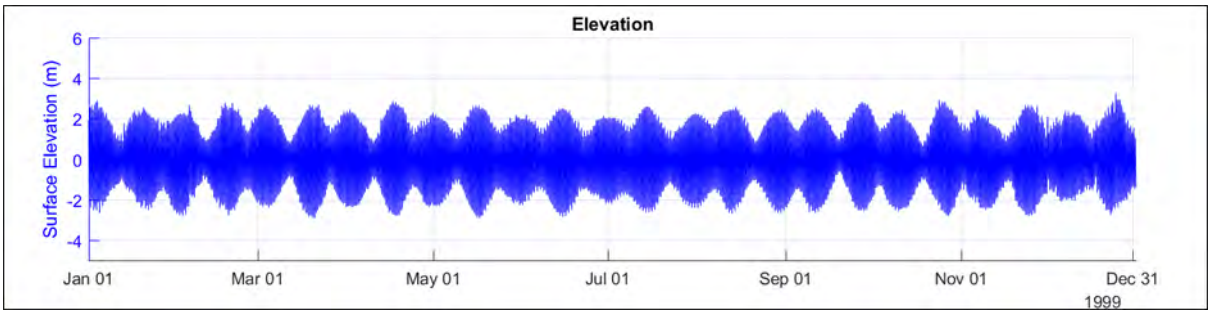

Figure 16 - Time series water level data for model inspection point 4

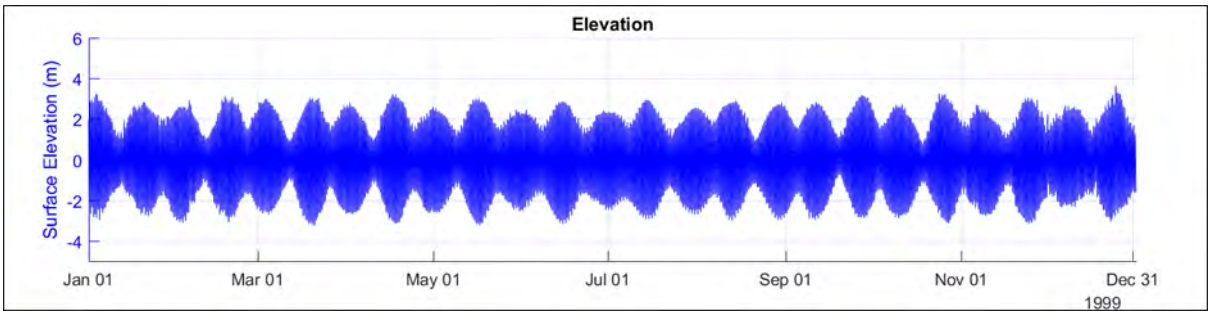

Figure 17 - Time series water level data for model inspection point 5

Tidal Flows

3.2.1.3. The temporal variation of tidal flow velocities in the Channel during a flooding Spring tide and an ebbing Spring tide are presented as vector plots overlain a spatial plot of the model domain in Figure 18 to Figure 24 and Figure 25 to Figure 31, respectively.

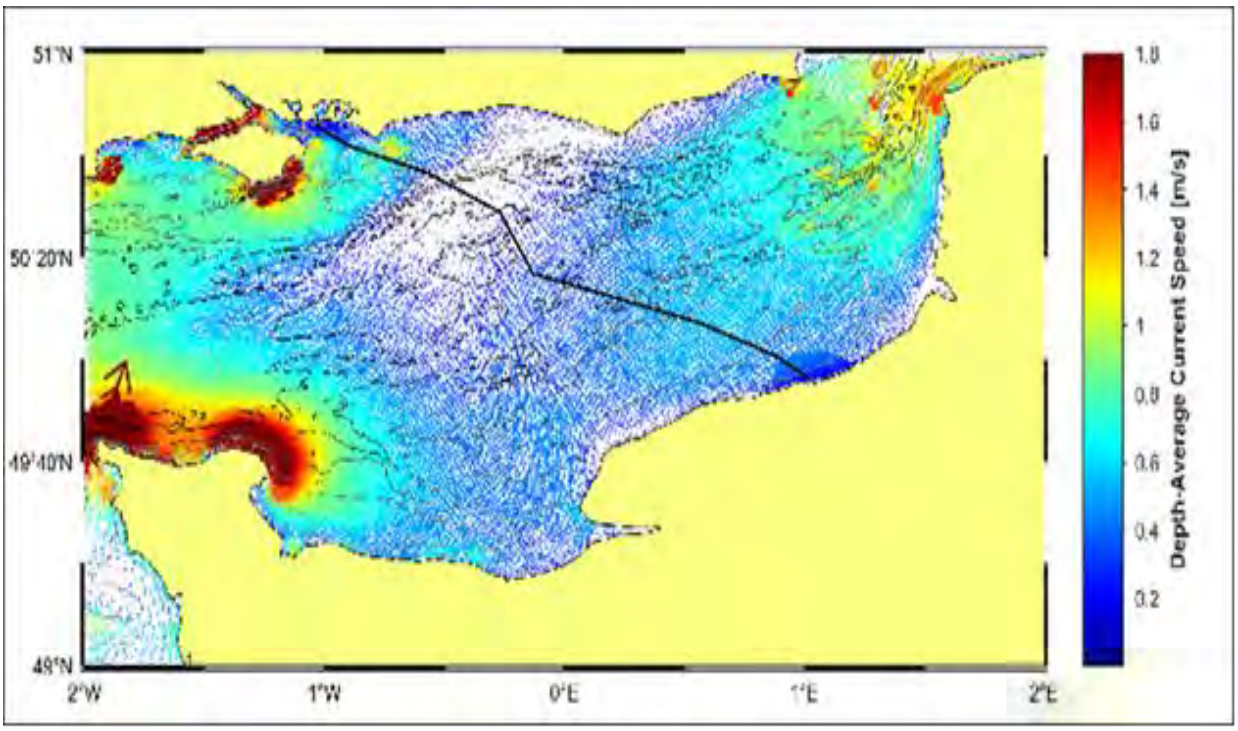

Figure 18 - Distribution of tidal currents in the Channel during Spring flood tides (High Water - 6 hours)

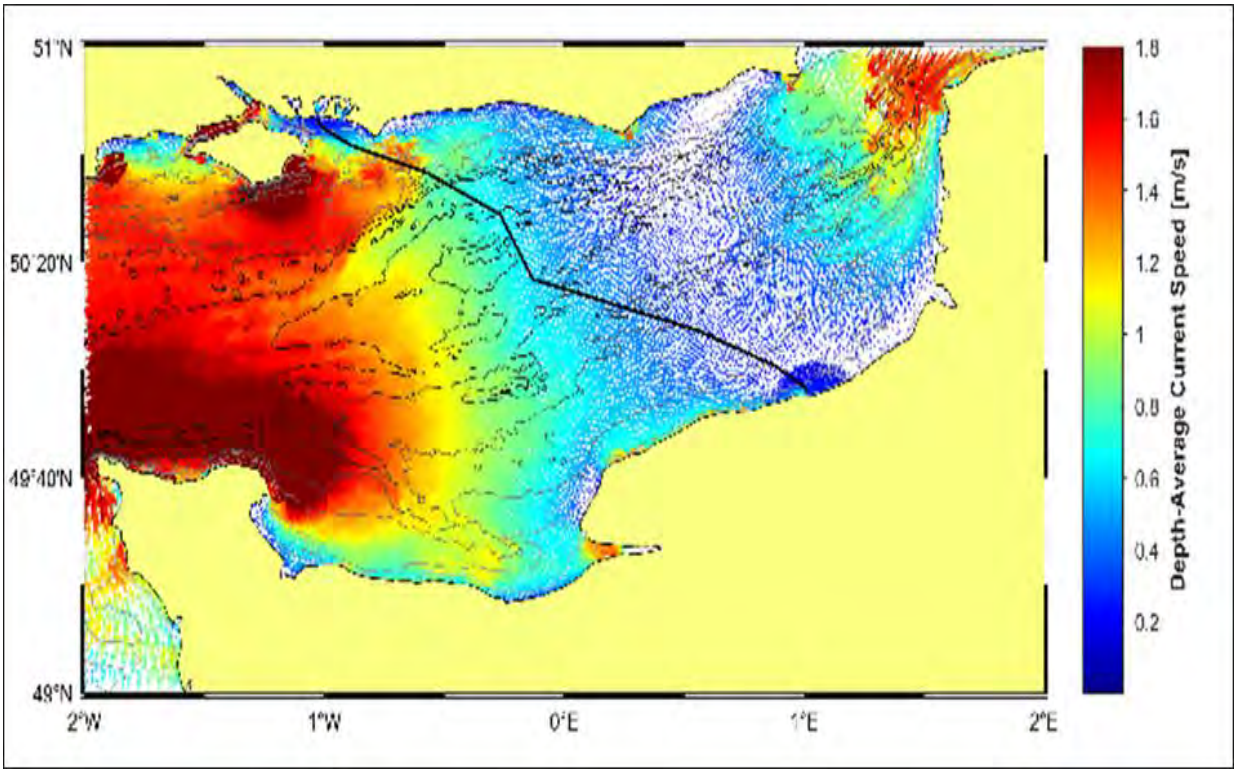

Figure 19 - Distribution of tidal currents in the Channel during Spring flood tides (High Water - 5 hours)

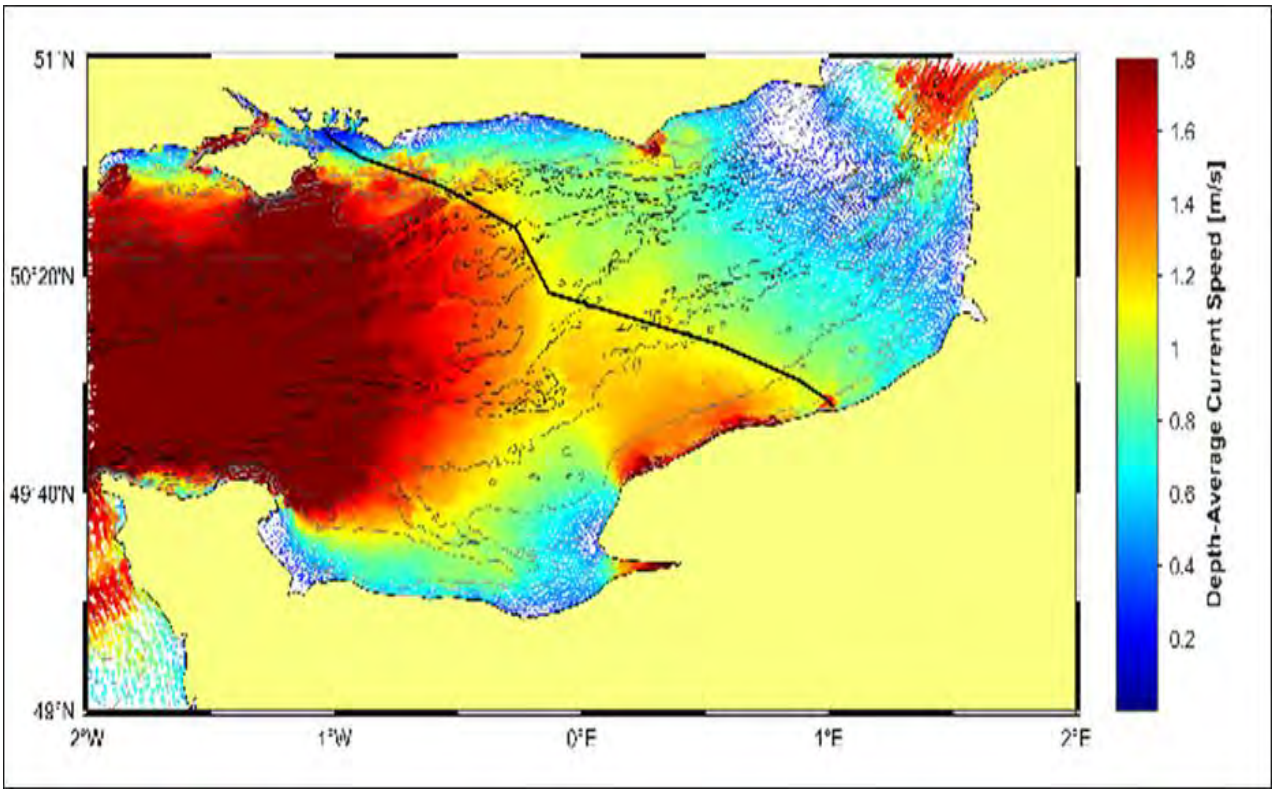

Figure 20 Distribution of tidal currents in the Channel during Spring flood tides (High Water - 4 hours)

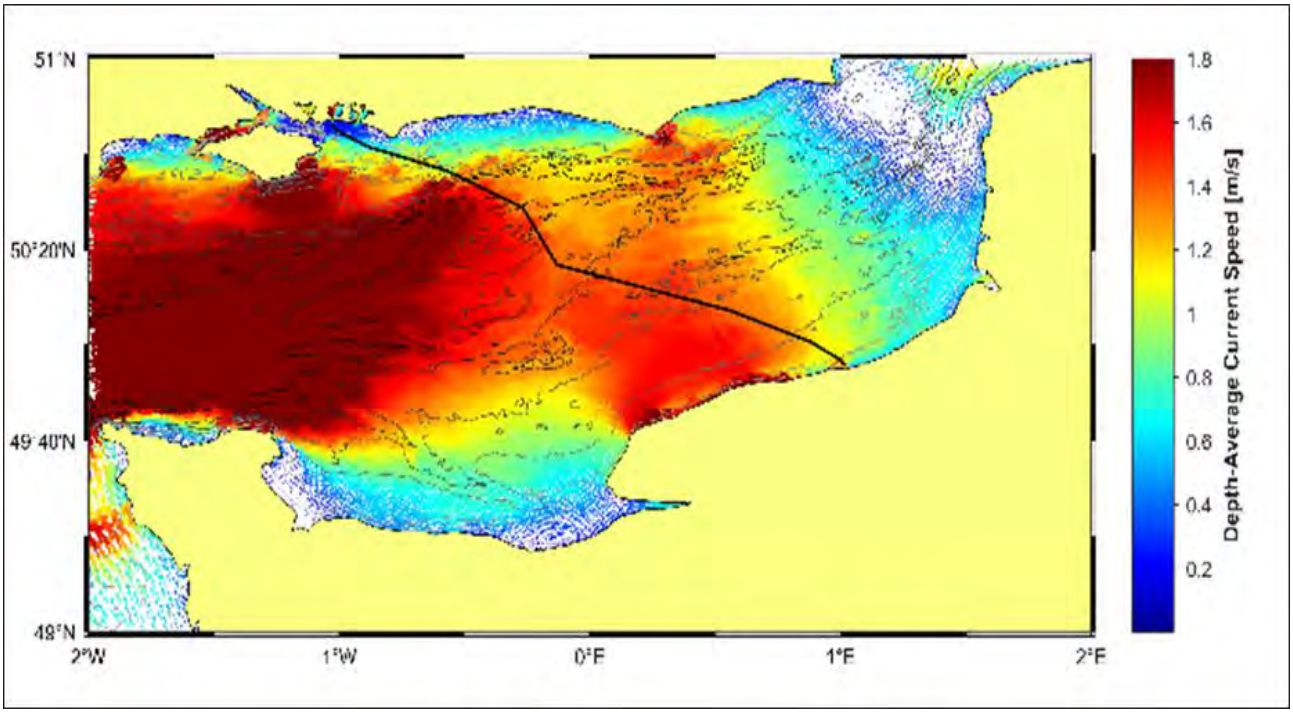

Figure 21 - Distribution of tidal currents in the Channel during Spring flood tides (High Water - 3 hours)

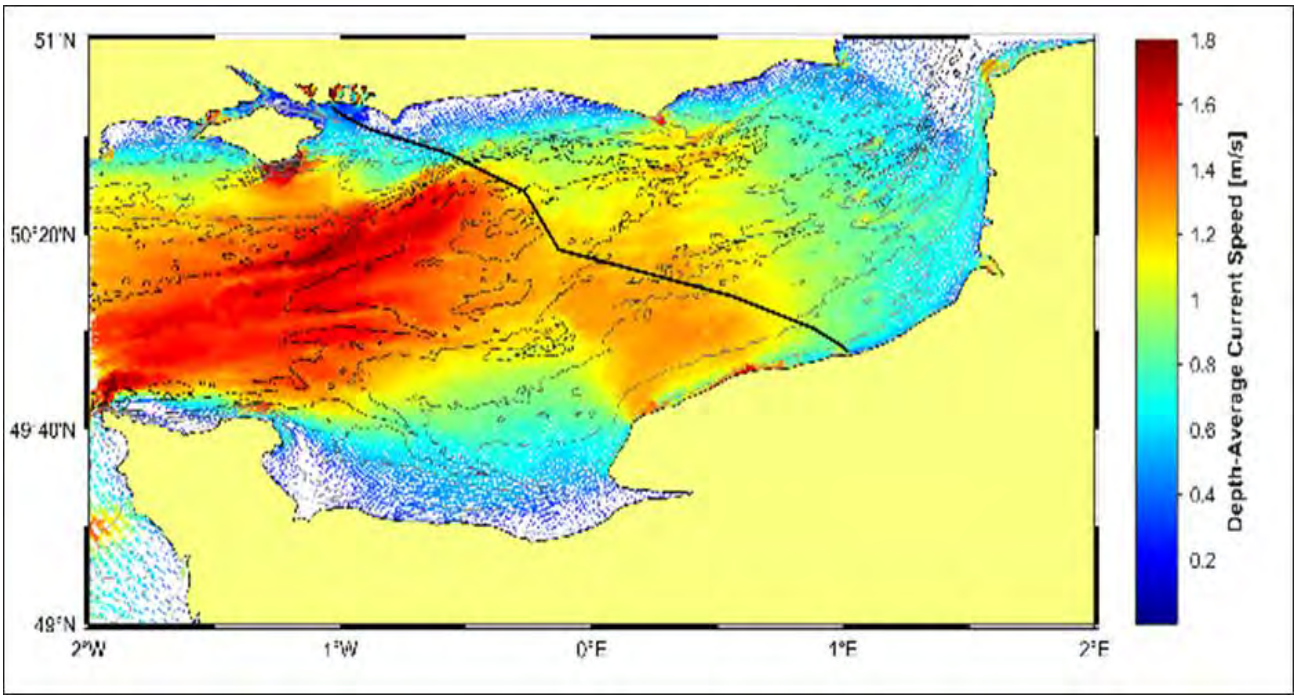

Figure 22 - Distribution of tidal currents in the Channel during Spring flood tides (High Water - 2 hours)

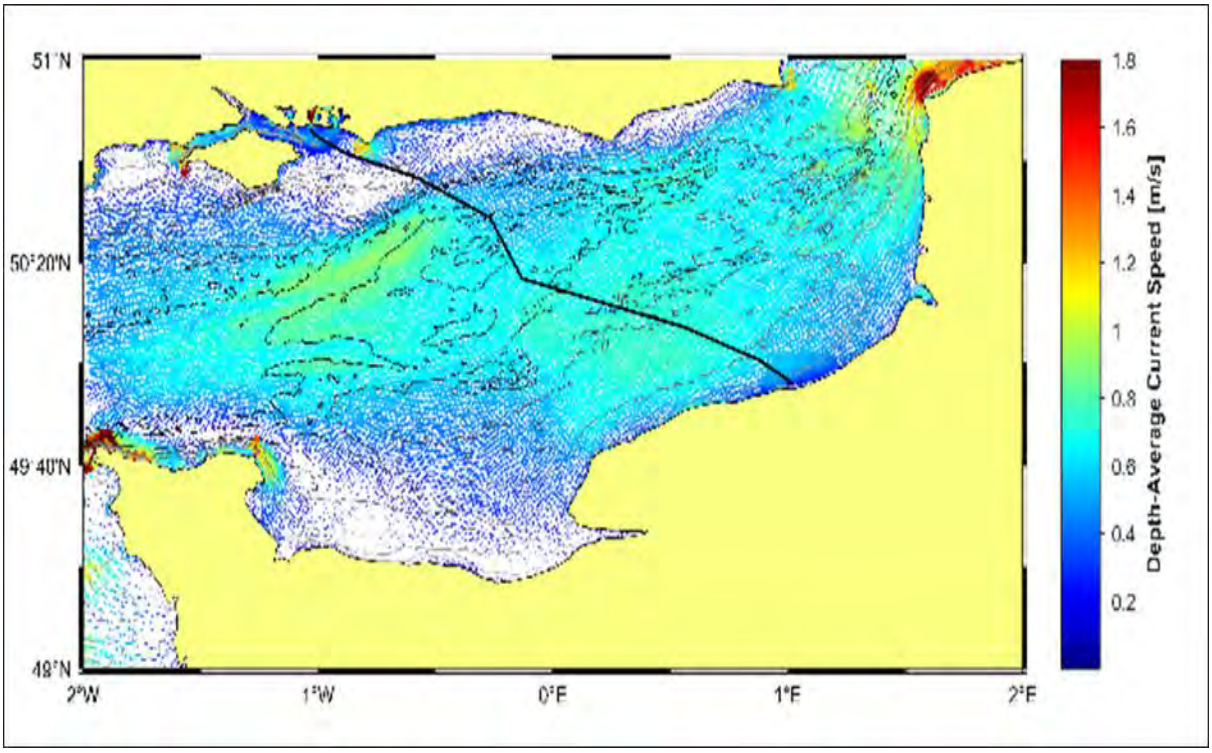

Figure 23 - Distribution of tidal currents in the Channel during Spring flood tides (High Water - 1 hour)

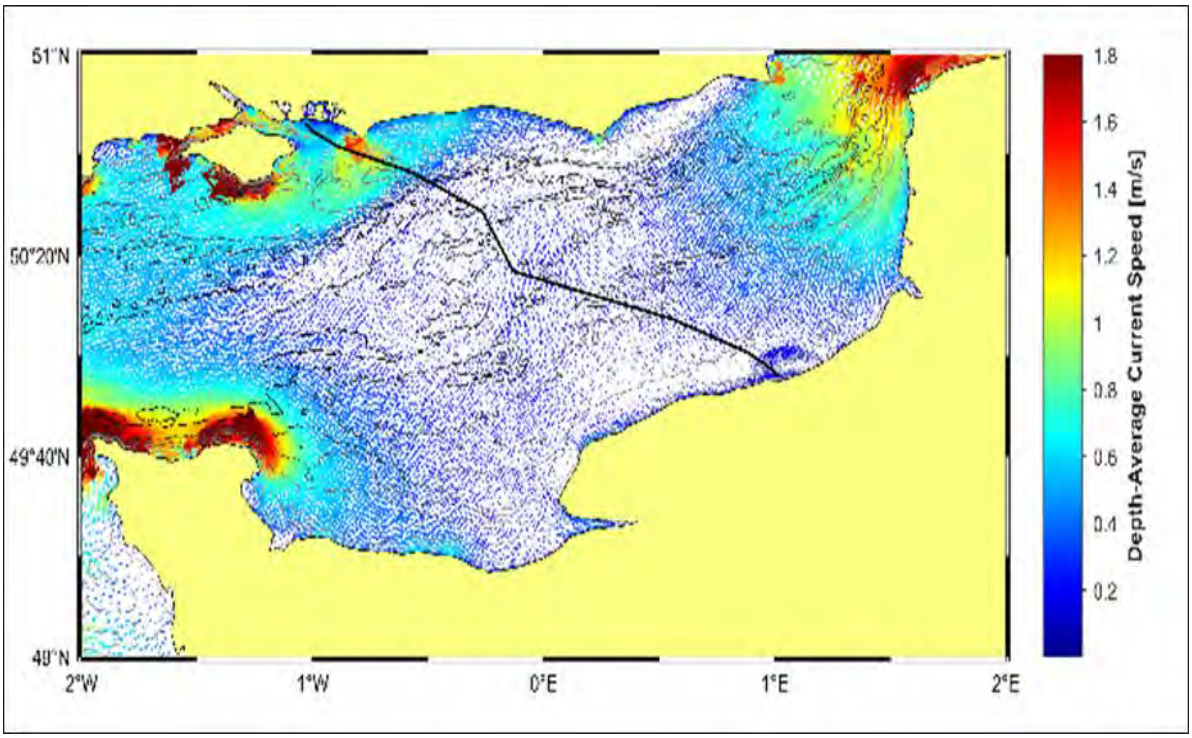

Figure 24 - Distribution of tidal currents in the Channel during Spring flood tides (High Water - 0 hours)

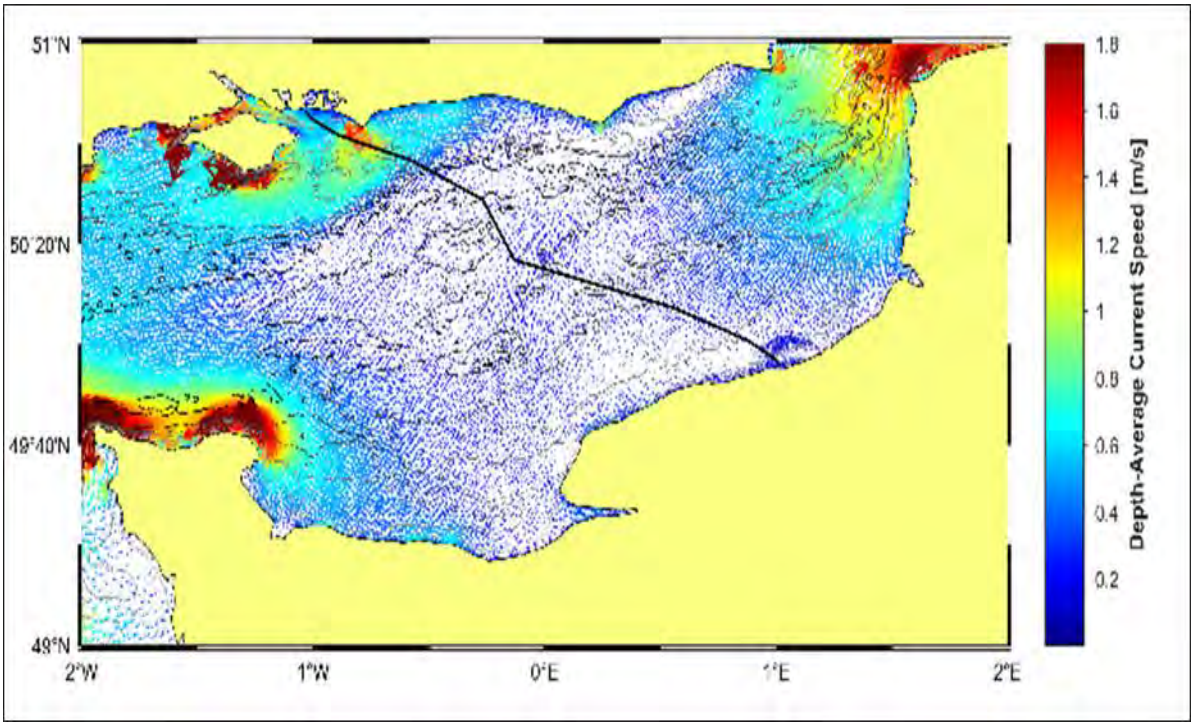

Figure 25 - Distribution of tidal currents in the Channel during Spring ebb tides (High Water - 0 hours)

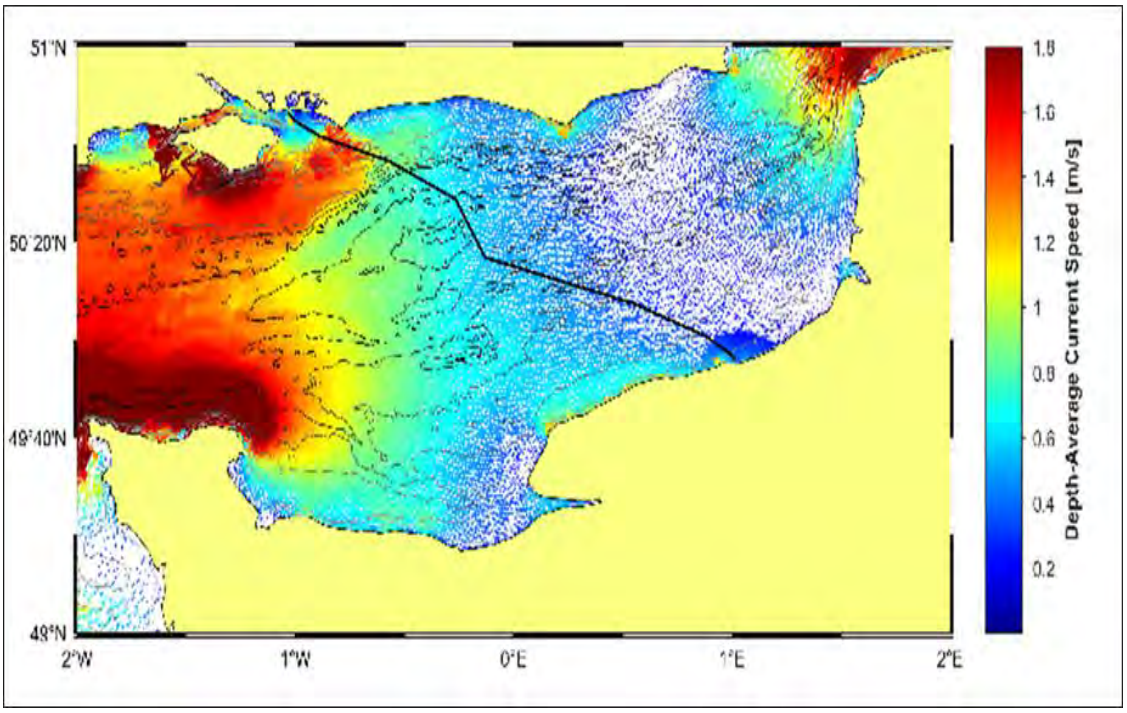

Figure 26 - Distribution of tidal currents in the Channel during Spring ebb tides (High Water + 1 hour)

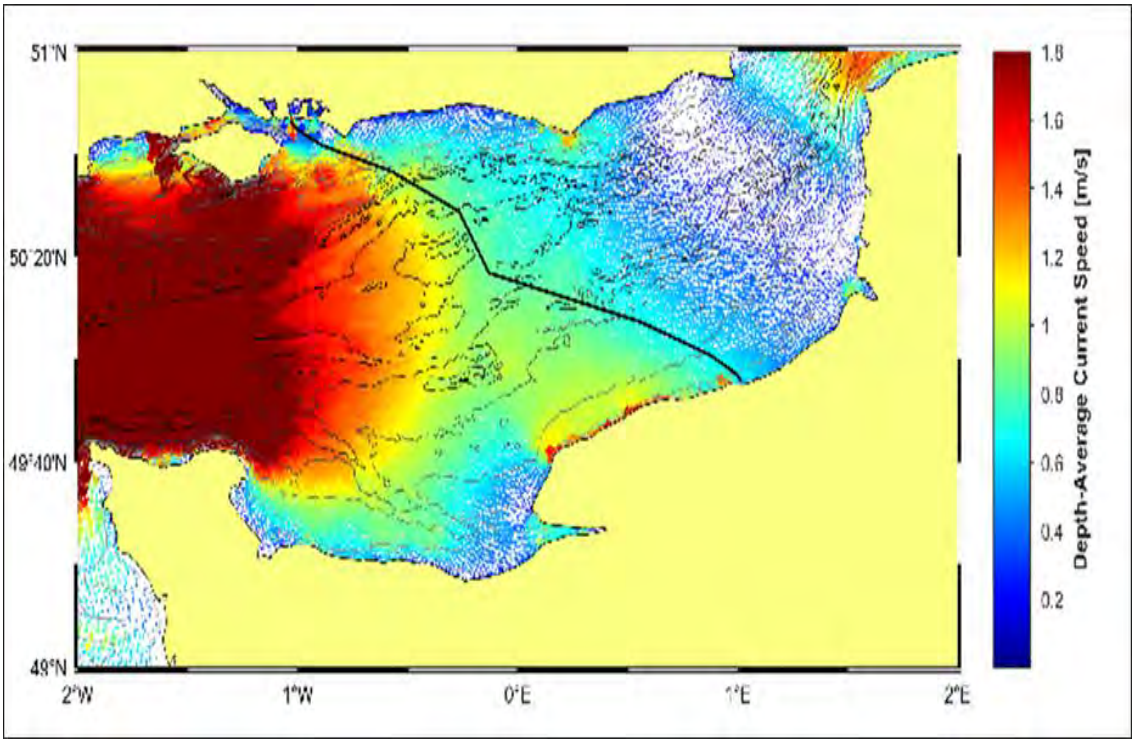

Figure 27 - Distribution of tidal currents in the Channel during Spring ebb tides (High Water + 2 hours)

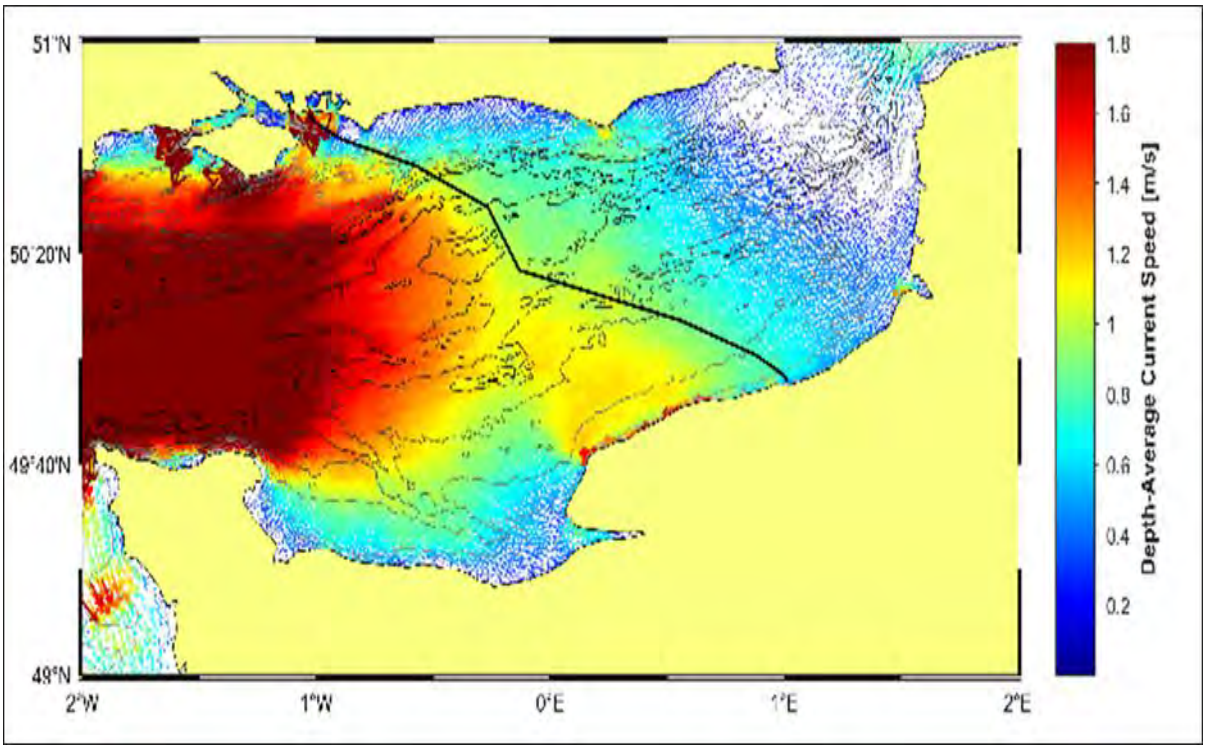

Figure 28 - Distribution of tidal currents in the Channel during Spring ebb tides (High Water + 3 hours)

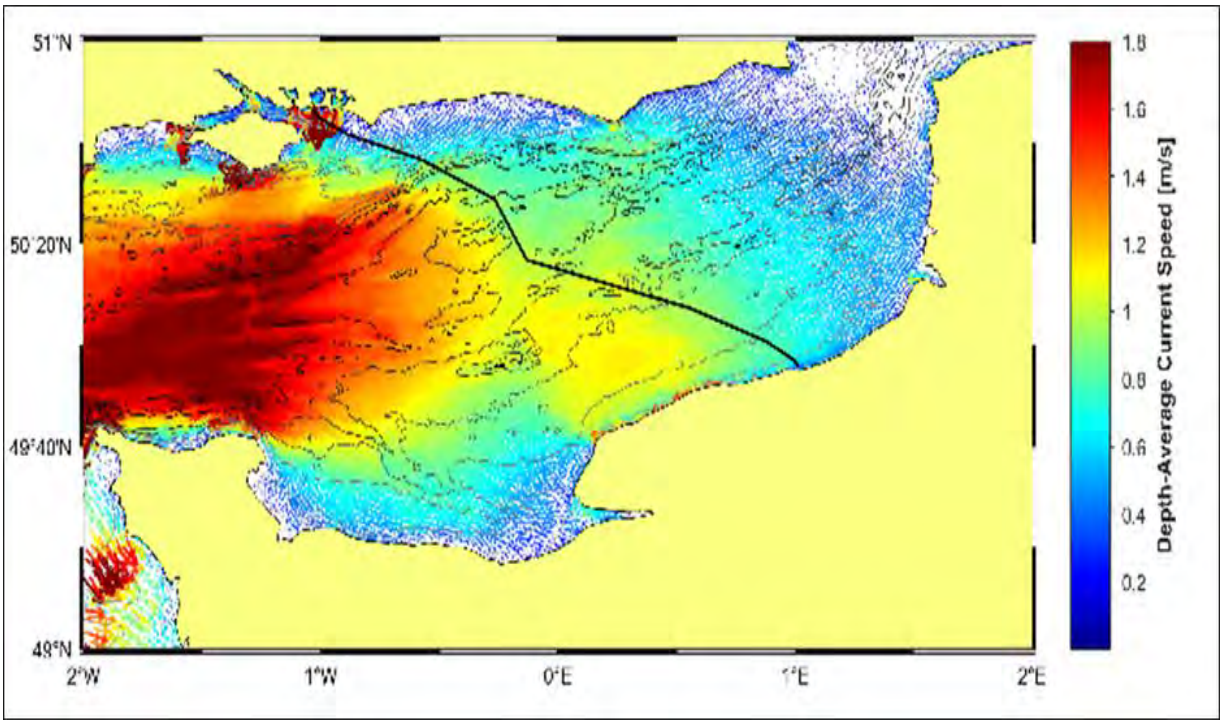

Figure 29 - Distribution of tidal currents in the Channel during Spring ebb tides (High Water + 4 hours)

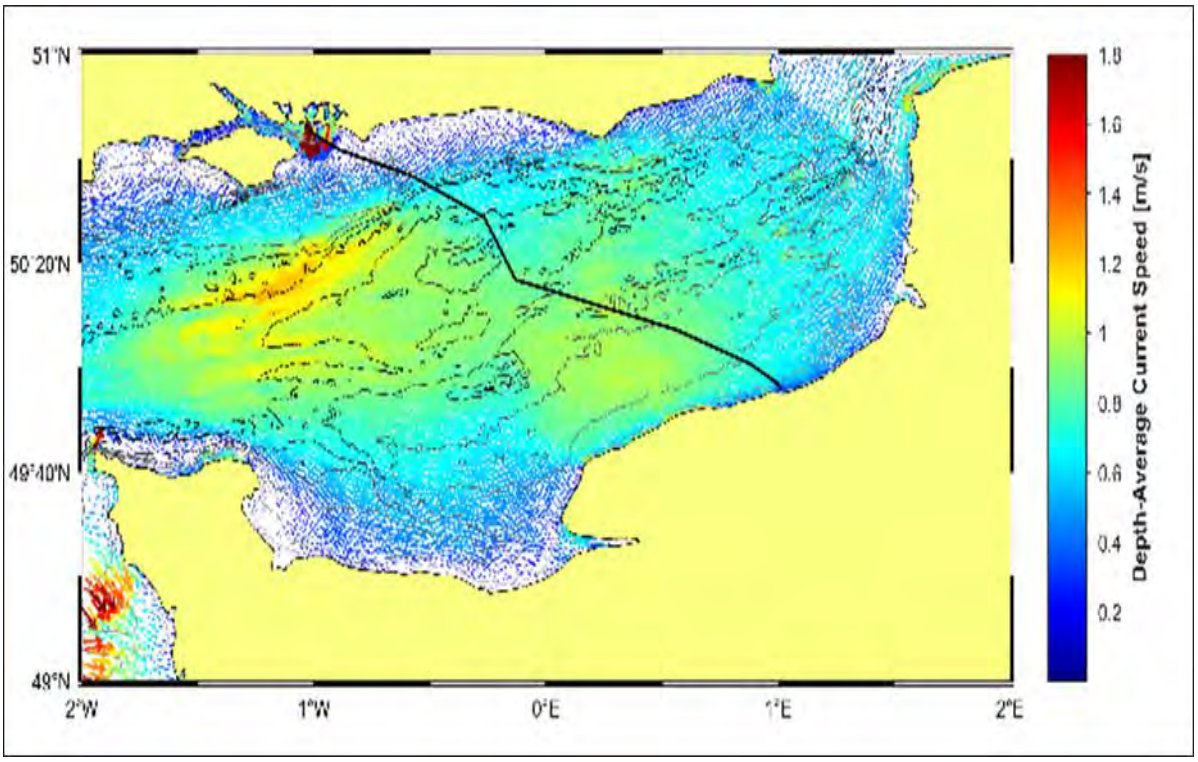

Figure 30 - Distribution of tidal currents in the Channel during Spring ebb tides (High Water + 5 hours)

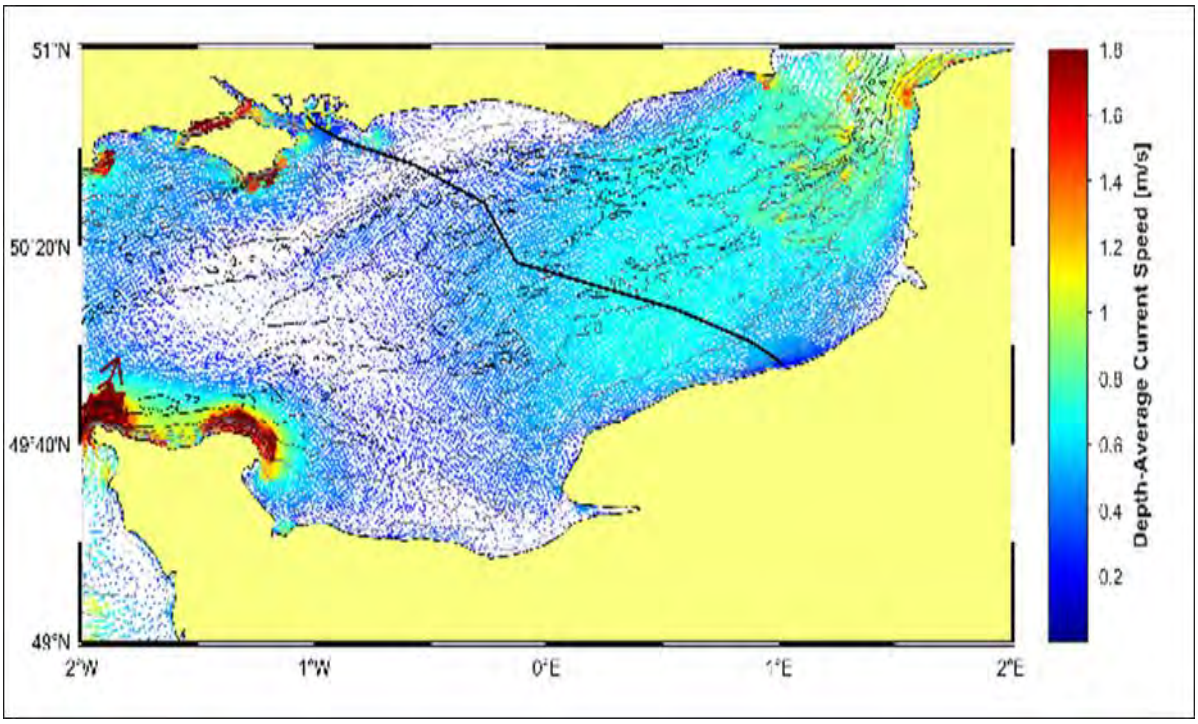

Figure 31 - Distribution of tidal currents in the Channel during Spring ebb tides (High Water + 6 hours)

3.2.1.4. A Eulerian view of the current velocities is presented in abstracted time-series of magnitude and direction (see Figure 32 to Figure 36). Additionally, Figure 37 to Figure 41 display flow direction vs magnitude at each of the model points in the form of rose diagrams which provides for a visually simple appreciation of the predominant tidal axis.

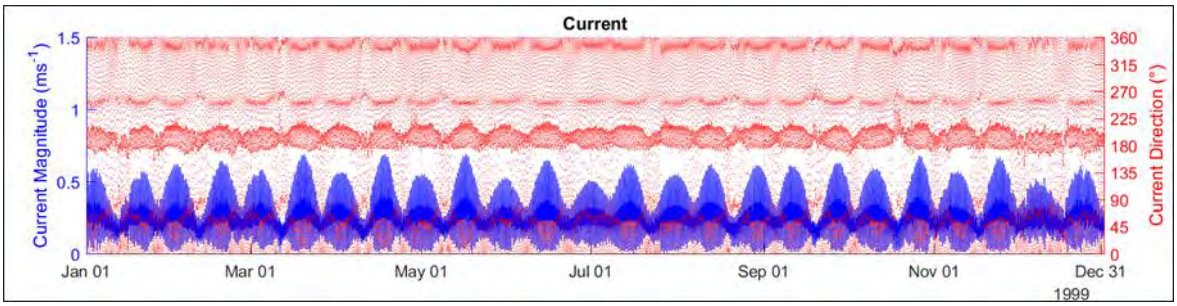

Figure 32 - Time series showing depth averaged current magnitude and current direction derived from the HD model at model point 1

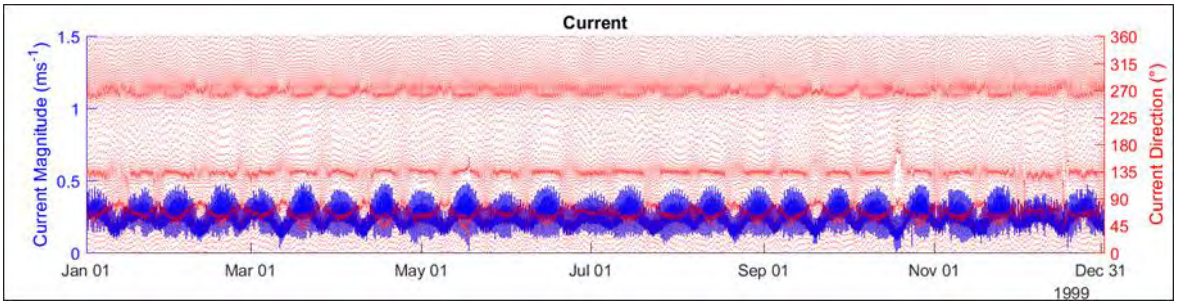

Figure 33 - Time series showing depth averaged current magnitude and current direction derived from the HD model at model point 2

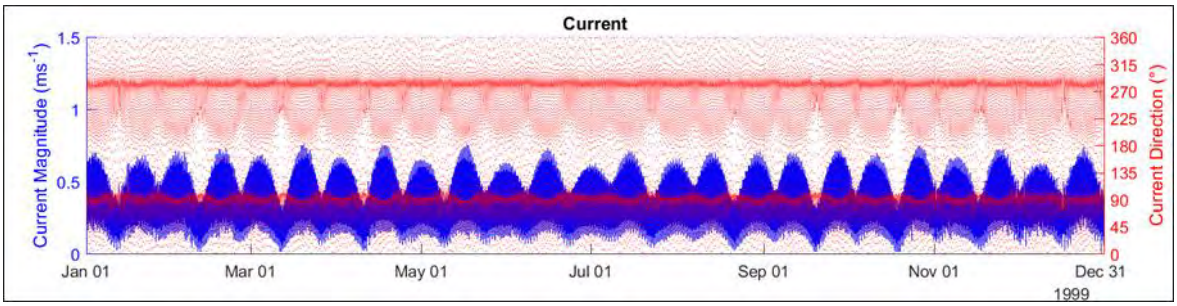

Figure 34 - Time series showing depth averaged current magnitude and current direction derived from the HD model at model point 3

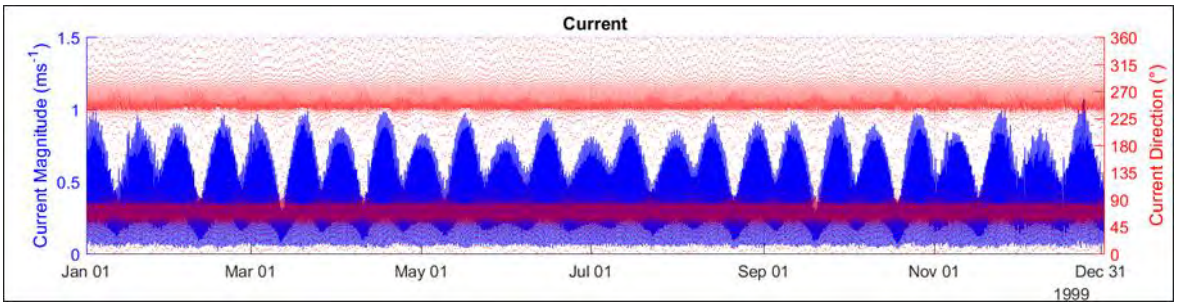

Figure 35 - Time series showing depth average current magnitude and current direction derived from the HD model at model point 4

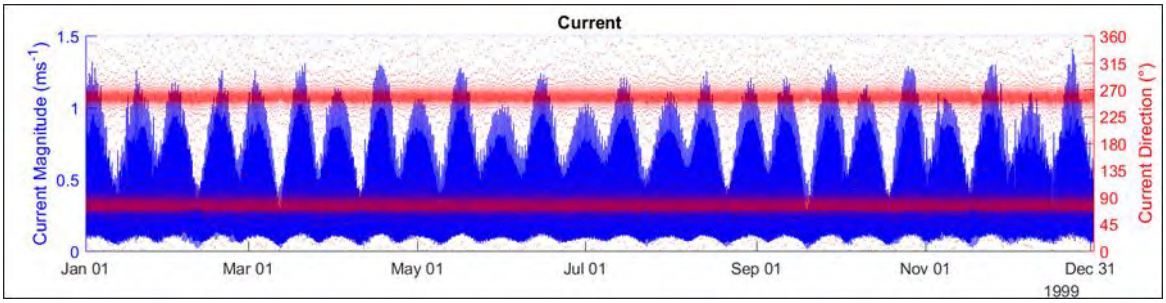

Figure 36 - Time series showing depth averaged current magnitude and current direction derived from the HD model at model point 5

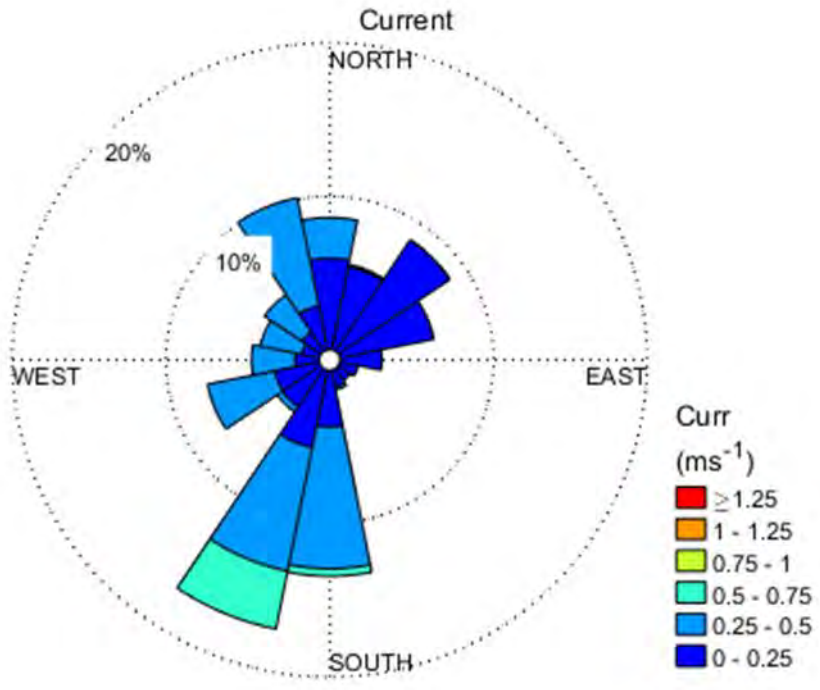

Figure 37 - Rose diagram displaying current magnitude vs direction derived from the HD model ('AIMS') at model point 1

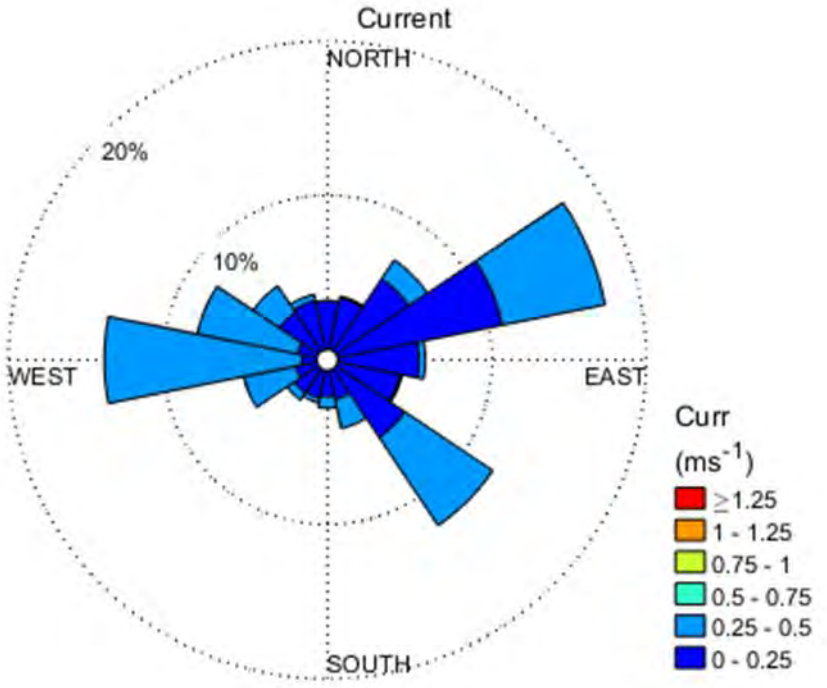

Figure 38 - Rose diagram displaying current magnitude vs direction derived from the HD model (AIMS) at model point 2

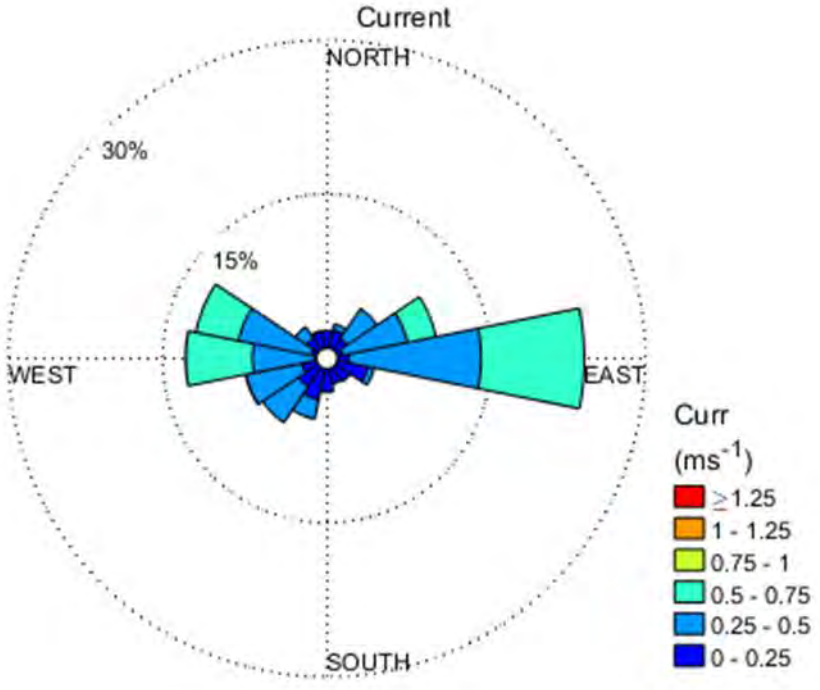

Figure 39 - Rose diagram displaying current magnitude vs direction derived from the HD model (AIMS) at model point 3

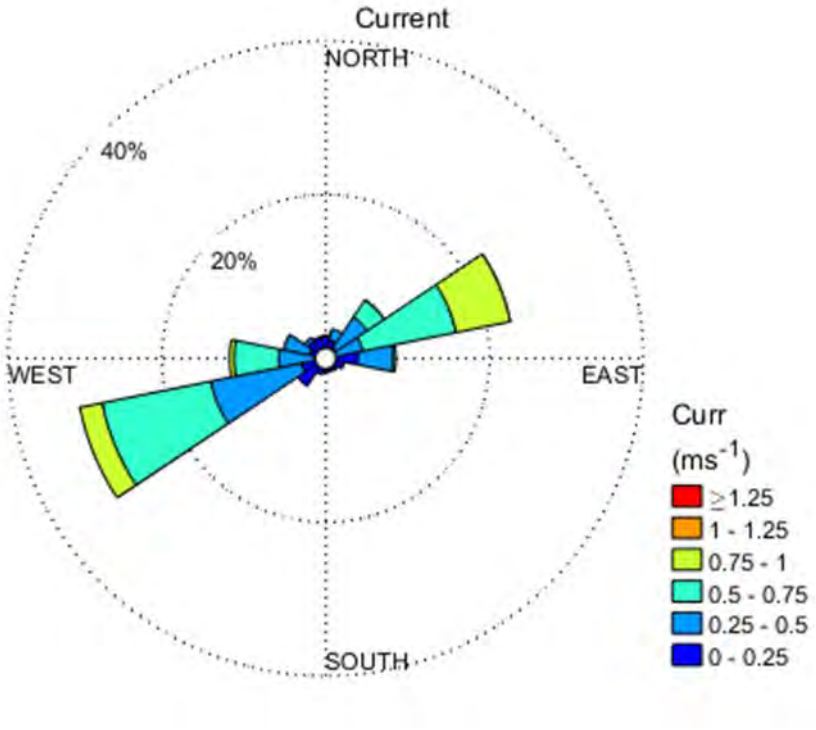

Figure 40 - Rose diagram displaying current magnitude vs direction derived from the HD model (AIMS) at model point 4

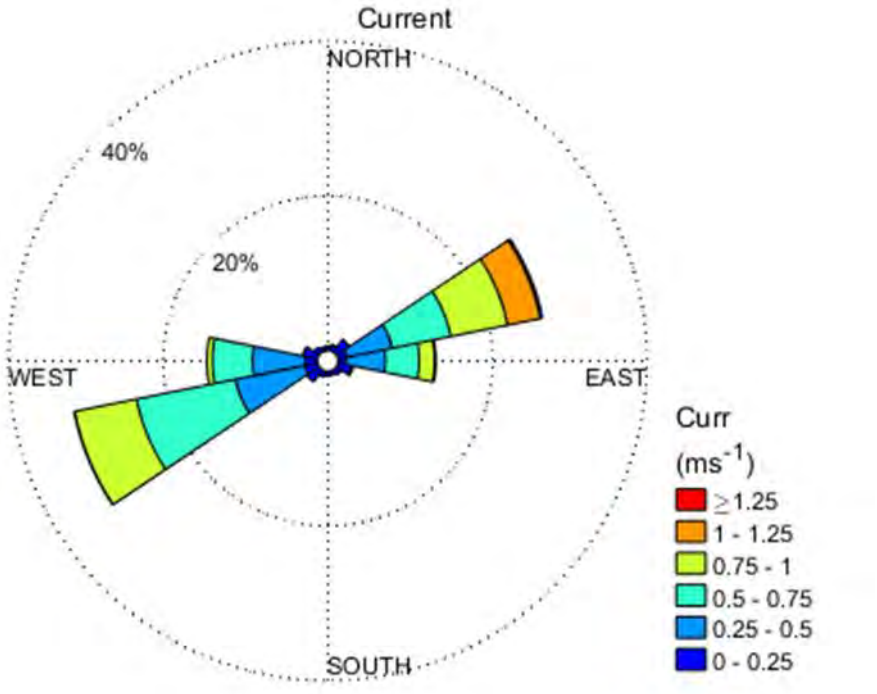

Figure 41 - Rose diagram displaying current magnitude vs direction derived from the HD model (AIMS) at model point 5

3.2.1.5. Tidal asymmetry is assessed via analysis of the magnitude and duration of an ebbing and flooding tide, during spring and neap tidal phases. The key statistics related to the 10 weakest neap tides and 10 strongest spring tides at model point inspection 3, 4 and 5 are presented in Table 4, Table 5 and Table 6, respectively.

Table 4 - Durations and magnitudes of depth averaged current for the 10 weakest Neap and 10 strongest Spring tides, at model point 3

Metric	Tide Number (ranked)									
	1	2	3	4	5	6	7	8	9	10
Strongest Spring Tides										
Spring flood duration (hrs)	06:10	06:00	06:00	06:10	05:50	06:00	06:00	06:00	06:00	06:00
Spring total duration (hrs)	12:40	12:30	12:40	12:50	12:10	12:20	12:30	12:20	12:30	13:10
Spring peak ebb u (ms^{-1})	-0.77	-0.77	-0.78	-0.78	-0.78	-0.78	-0.79	-0.79	-0.79	-0.79
Spring peak flood u (ms^{-1})	0.67	0.6	0.67	0.67	0.67	0.66	0.66	0.66	0.66	0.62
Weakest Neap tides										
Neap flood duration (hrs)	06:10	06:30	06:10	06:10	06:20	06:10	06:20	06:00	07:00	06:10
Neap total duration (hrs)	12:40	12:40	12:40	12:50	13:20	13:30	12:50	13:20	13:50	12:40
Neap peak ebb u (ms^{-1})	-0.27	-0.26	-0.28	-0.28	-0.29	-0.29	-0.29	-0.3	-0.27	-0.3
Neap peak flood u (ms^{-1})	0.26	0.28	0.28	0.25	0.28	0.28	0.3	0.29	0.3	0.25

Table 5 - Durations and magnitude of depth averaged currents for the 10 weakest Neap and 10 strongest Spring tides, at model point 4

Metric	Tide Number (ranked)									
	1	2	3	4	5	6	7	8	9	10
Strongest Spring Tides										
Spring flood duration (hrs)	06:10	06:00	06:00	05:50	05:50	06:20	06:40	06:00	06:20	06:20
Spring total duration (hrs)	12:40	12:50	12:30	12:30	12:40	12:30	12:10	12:20	12:50	12:30
Spring peak ebb u (ms^{-1})	-0.78	-0.82	-0.81	-0.84	-0.85	-0.76	-0.61	-0.77	-0.8	-0.71
Spring peak flood u (ms^{-1})	1.03	1.03	1.03	1.03	1.03	1.04	1.04	1.04	1.05	1.07
Weakest Neap tides										
Neap flood duration (hrs)	05:40	06:00	05:50	06:40	05:50	05:40	05:50	06:00	06:10	06:10
Neap total duration (hrs)	12:40	13:30	13:00	12:50	12:50	13:00	13:10	13:20	12:30	12:50
Neap peak ebb u (ms^{-1})	-0.28	-0.29	-0.3	-0.23	-0.3	-0.31	-0.31	-0.28	-0.25	-0.27
Neap peak flood u (ms^{-1})	0.25	0.29	0.29	0.3	0.27	0.31	0.3	0.31	0.31	0.31

Table 6 - Durations and magnitudes of depth averaged currents for the 10 weakest Neap and 10 strongest Spring tides, at model point 5

Metric	Tide Number (ranked)									
	1	2	3	4	5	6	7	8	9	10
Strongest Spring Tides										
Spring flood duration (hrs)	06:00	06:20	06:10	06:10	06:20	06:10	06:20	06:30	06:50	06:50
Spring total duration (hrs)	12:40	12:30	12:40	12:30	12:20	12:40	12:40	12:50	12:30	12:50
Spring peak ebb u (ms^{-1})	-1	-0.92	-0.98	-0.96	-0.81	-0.98	-0.97	-0.92	-0.84	-0.91
Spring peak flood u (ms^{-1})	1.37	1.37	1.37	1.38	1.38	1.38	1.39	1.4	1.41	1.45
Weakest Neap tides										
Neap flood duration (hrs)	05:30	06:10	06:00	06:30	05:40	06:10	06:00	05:40	06:10	06:00
Neap total duration (hrs)	12:30	13:20	13:20	12:30	12:40	12:40	12:50	12:50	13:10	13:10
Neap peak ebb u (ms^{-1})	-0.31	-0.32	-0.33	-0.26	-0.33	-0.28	-0.33	-0.34	-0.34	-0.34
Neap peak flood u (ms^{-1})	0.25	0.33	0.33	0.33	0.32	0.33	0.29	0.33	0.32	0.33

Waves

3.2.1.6. For each model inspection point, wave roses showing the significant wave height ($H_m{}^0$) (defined as the mean wave height, trough to crest, of the highest third of the waves observed) vs direction are presented in Figure 42 to Figure 46. In addition, wave roses showing the zero up-crossing wave period (T_z) (defined as the time interval between two successive up-crossings of the mean water level) vs direction are presented in Figure 47 and Figure 51.

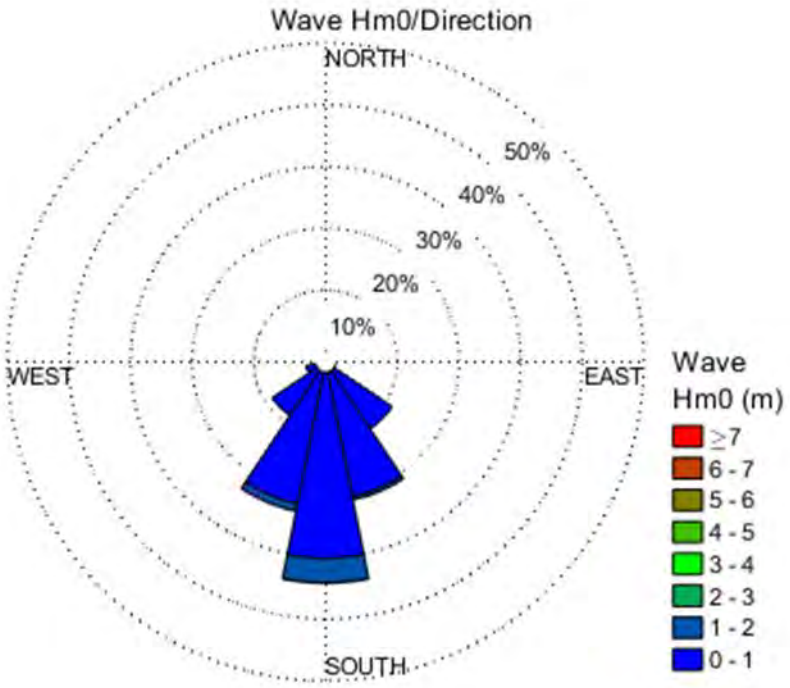

Figure 42 - Wave rose showing significant wave height (H_{m0}) and the associated direction at model point 1

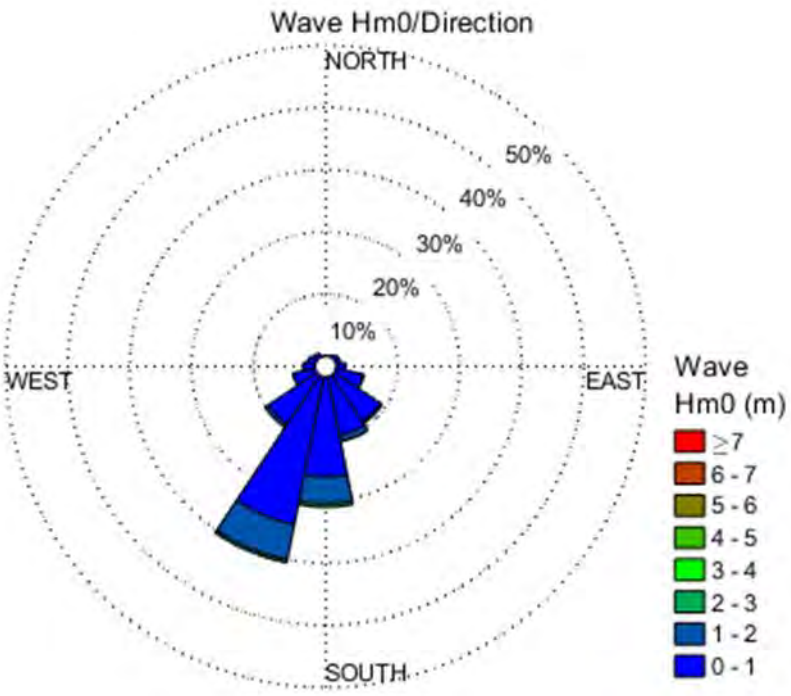

Figure 43 - Wave rose showing significant wave height (H_{m0}) and the associated direction at model point 2

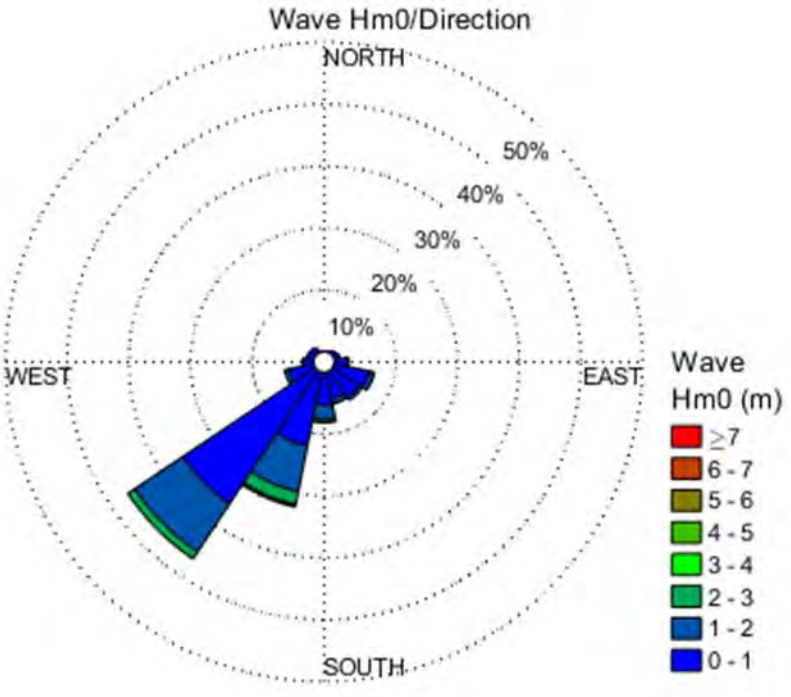

Figure 44 - Wave rose showing significant wave height (H_{m0}) and the associated direction at model point 3

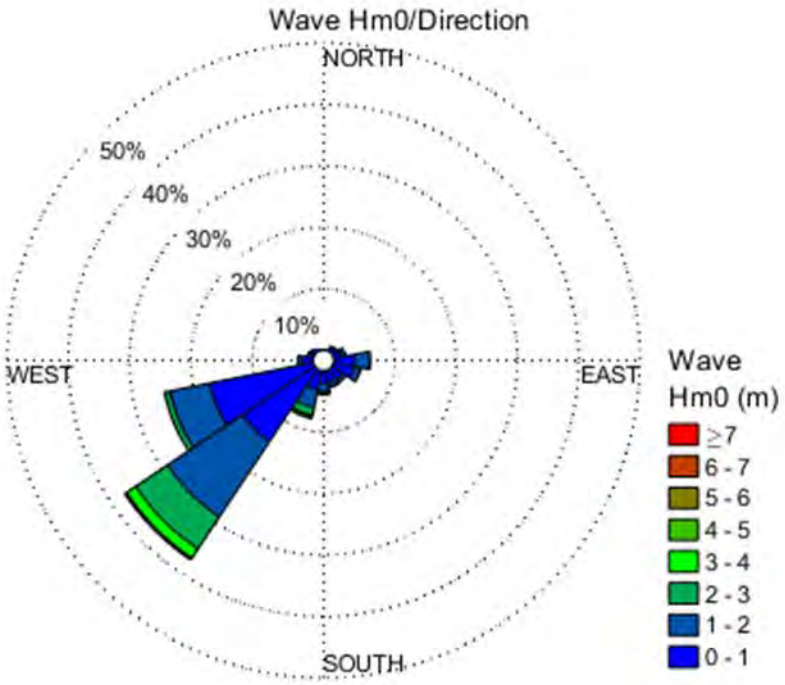

Figure 45 - Wave rose showing significant wave height (H_{m0}) and the associated direction at model point 4

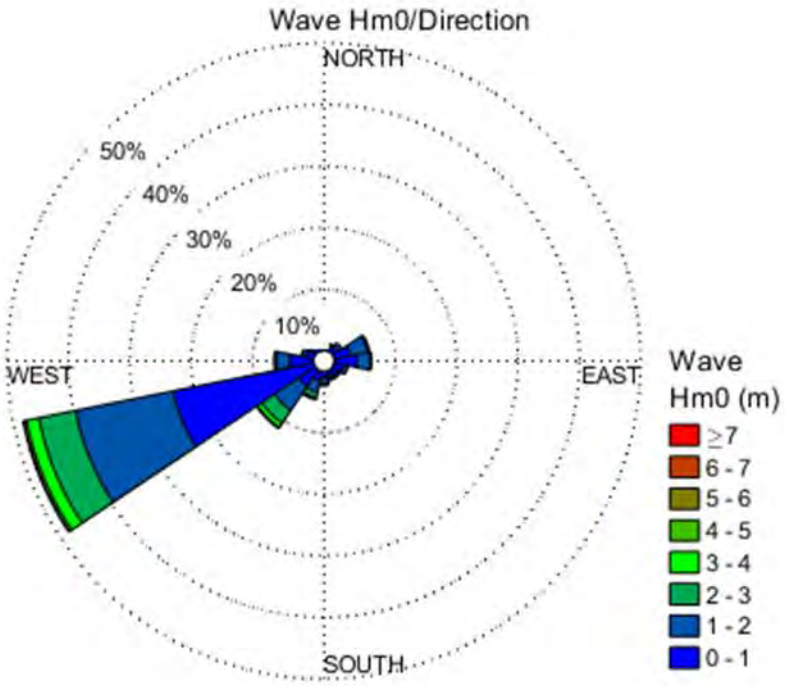

Figure 46 - Wave rose showing significant wave height (H_{m0}) and the associated direction at model point 5

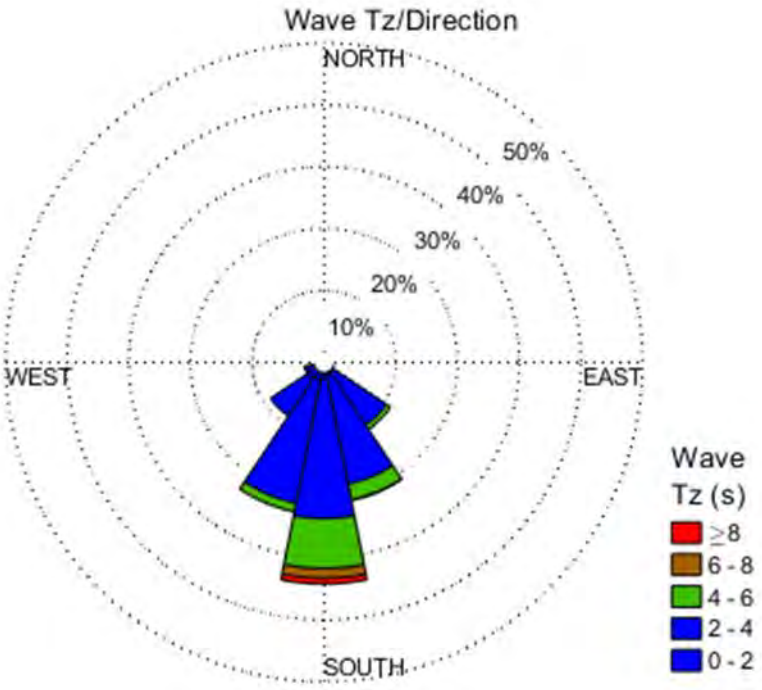

Figure 47 - Wave rose showing zero up-crossing wave period (T_z) and the associated direction at model point 1

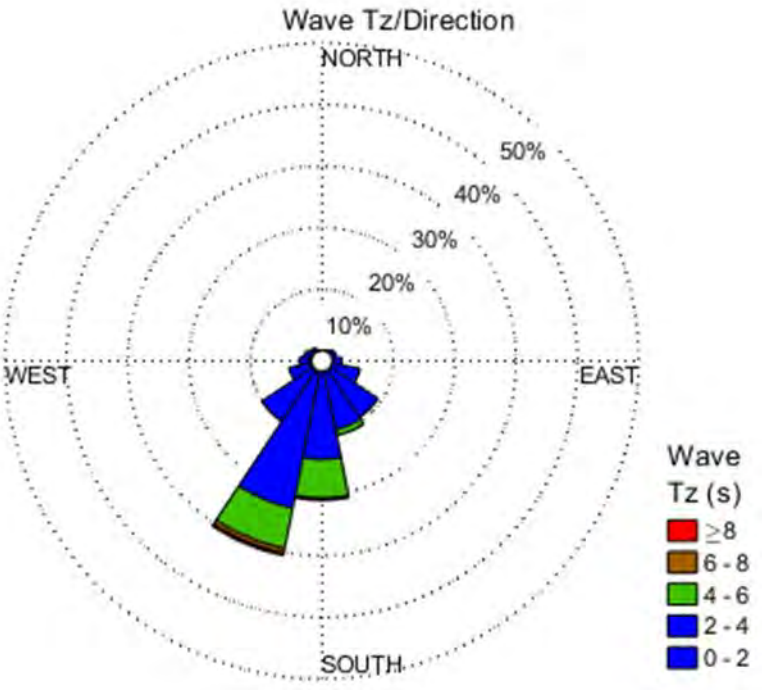

Figure 48 - Wave rose showing zero up-coming wave period (T_z) and the associated direction at model point 2

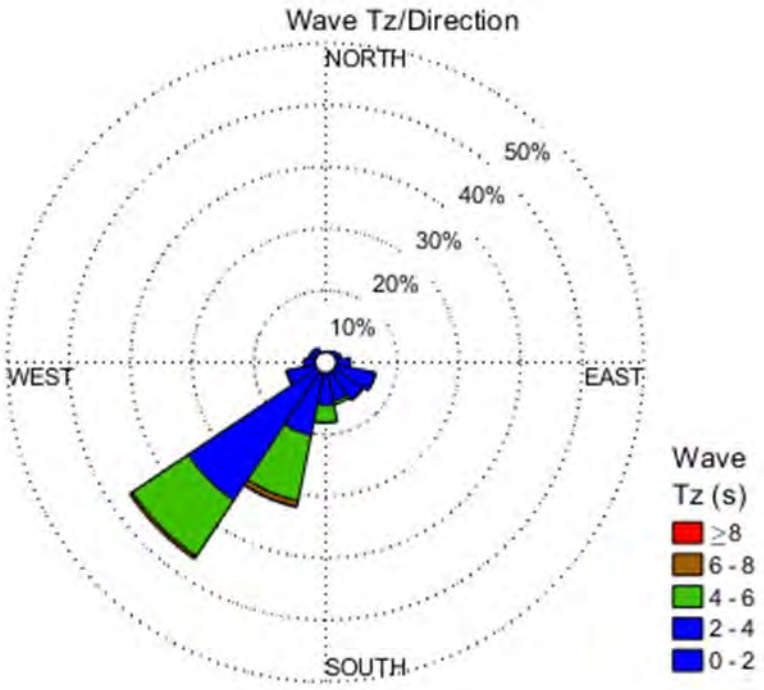

Figure 49 - Wave rose showing zero up-coming waver period (T_z) and the associated direction at model point 3

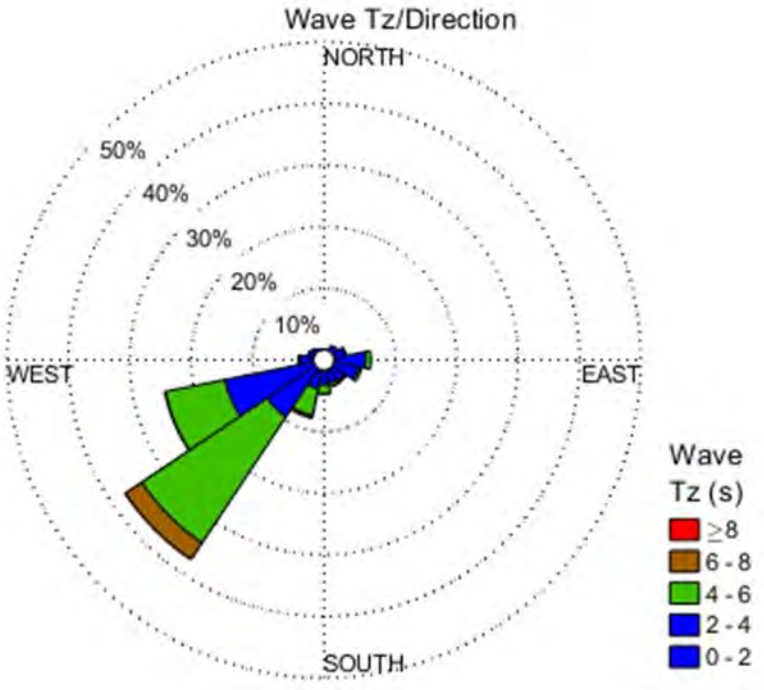

Figure 50 - Wave rose showing zero up-coming wave period (T_z) and the associated direction at model point 4

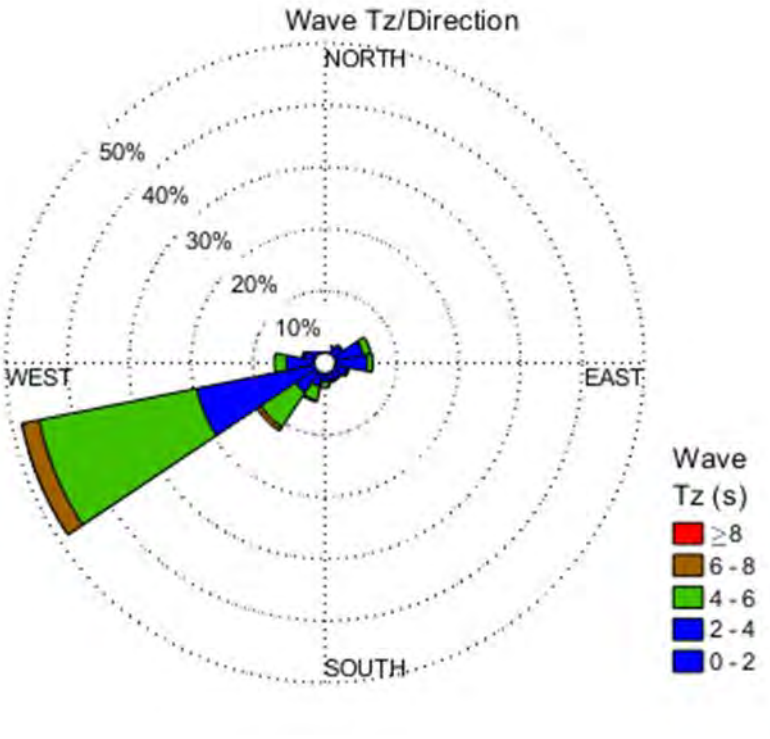

Figure 51 - Wave rose showing zero up-coming wave period (T_z) and the associated direction at model point 5

3.2.1.7. A 12-month record (from the year 1998) of predicted significant wave heights ($H_m{}^0$) at each model inspection point is presented in the form of time series (Figure 52 to Figure 56).

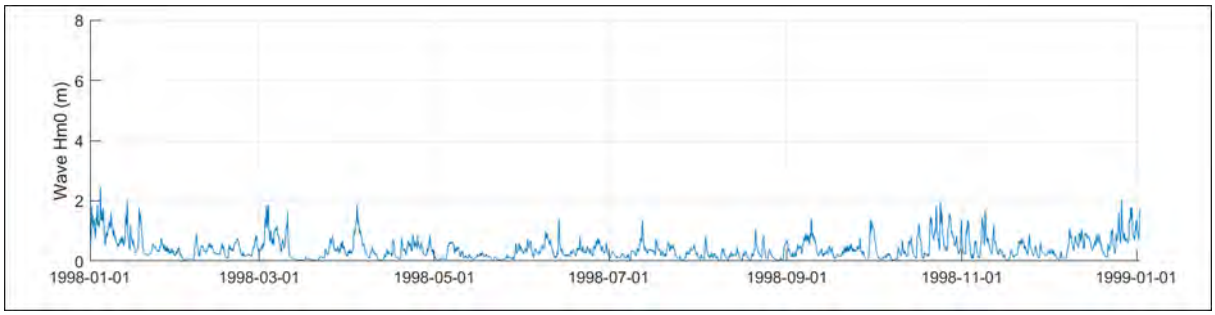

Figure 52 - Time series of significant wave height ($H_m{}^0$) derived from the AIMS coupled SWAN and HD model, at model point 1

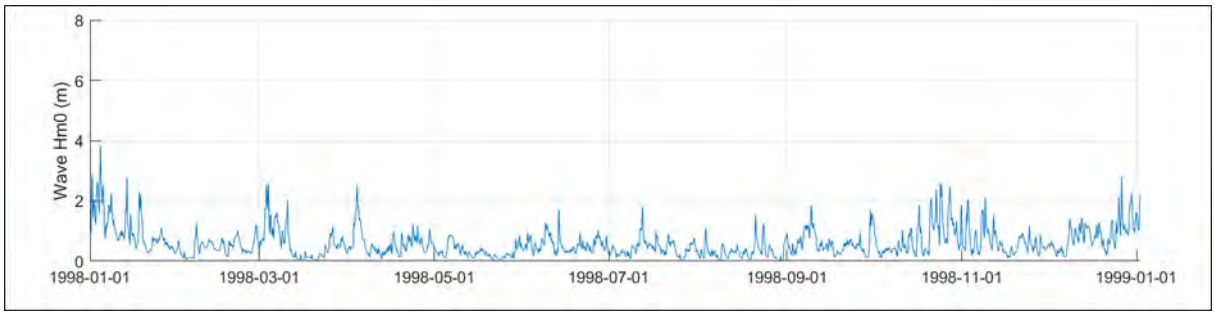

Figure 53 - Time series of significant wave height ($H_m{}^0$) derived from the AIMS coupled SWAN and HD model, at model point 2

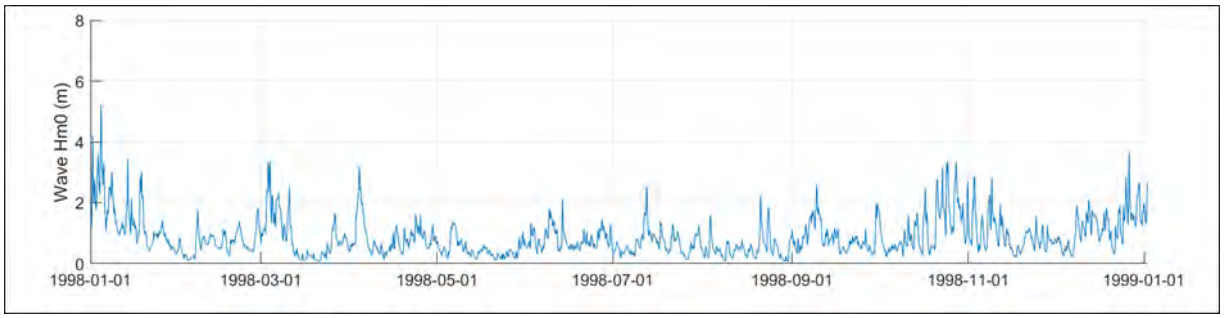

Figure 54 - Time series of significant wave height ($H_m{}^0$) derived from the AIMS coupled SWAN and HD model, at model point 3

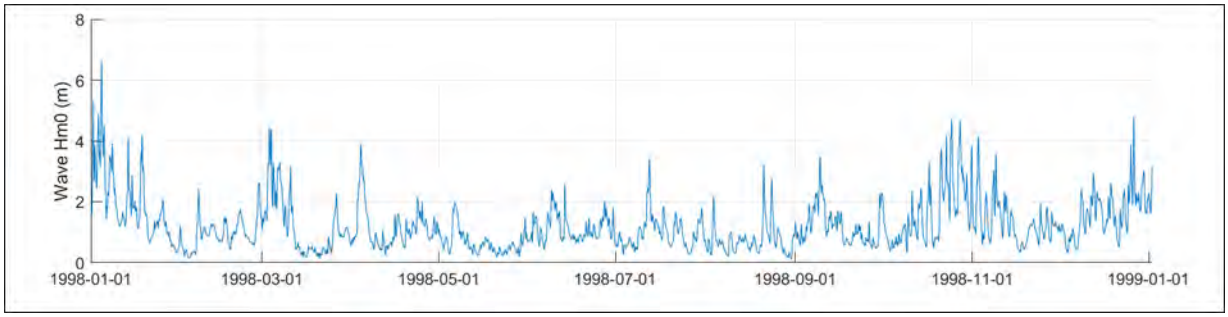

Figure 55 - Time series of significant wave height ($H_m{}^0$) derived from the AIMS coupled SWAN and HD model, at model point 4

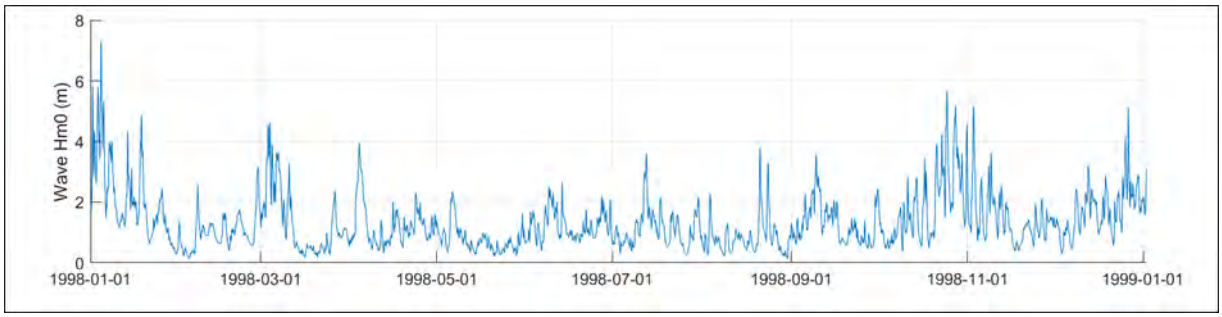

Figure 56 - Time series of significant wave height ($H_m{}^0$) derived from the AIMS coupled SWAN and HD model, at model point 5

3.2.1.8. A more accurate assessment of the frequency – magnitude of the wave climate along the Proposed Development is accessible via Figure 57 to Figure 61 which present joint probability distributions with respect to significant wave height (H_{m^0}) and wave approach (compass quadrants), and significant wave height and wave period (T_z) for each model inspection point.

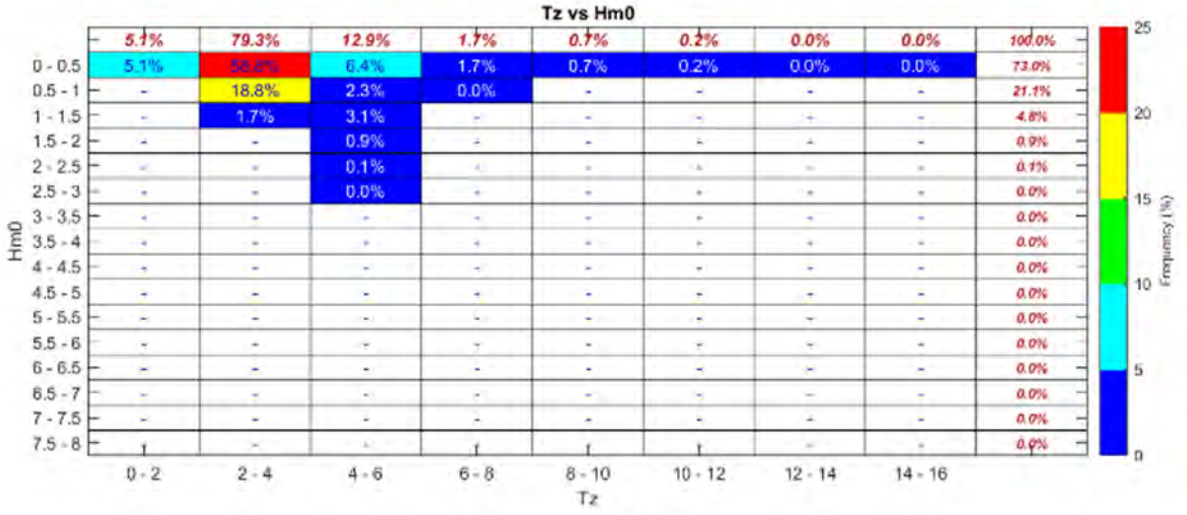

Figure 57 - Joint probability distribution of significant wave heights (H_{m0}) and wave period (T_z) derived from the AIMS coupled SWAN and HD model at model point 1

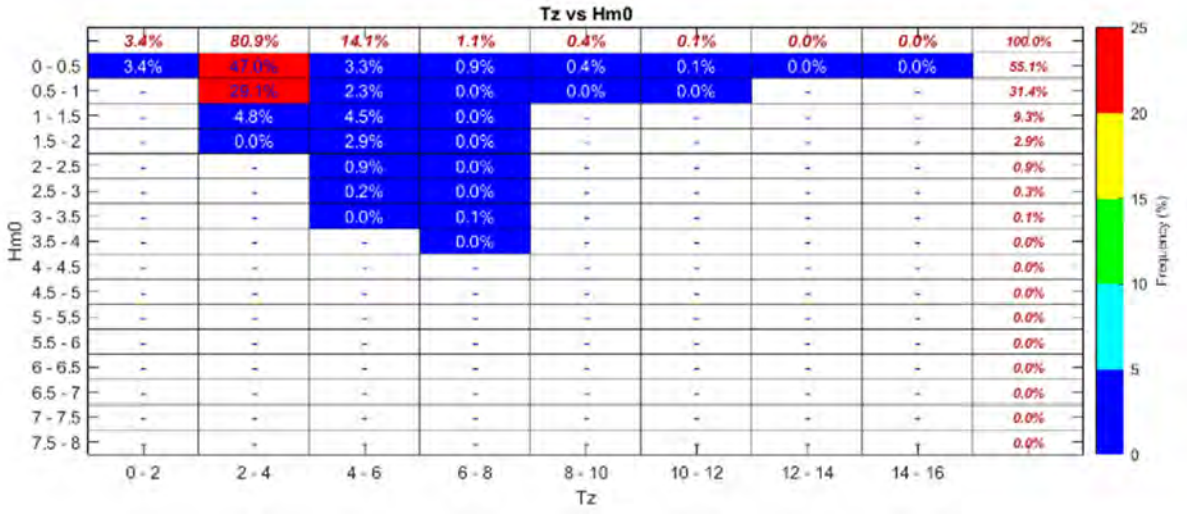

Figure 58 - Joint probability distribution of significant wave heights (H_{m0}) and wave period (T_z) derived from the AIMS coupled SWAN and HD model at model point 2

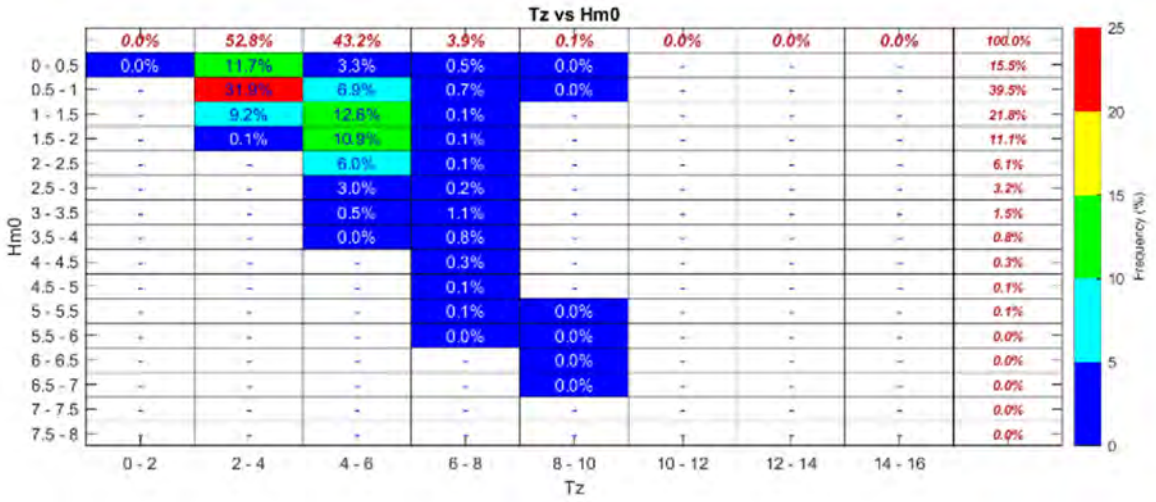

Figure 59 - Joint probability distribution of significant wave heights (H_{m0}) and wave period (T_z) derived from the AIMS coupled SWAN and HD model at model point 3

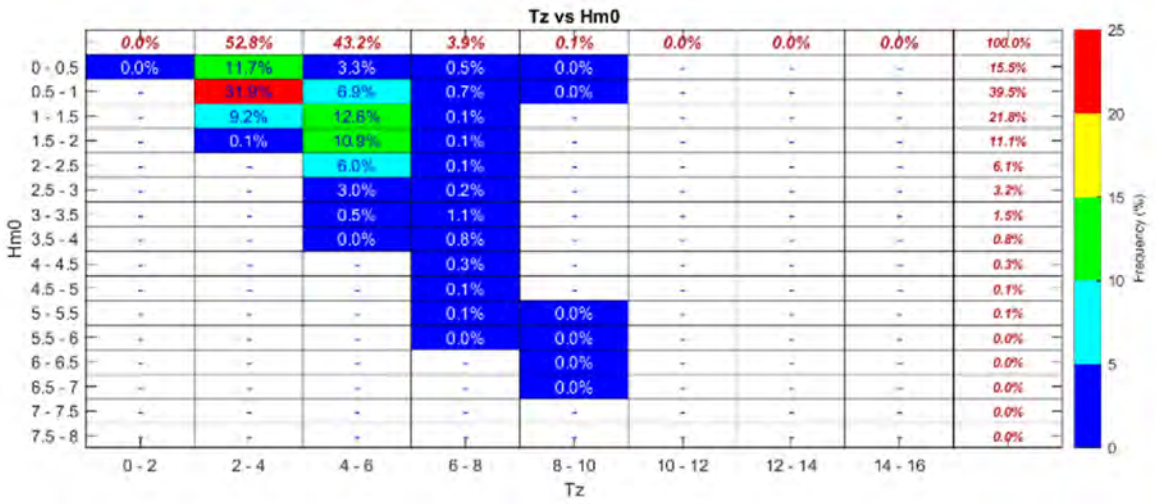

Figure 60 - Joint probability distribution of significant wave heights (H_{m0}) and wave period (T_z) derived from the AIMS coupled SWAN and HD model at model point 4

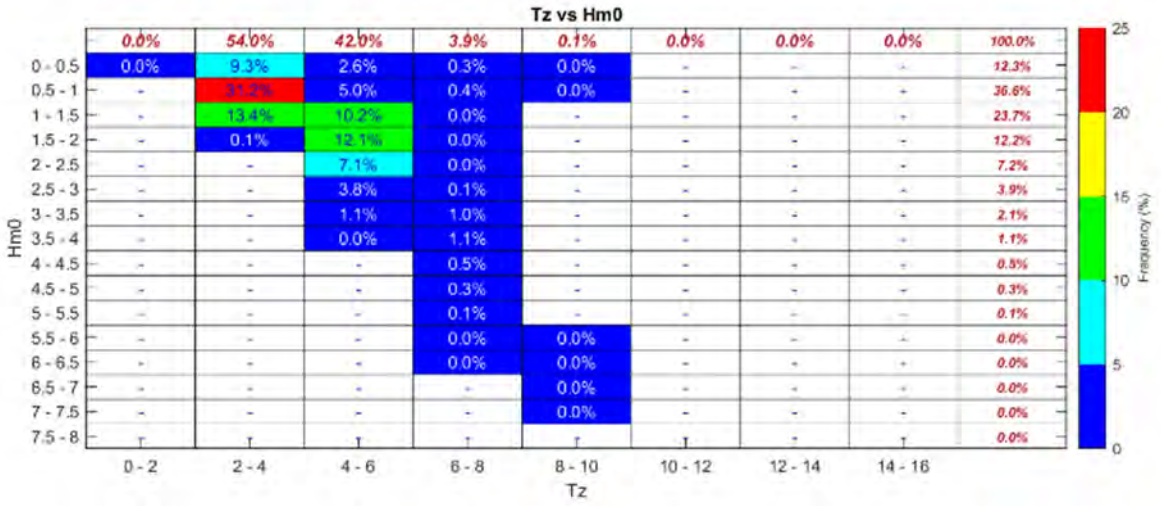

Figure 61 - Joint probability distribution of significant wave heights (H_{m0}) and wave period (T_z) derived from the AIMS coupled SWAN and HD model at model point 5

Sediment Mobility

3.2.1.9. To determine the shear stress acting on the bed due to tidal flows, the mean depth velocity was converted to the velocity 1 m above the bed (u_{100}) using the 1/7th power law velocity profile. The bed shear stress acting on the bed is then derived using the standard quadratic friction law based on an estimated friction coefficient (C_D, C_{100}) following the method of Soulsby (1997). This representation allows for a simple and direct appreciation of the mobility of these grain sizes by tidal currents alone. These analyses are summarised for each model inspection point in Figure 62 to Figure 65.

Model inspection point 1

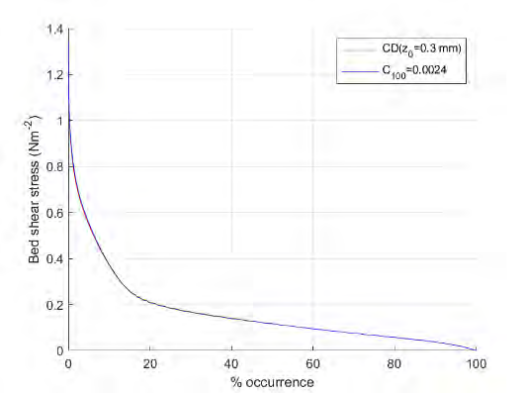

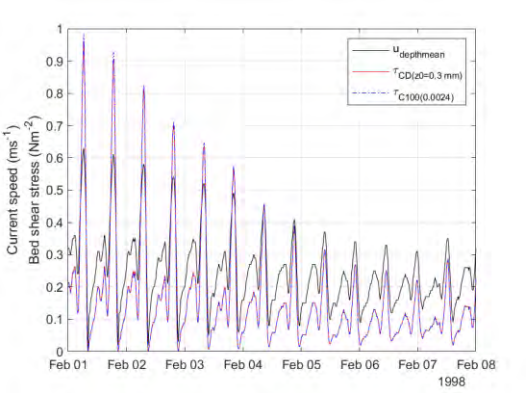

Model inspection point 2

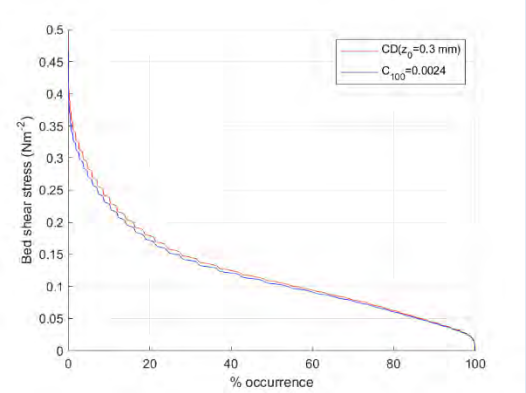

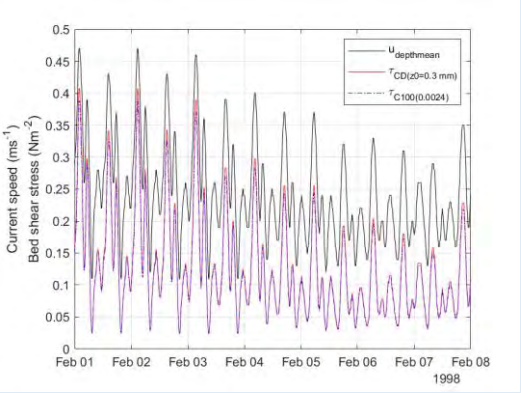

Model inspection point 3

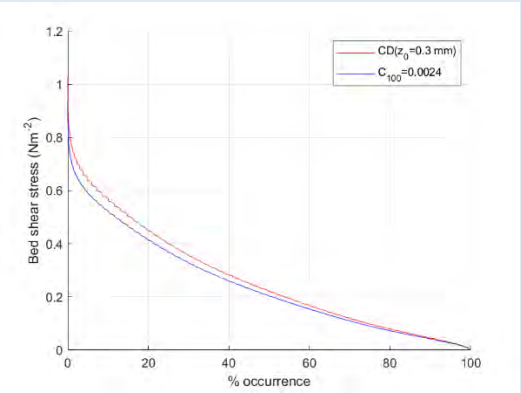

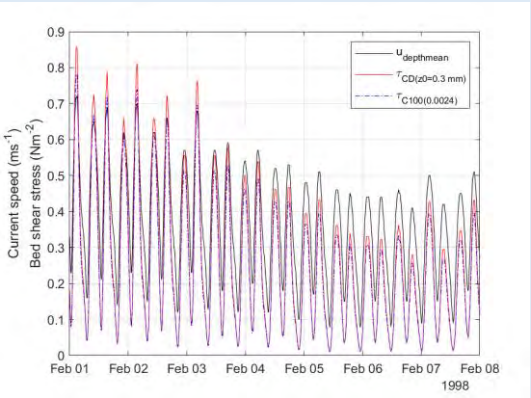

Model inspection point 4

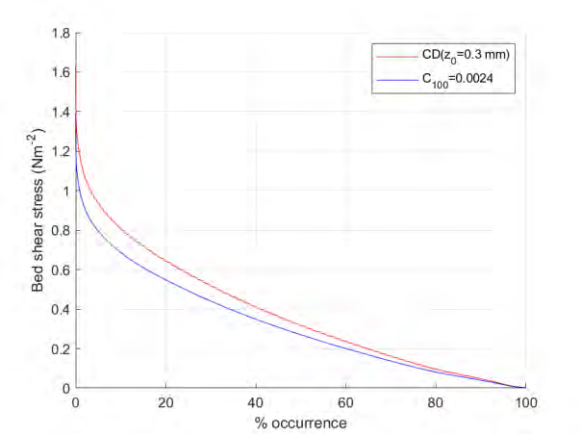

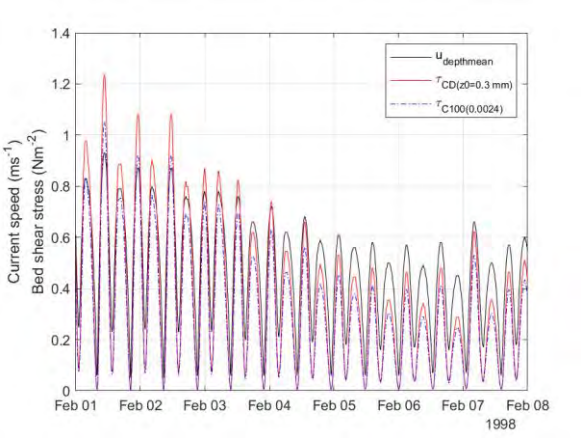

Model inspection point 5

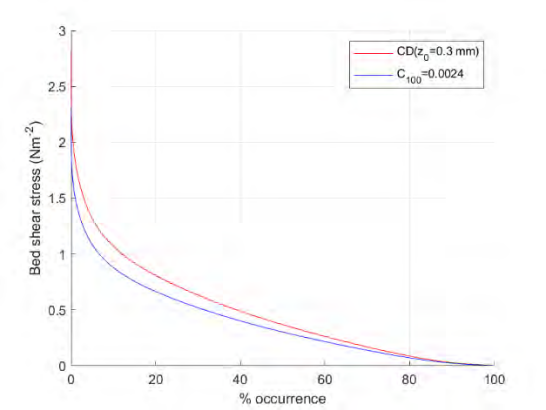

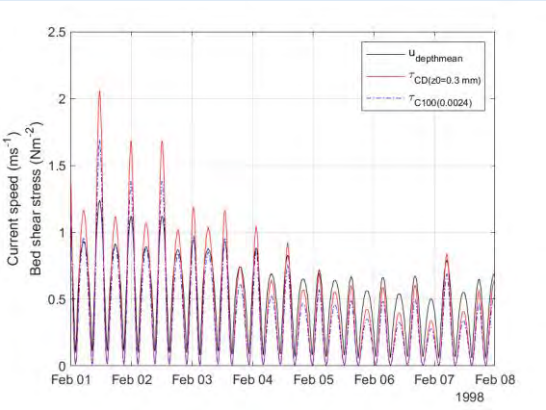

Figure 62 - Tidally induced bed shear stress acting on the seabed at each model point location (left panel) and overlaid a time series of current velocities observed during a typical spring – neap cycle. Total stress is derived from two drag or friction coefficients (C_D,C_{100}) presented by Soulsby (1997). The critical threshold for motion (i.e. the point of incipient motion) of sediments (based on the median grain size) of size fraction 'coarse sand and gravel' is plotted. Please note that in this instance as the threshold is not exceeded this does not appear on either plot.

Model inspection point 1

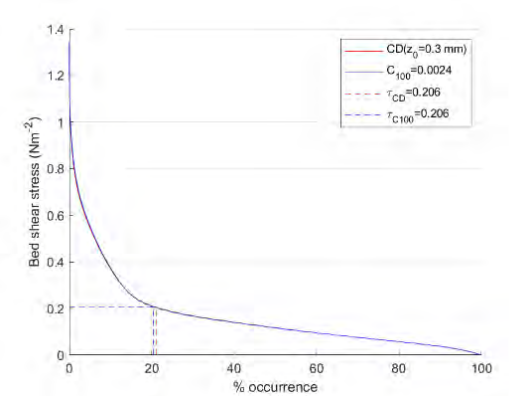

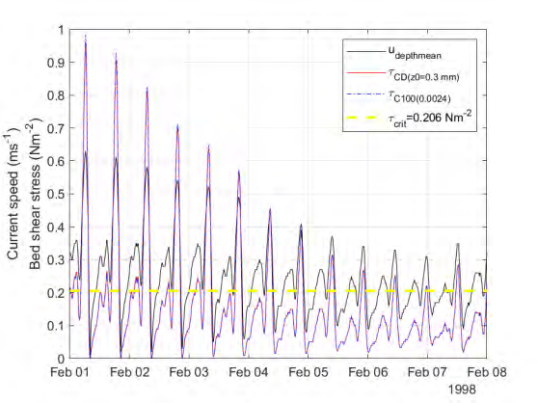

Model inspection point 2

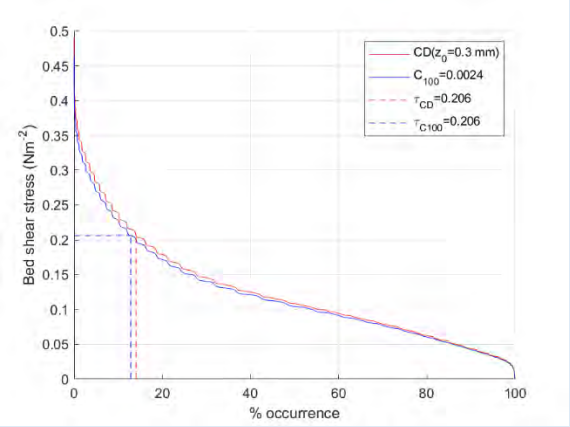

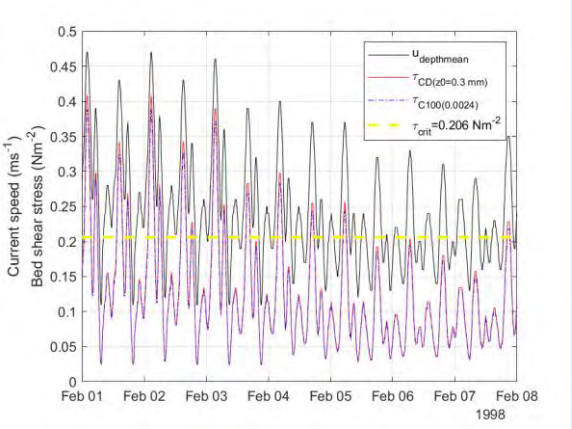

Model inspection point 3

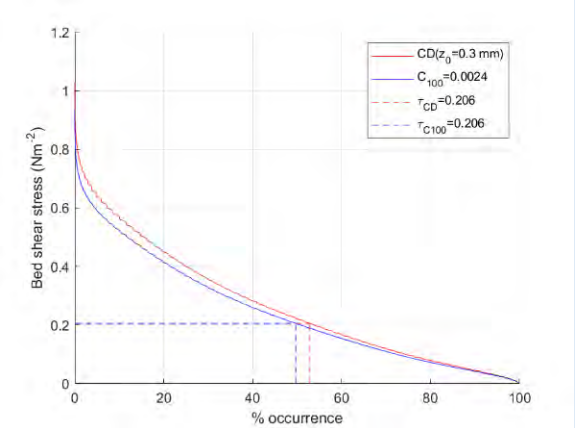

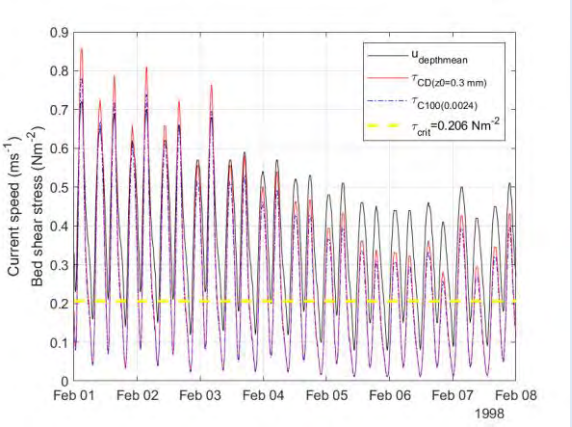

Model inspection point 4

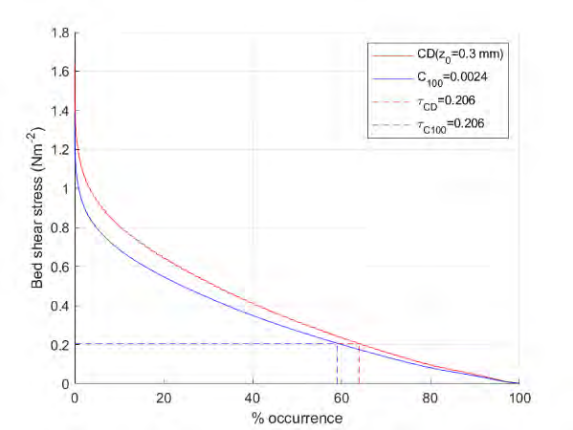

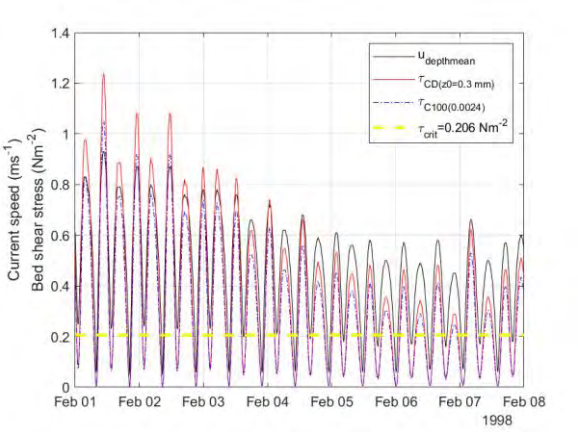

Model inspection point 5

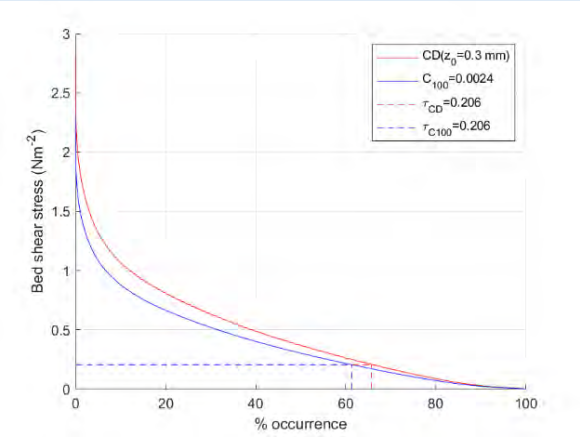

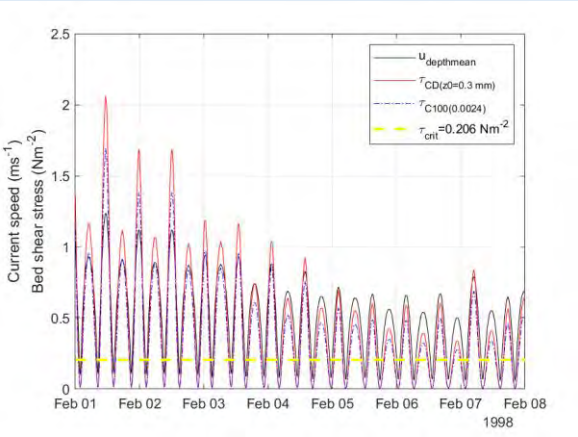

Figure 63 - Tidally induced bed shear stress acting on the seabed at each model point location (left panel) and overlaid a time series of current velocities observed during a typical spring – neap cycle Total stress is derived from two drag or friction coefficients (C_D,C_{100}) presented by Soulsby (1997). The critical threshold for motion (i.e. the point of incipient motion) of sediments (based on the median grain size) of size fraction 'medium sand' is plotted.

Model inspection point 1

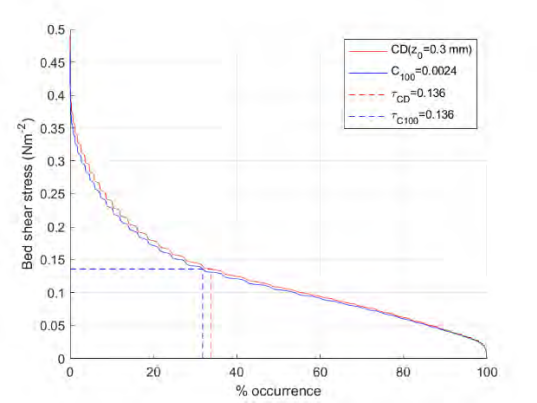

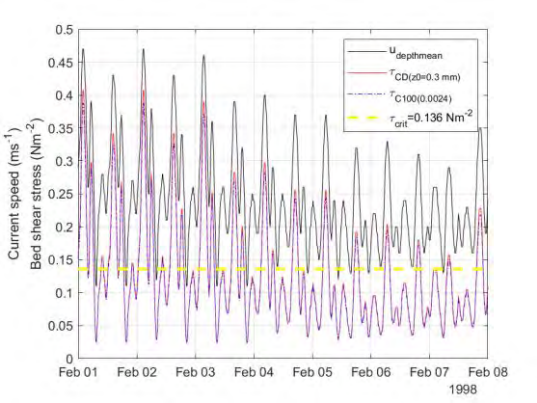

Model inspection point 2

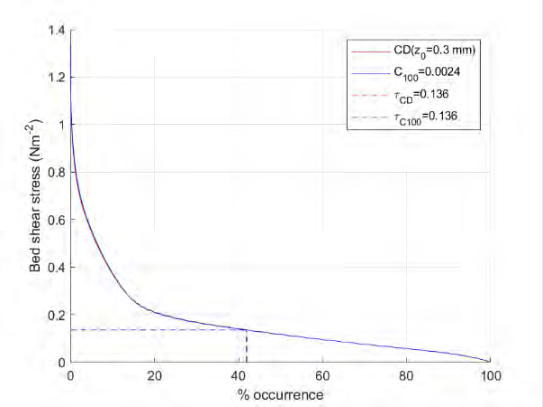

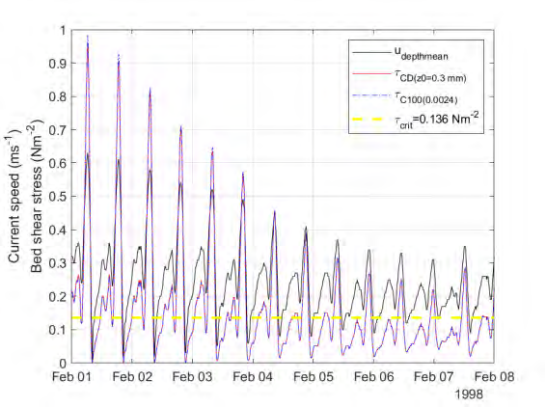

Model inspection point 3

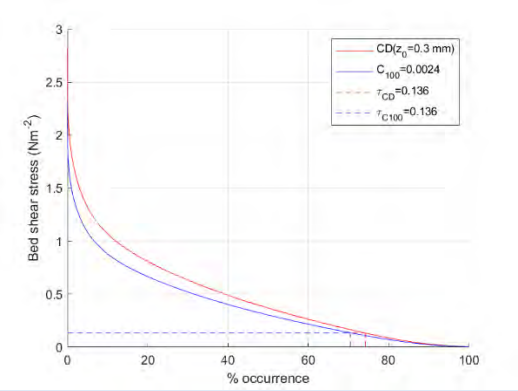

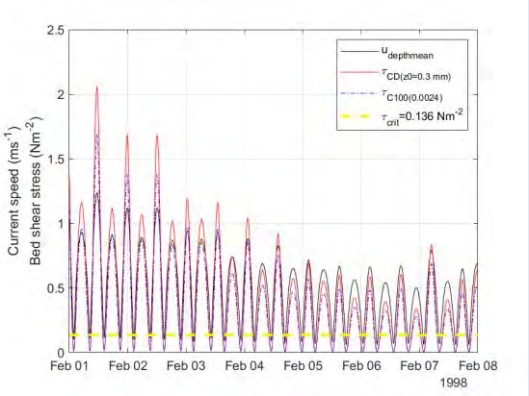

Model inspection point 4

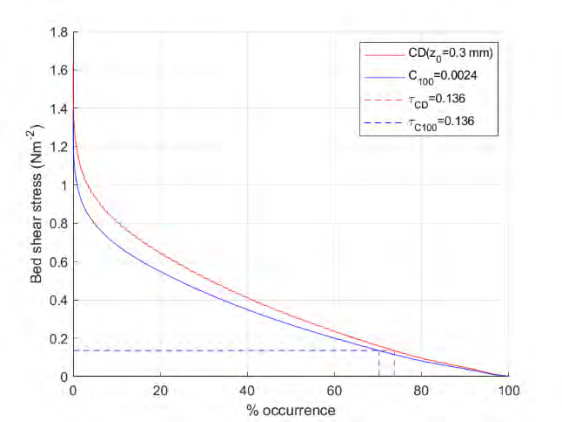

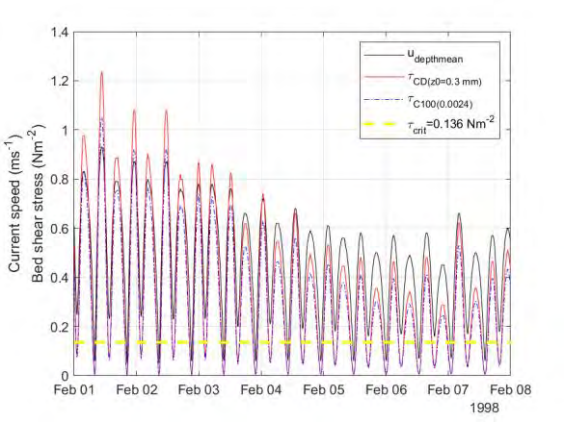

Model inspection point 5

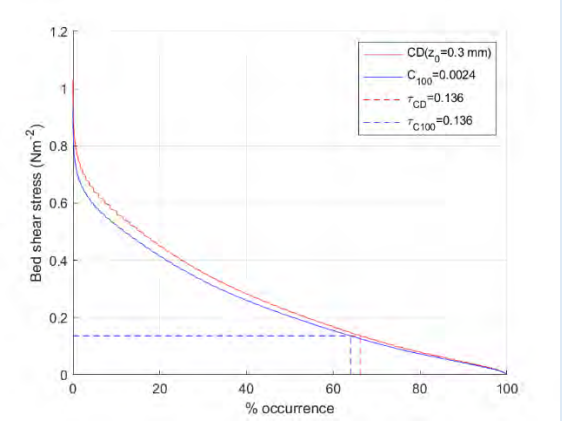

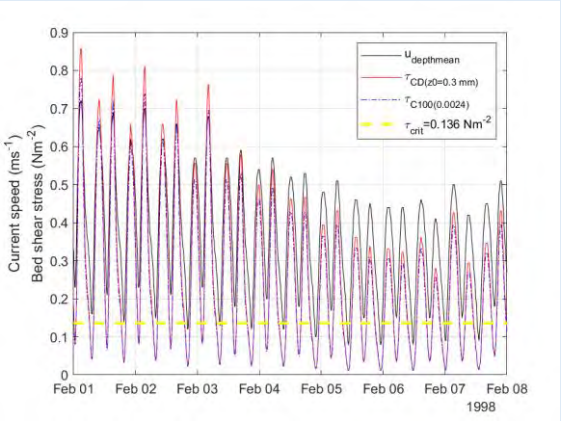

Figure 64 - Tidally induced bed shear stress acting on the seabed at each model point location (left panel) and overlaid a time series of current velocities observed during a typical spring – neap cycle Total stress is derived from two drag or friction coefficients (C_D,C_{100}) presented by Soulsby (1997). The critical threshold for motion (i.e. the point of incipient motion) of sediments (based on the median grain size) of size fraction 'coarse silt and fine sand' is plotted.

Model inspection point 1

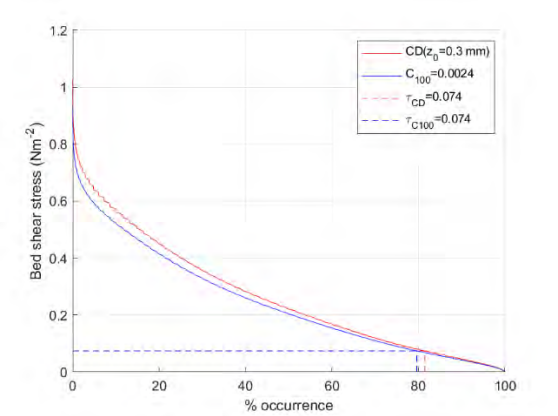

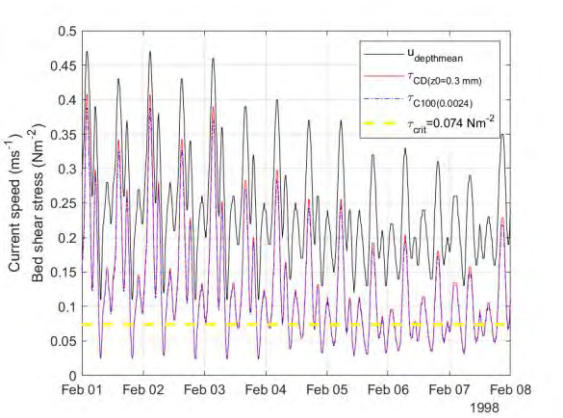

Model inspection point 2

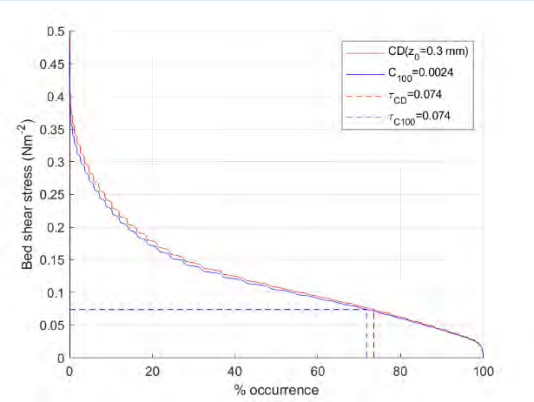

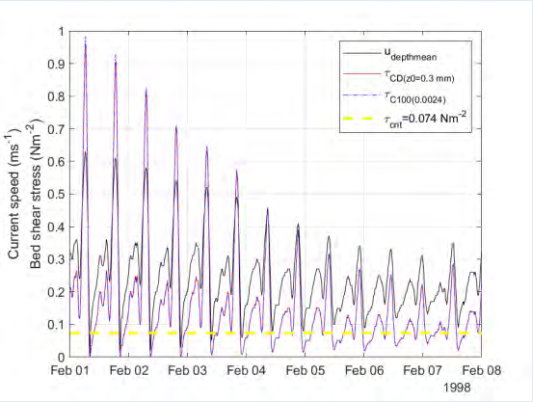

Model inspection point 3

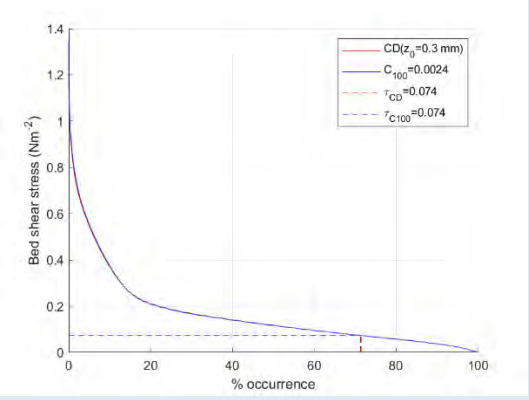

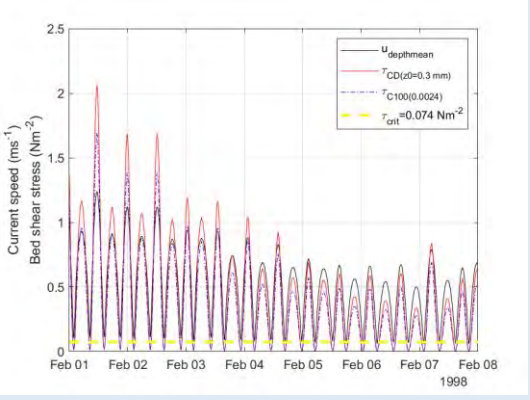

Model inspection point 4

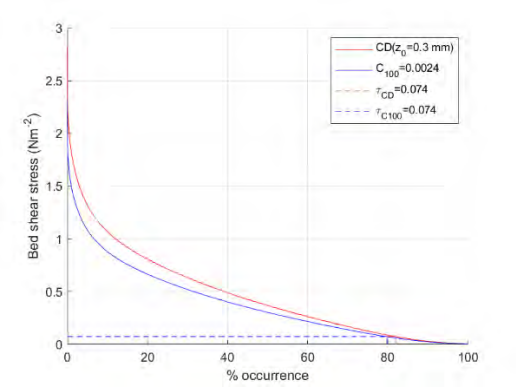

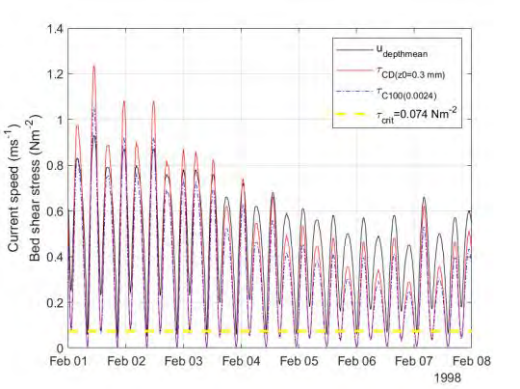

Model inspection point 5

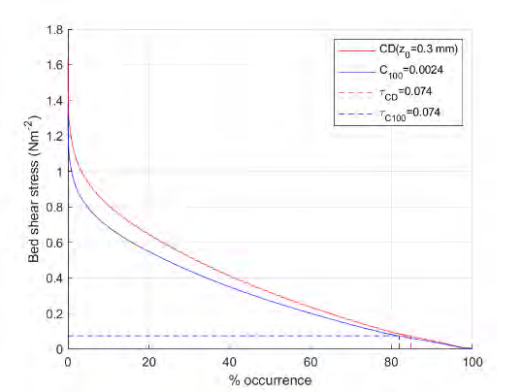

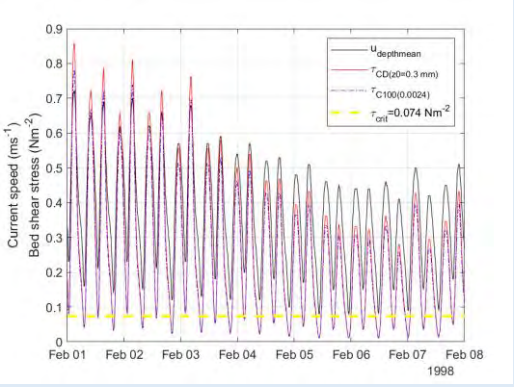

Figure 65 - Tidally induced bed shear stress acting on the seabed at each model point location (left panel) and overlaid a time series of current velocities observed during a typical spring – neap cycle Total stress is derived from two drag or friction coefficients (C_D,C_{100}) presented by Soulsby (1997). The critical threshold for motion (i.e. the point of incipient motion) of sediments (based on the median grain size) of size fraction 'clay and silt' is plotted.

4. PLUME DISPERSION MODELLING

4.1. ENVIRONMENTAL AND ENGINEERING CONSTRAINTS

4.1.1.1. At various locations along the Marine Cable Route, dredging is required for the purposes of large ripple and sandwave clearance and engineering of Horizontal Directional Drilling ('HDD') exit / entry points (depending on whether HDD is undertaken from onshore to offshore, or offshore to onshore). It is intended that sediment arising from dredging operations will be disposed of within the Marine Cable Corridor at a designated marine disposal site, ideally in proximity (if possible) to the dredging works. The Particle Tracking module of MIKE 21 Flow Model was utilised for undertaking plume dispersion modelling to assess the fate of the plumes of suspended sediments created during disposal operations.

4.1.1.2. Prior to undertaking plume dispersion modelling a constraints mapping exercise, designed to identify both engineering and environmental constraints related to disposal of dredge material, was conducted to identify areas along the Marine Cable Corridor considered unsuitable for the disposal of dredge material and in turn, define areas which were considered suitable for disposal. This exercise identified several constraints;

4.1.1.3. The engineering constraints included;

- Disposal will not occur outside the Marine Cable Corridor;
- Disposal will not occur at locations of existing large ripples or sandwaves to ensure that the deposited material does not unintentionally back-fill the dredged area;
- Disposal will not occur at locations where water depth is too shallow for the dredger to operate;
- Disposal will not occur at the HDD exit/entry location or inshore of this point;
- Disposal will not occur in areas within 500 m of in-service cable crossings;
- Disposal will not occur within areas within 100 m of identified potential wrecks, and;
- Post disposal, the deposited thickness of sediment on the seabed is such that it will not significantly impact upon the navigable depth (i.e. the navigable depth will not be reduced by > 5 %).

4.1.1.4. The environmental constraints included;

- Disposal of material will not occur within 3 km from any identified WFD water bodies; and;
- In order to avoid sensitive habitats, disposal will not occur within;
    - 500 m of habitat A5.445 (*Ophiothrix fragilis* and/or *Ophiocomina nigra* brittlestar beds on sublittoral mixed sediment); and

- 100 m of habitat A4.2 (moderate energy circalittoral rock).

4.1.1.5. The results of this exercise designated areas deemed suitable for offshore disposal and therefore this area is to be characterised as a marine disposal site; being between KP 21 and KP 109 in UK waters as shown in Figure 66.

4.2. MODEL SETUP

4.2.1.1. To conduct the assessment of plume dispersion utilising the particle tracking module, the spatial resolution of the hydrodynamic model in the Channel was increased[1] to 500 m (triangular mesh side lengths), allowing:

- Increased spatial resolution of the hydrodynamic processes driving plume advection, particularly in areas of complex flow, such as the Solent, and;
- Increased spatial resolution of the outputs from the plume dispersion scenario, since, in the MIKE software, the outputs are presented on the hydrodynamic grid/mesh.

4.2.1.2. The driving hydrodynamic input for the plume dispersion scenario was derived from a hydrodynamic hindcast conducted for a period of four months (from 1st April 2013 to 1st August 2013), encompassing typical and highest astronomical range, spring and neap tidal cycles.

4.2.1.3. Within the model, the sediment (i.e. each individual particle class) is considered as particles, with inherent hydraulic characteristics (e.g. settling, moving sources and horizontal and vertical dispersion), being advected within the surrounding water body and dispersed as a result of random (turbulent) processes in two dimensions. A corresponding mass is assigned to each particle released within the model. The model was not configured to provide information regarding erosion/transport of sediments on the seabed.

1 As the resolution of the model was increased, the validation of the hydrodynamic model was re-checked to ensure that the performance of the hydrodynamic model was not significantly affected. The results of this exercise showed that the change in spatial resolution did not appreciably affect the performance of the hydrodynamic model.

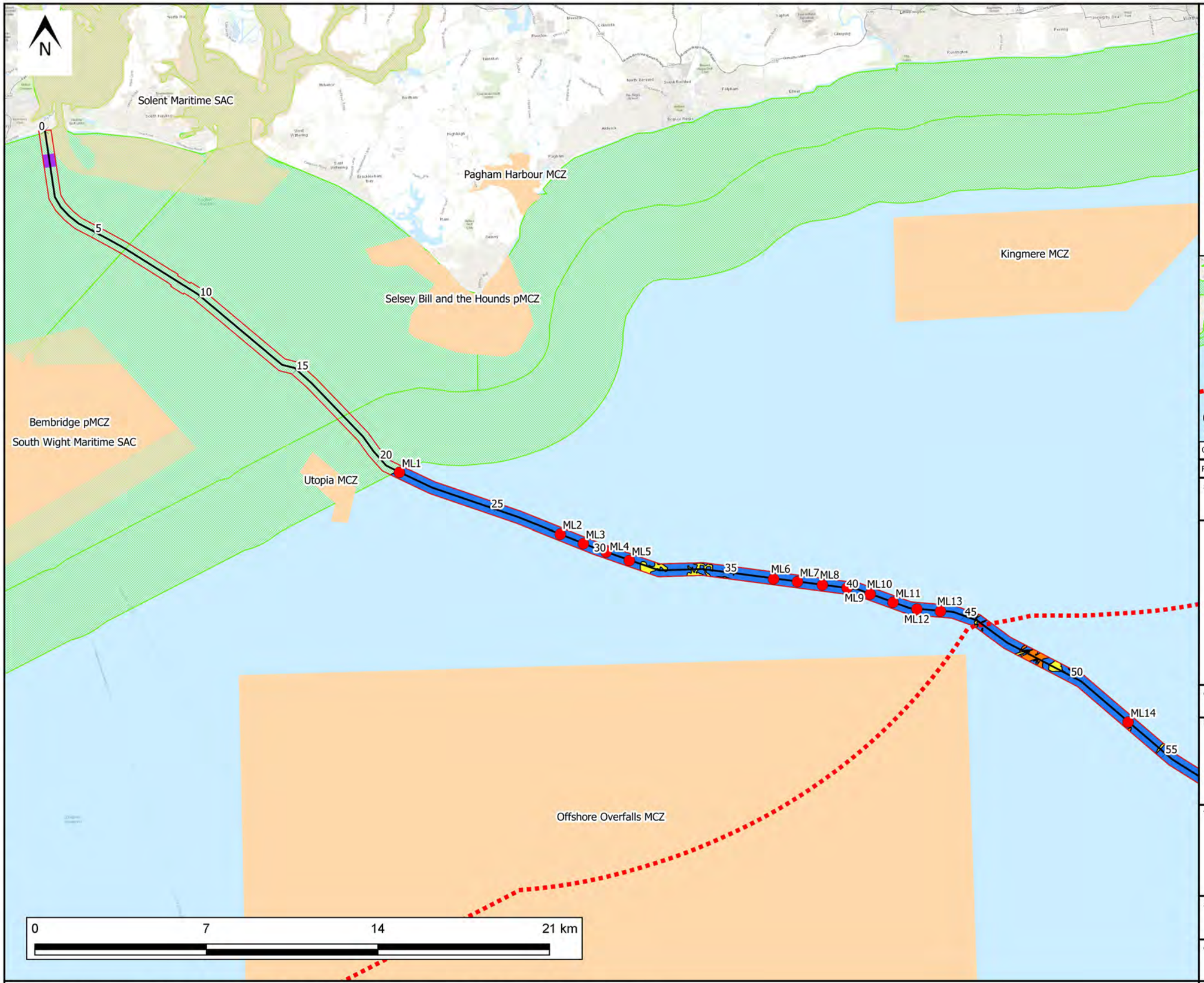

KEY:

- Survey Centre Line
- Marine Cable Corridor
- Exclusive Economic Zone
- UK 12 Nautical Mile Limit
- Proposed Dredge Disposal Area

Constraints

- Designated Sites
- Large Ripples
- Sand Waves
- HDD Entry / Exit Locations
- Cable Crossings 500m Disposal Exclusion Zone
- WFD Water Bodies with 3 km buffer

Modelling Locations

- Potential worst case modelling location for diposal of maximum volume

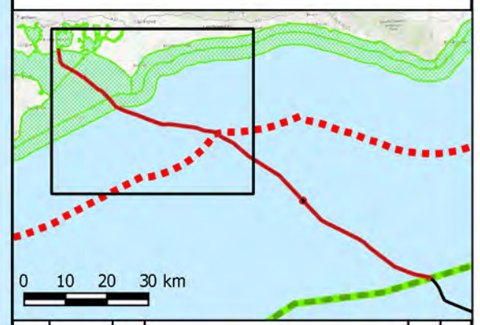

REV	DATE	BY	DESCRIPTION	CHK	APP
0.93	26/04/19	CP	DRAFT		CL

STATUS: FOR INFORMATION ONLY

WSP | Parsons Brinckerhoff, Amber Court, William Armstrong Drive, Newcastle upon Tyne, NE4 7YQ
Tel: +44(0) 191 298 1000
www.wsp-pb.com

CLIENT: AQUIND LTD

PROJECT: UK - FRANCE INTERCONNECTOR

TITLE: FIGURE 66 UK PROPOSED DREDGE DISPOSAL AREA MAP

SCALE @A3:	CHECKED:	APPROVED:
1:150,000		CL
QGIS FILE:	DRAWN: 26/04/19	DATE: 26/04/19

PROJECT No:	DRAWING No:	REV:
62100616		0.93

THE PROPERTY OF THIS DRAWING AND DESIGN IS VESTED IN WSP AND MUST NOT BE COPIED OR REPRODUCED IN ANY WAY WITHOUT THEIR WRITTEN CONSENT
© BRITISH CROWN COPYRIGHT, 2019 ALL RIGHTS RESERVED

Created by: UKCJP003 - 2019-04-26 13:23:28 - \\uk.wspgroup.com\central data\Projects\62100xxx\62100616 - Aquind VO No.3\E Models and Drawings\GIS\QGIS Marine\Drawings\Workspace\Dredge Disposal Constraint Map\Dredge Disposal Locations.qgs

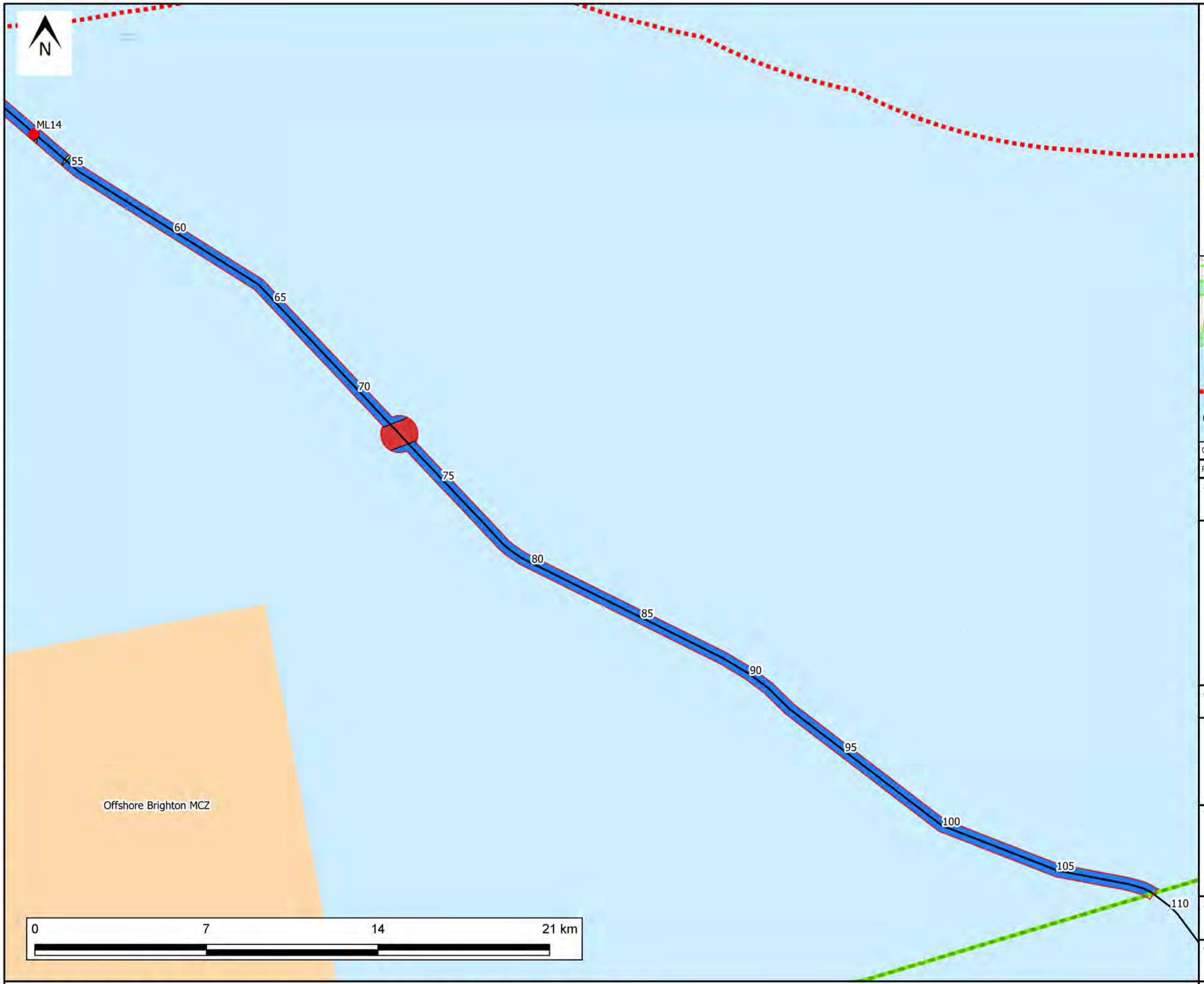

KEY:

- Survey Centre Line
- Marine Cable Corridor
- Exclusive Economic Zone
- UK 12 Nautical Mile Limit
- Proposed Dredge Disposal Area

Constraints

- Designated Sites
- Large Ripples
- Sand Waves
- HDD Entry / Exit Locations
- Cable Crossings 500m Disposal Exclusion Zone
- WFD Water Bodies with 3 km buffer

Modelling Locations

- Potential worst case modelling location for diposal of maximum volume

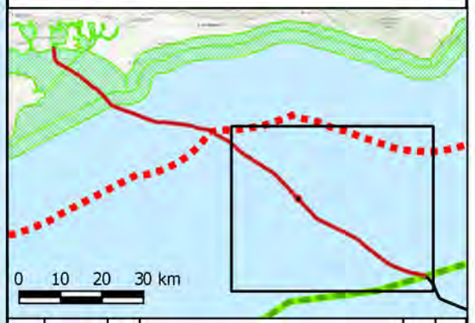

REV	DATE	BY	DESCRIPTION	CHK	APP
0.93	26/04/19	CP	DRAFT		CL

STATUS: FOR INFORMATION ONLY

WSP | Parsons Brinckerhoff, Amber Court, William Armstrong Drive, Newcastle upon Tyne, NE4 7YQ
Tel: +44(0) 191 298 1000
www.wsp-pb.com

CLIENT: AQUIND LTD

PROJECT: UK - FRANCE INTERCONNECTOR

TITLE: FIGURE 66 UK PROPOSED DREDGE DISPOSAL AREA MAP

SCALE @A3:	CHECKED:	APPROVED:
1:150,000		CL
QGIS FILE:	DRAWN: 26/04/19	DATE: 26/04/19

PROJECT No:	DRAWING No:	REV:
62100616		0.93

THE PROPERTY OF THIS DRAWING AND DESIGN IS VESTED IN WSP AND MUST NOT BE COPIED OR REPRODUCED IN ANY WAY WITHOUT THEIR WRITTEN CONSENT
© BRITISH CROWN COPYRIGHT, 2019 ALL RIGHTS RESERVED

Created by: UKCJP003 - 2019-04-26 13:23:38 - \\uk.wspgroup.com\central data\Projects\62100xxx\62100616 - Aquind VO No.3\E Models and Drawings\GIS\QGIS Marine\Drawings\Workspace\Dredge Disposal Constraint Map\Dredge Disposal Locations.qgs

4.2.2. MODEL PARAMETERISATION

4.2.2.1. When dredge vessels discharge material, a distinction is made between near-field and far-field plume motions, based on the differences in the physical processes governing the spreading mechanisms. A 'dynamic plume' descends rapidly to the seabed because of its high density relative to the surrounding seawater. A 'passive plume' forms as the dynamic plume mixes due to turbulent processes and interaction with the ambient seawater.

4.2.2.2. To account for these processes within the model, an empirical coefficient which limits the volume of fine sediment released into the water column is utilised. In this scenario a conservative 10 % rate of loss (to the passive plume) of fine sediment (sand, silt and clay) was applied, based on findings reported by Becker ***et al.*** (2015) and data garnered from other dredge disposal plume dispersion studies (detailed in Table 7). Coarser gravel sized material was assumed to be deposited almost immediately on the seabed in the vicinity of the disposal location, and therefore is not available for transport in the passive plume.

Table 7 - Similar dredge plume studies and the passive plume coefficients employed for fine material released into the water column during modelled dispersion assessments

Dredge Disposal Plume Dispersion Study	Date	Percentage of fine material released into water column (passive plume)
HR Wallingford – Falmouth Cruise Terminal	2008	5
RHDHV/HR Wallingford - York Potash Harbour: Facilities Order Disposal at Tees Bay C	2015	10
Golder Associates - Permitting of Dredged Material Disposal at Sea – Rio Tinto Alcan: Modelling Dredged Material Deep Water Placement in Upper Kitimat Arm, British Columbia	2015	5-7
Land and Bray	1998	10
URS Northern Territory (Australia) - East Arm Wharf- Dredge dispersion modelling	2011	5
Aarninkhof (Boskalis) and Luijendijk (Deltares) - Ras Laffan Port Expansion Programme (Qatar)	2010	10

4.2.2.3. The model was parameterised using site specific sedimentological data derived from vibrocores collected during the AQUIND geotechnical field campaign and sediment transport coefficients detailed by Soulsby (1997). Several sediment samples have been collected directly from features to be dredged (sandwaves [$n = 2$] and large ripples [$n =$

14]). For the purposes of model parameterisation, the mean value of each grain size class derived from samples collected directly from the features to be dredged, was utilised. Three grain size classes were defined for input to the model (Table 8). For material dredged at the HDD entry/exit pit location, sedimentological data was derived from the downcore logs gathered from the nearest borehole, where boreholes were equidistant (or nearly equidistant) from the location of the HDD exit pit, data from both boreholes was utilised, and a mean value calculated.

Table 8 - The grain size classes, and sedimentological characteristics of each class, defined for input to the plume dispersion model scenario

Grain Size Class	Size Range (mm)	Median grain size (mm)	Mean split for features to be dredged (%)	Settling Velocity (ms^{-1})
Coarse Sand and Gravel	0.600 – 64.000	32.30	35	N/A*
Fine to Medium Sand	0.064 – 0.590	0.33	56	0.042
Clay and Silt	0.001 – 0.063	0.03	9	0.001

* **Note an arbitrary high value was chosen to ensure that this material is immediately deposited on the seabed.**

4.2.2.4. Dredge volumes were calculated and reported by WSP Marine Engineering Team, (2019). Table 9 summarises the worst-case maximum volumes of dredge material disposed within the model scenario. The volume of material to be dredged was determined from the geophysical survey data, identifying areas of potentially mobile bedforms that could constrain cable installation operations, with subsequent GIS-based comparison of the existing seabed level. A Stable Seabed Level Assessment was then undertaken (informed by a review of the latest and historic survey data) to identify the level below which sediment is not anticipated to be mobile, and a comparison was made between the existing seabed level and the stable seabed level to inform the volumes. The volumes have also, as far as is possible at this stage, considered forecasts of seabed level changes and account for some estimated migration rates of mobile bedforms.

Table 9 - Volumes of material to be dredged in UK waters and disposed of within the proposed marine disposal site. Data source: WSP (2019)

KP start	KP end	Maximum Dredge Volumes m^3 *
UK Waters		
31.49	32.17	208, 824
32.50	32.65	40,437
33.67	34.5	74,112
35.37	35.42	15,601
45.35	46.05	310,931
47.75	48.00	54,109
47.99	48.69	151,310
49.00	49.80	895,405
HDD pit		2,700
Total		**1,753,428**

*** Note: volumes assume excavation batter slopes of 18 degrees and a bulking factor of 1.3.**

Model Scenarios

4.2.2.5. Model scenarios were run to best represent what is most likely to occur during disposal operations, to reflect as best as possible the 'realistic worst-case scenario'. The scenario that was modelled was based upon release of the worst-case maximum dredge material volumes identified in Table 9 (i.e. 1,753,428 m^3, disposed in UK waters).

Dredge Operations Simulated

4.2.2.6. Model scenarios simulated a single Trailing Suction Hopper Dredger ('TSHD'), working 24-hour operations, across an approximate 11-day period (referred to as the operational cycle). The excavation of the HDD pit(s) (predicted to occur between KP 1 and 1.6) was simulated using a backhoe dredger and barge as the draft of a TSHD vessel would exceed the working water depths at these locations. Within each model scenario, operations commenced on the UK coast, progressing into French waters. Timings are calculated from available vessel specification information, for the TSHD vessel *'Queen of the Netherlands'* and the split hopper barge '*Terraferre 502'* under steam from a tug vessel '*Union Topaz'* (Figure 67 and Table 10).

Figure 67: The *Queen of the Netherlands* (left) and the *Terraferre 502* under steam from the *Union Topaz*. Source: Boskalis (2019).

Table 10 - The features and specification of the *Queen of the Netherlands* and the *Terraferre 502* under steam from the *Union Topaz*. Source: Boskalis (2019).

Features	Vessel Specification	
	Queen of the Netherlands	***Terraferre 502***
Length overall	230.71 m	94.3 m
Breadth	32.00 m	16.55 m
Hopper Capacity	35,500 m^3	3823 m^3
Sailing speed loaded	16.0 kn	~10 kn
Discharge systems	Bottom door / pump ashore / rainbow installation / back dumping	Split hopper

4.2.2.7. Within the model, disposal of dredged material occurred locally relative to the features dredged i.e. towards the edge of the Marine Cable Corridor, 1,000 m from the dredging area in the negative (i.e. towards the shore and shallower water). This approach aimed to ensure that the disposed sediment remains in the vicinity of the sediment transport system from where the material was derived, but far enough away to not impact upon trenching and cable lay operations. In total, disposal of material at 13 disposal locations in UK waters are simulated in the model scenario. In calculating the position of these disposal locations, the following rules were applied:

- In UK waters, where a dredge location includes enough volume of material to fill the dredge hopper, the disposal is offset from the dredge location by 1.0 km in the negative chainage direction (i.e. towards the coast).
- This offset disposal position is checked against all other dredge KPs and is incrementally moved in the negative (or positive) chainage direction if it is within 1.0 km of any dredge site.
- Where dredge sites are located within zones where disposal is prohibited (due to environmental/engineering constraints), they are incrementally moved in the positive or negative chainage direction until the above rules are satisfied. For example,

material dredged from the UK HDD entry pit location in the nearshore is disposed at KP 21.

- The number of disposal locations required was calculated based on the engineering constraint that navigable depths cannot be reduced by > 5% at any disposal location. Material volumes dredged from each feature were evenly apportioned between the number of disposal locations.
- These disposal locations are then offset to the left-hand side of the Marine Cable Corridor by 250 m (i.e. to the edge of the cable corridor).

The disposal locations in UK waters during the worst-case scenario (i.e. where the maximum dredge volume is disposed) is presented in Figure 66.

4.3. PARTICLE TRACKING MODEL OUTPUTS

4.3.1.1. The model outputs were interrogated to establish the maximum and instantaneous suspended sediment concentration (mg l^{-1}) and maximum and instantaneous deposited sediment thickness (mm) arising from the disposal operations. These metrics are considered key output parameters required for the assessment of potential environmental impacts.

4.3.1.2. Model outputs included geospatial plots showing the suspended sediment concentration (presented as values above background) and increases in sediment thickness on the seabed, in the form of time-sliced snapshots and time series plots derived from each disposal location, and marine protected areas. Figure 68 shows the location of each model inspection point (where time series data were drawn) within designated areas within the Channel. Note; although data was retrieved and analysed from each inspection point, including those located within designated sites as illustrated in Figure 68, no significant impacts were predicted for all but the Offshore Overfalls Marine Conservation Zone ('MCZ'). Therefore, only the results for the Offshore Overfalls MCZ is presented in Section 4.4.

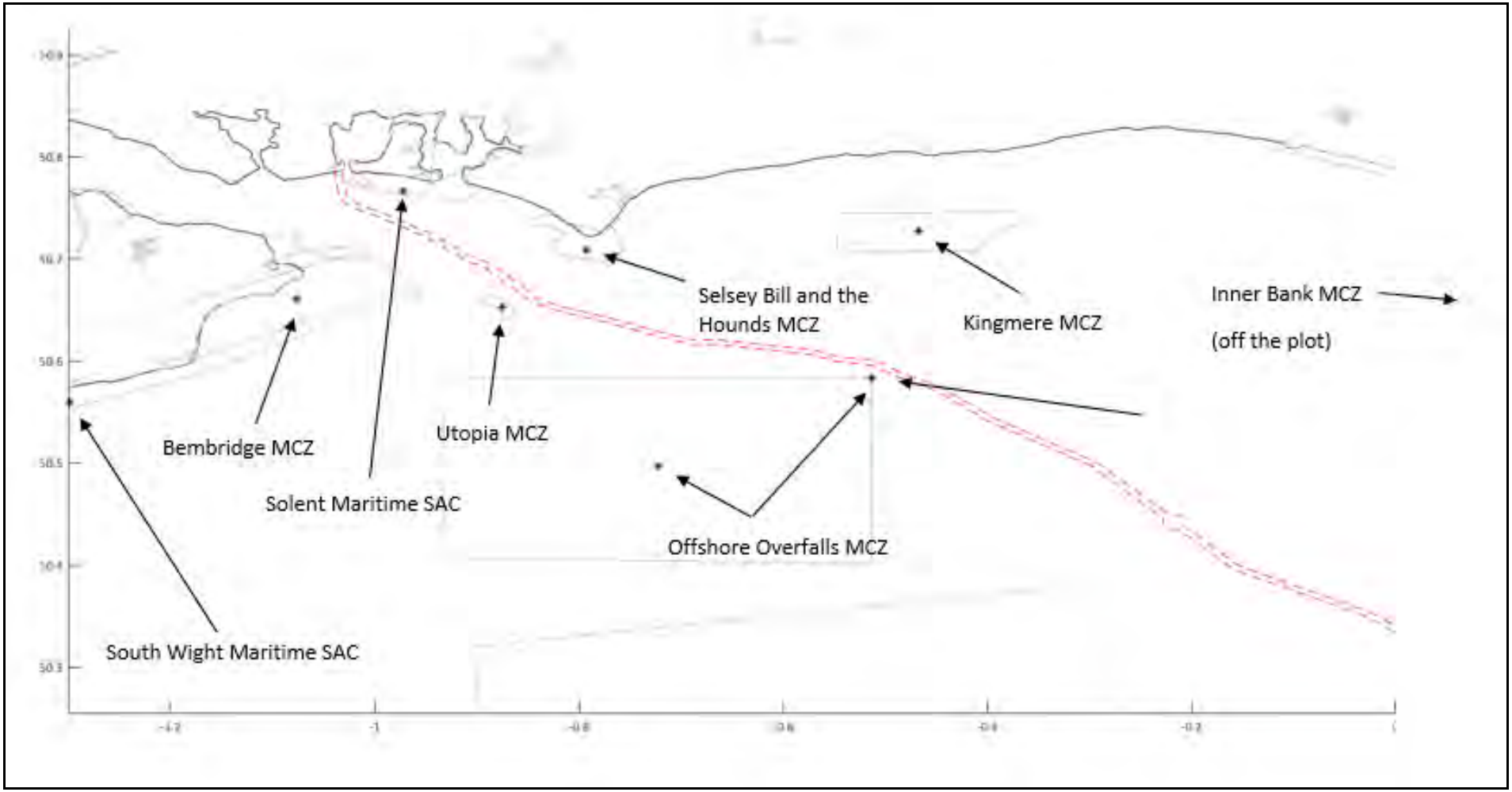

Figure 68 - The location of the model inspection points positioned within an MCZ or SAC in UK waters (location is indicated by a black star).

4.4. RESULTS

4.4.1.1. During the modelled worst-case scenario suspended sediment plumes created during dredge disposal operations were predicted to enhance suspended sediment concentrations, local to dredge operations, and across the wider environment, transiently. The maximum observed values at any time during the model run are presented in Figure 69 presenting the worst-case plume footprint.

4.4.1.2. This footprint extends up to circa 20 – 25 km in UK waters relative to the Marine Cable Corridor, along the dominant tidal axis both in the ebb and flood direction. The spatial extent of this footprint is mainly due to the presence of fine material at the extremities of the plume. Closer to the point of release, the plume also comprises sand sized sediments, but these are deposited rapidly, locally to the point of release (i.e. within 1000 m).

4.4.1.3. Figures 70 to 82 present time sliced snapshots showing the location (and predicted concentration) of suspended sediment plumes and predicted bed thickness captured 1 hour after disposal at each disposal location during the course of the simulation i.e. these figures show the evolution of the plume during the operational cycle.

4.4.1.4. Figures 83 to 95 present the suspended sediment concentrations at each disposal location in the form of a time series. These plots reveal predicted increases in suspended sediment concentrations in the order of 1000 mg l^{-1} at the point of release at several disposal locations (see Figure 88 for an example) along the Marine Cable Corridor, but again these are transient, rapidly decreasing as sand sized sediments deposit to the bed and finer sediments are dispersed.

4.4.1.5. In all instances, suspended sediment concentrations return to background levels within the timeframe of a few days. Predicted deposition of coarser sediments local to the point of release show thickness on the bed of between < 10 mm and 1.5 m (Figures 83 to 95).

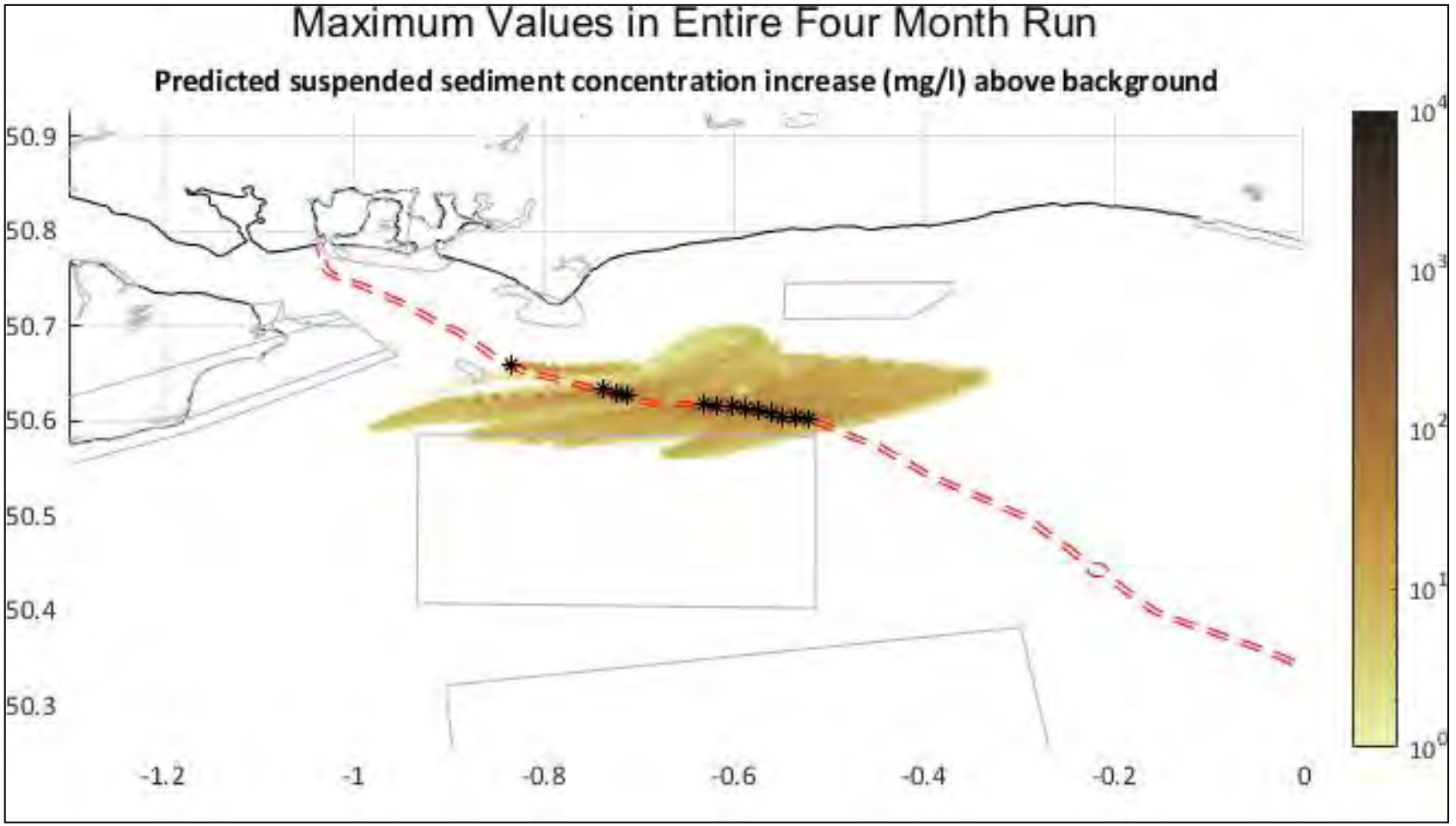

Figure 69 - Maximum values of predicted suspended sediment concentration increase above background UK Waters during the model run. *Note; this plot does not show the actual plume at any one time but rather the peak values attained at each location over the course of the whole simulation*.

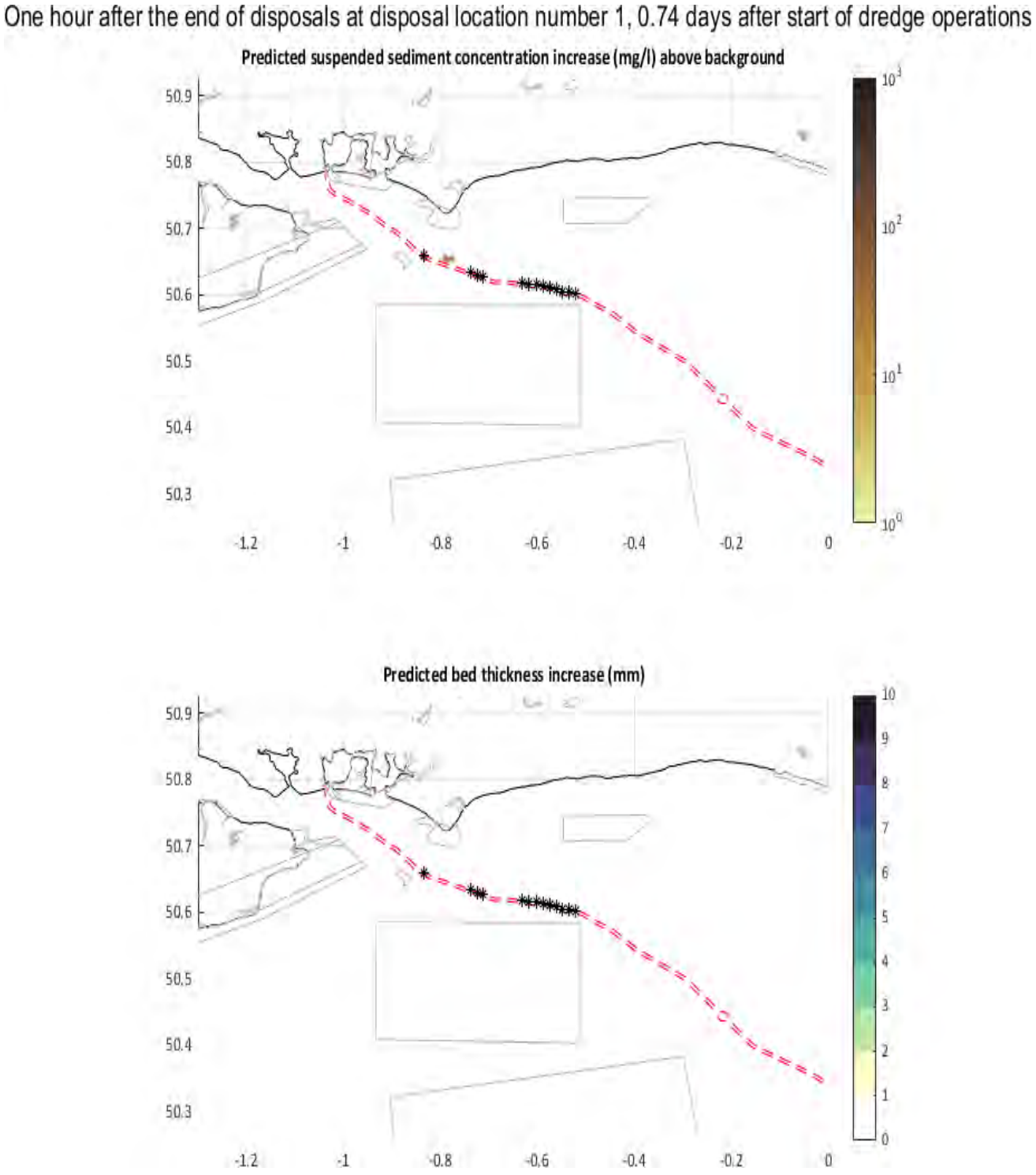

Figure 70 - Time sliced snapshot of the location and associated concentration of suspended sediment plumes and the predicted bed thickness created during disposal of dredge material in UK waters. The snapshot is captured 1 hour after disposal at location 1.

One hour after the end of disposals at disposal location number 2, 1.27 days after start of dredge operations

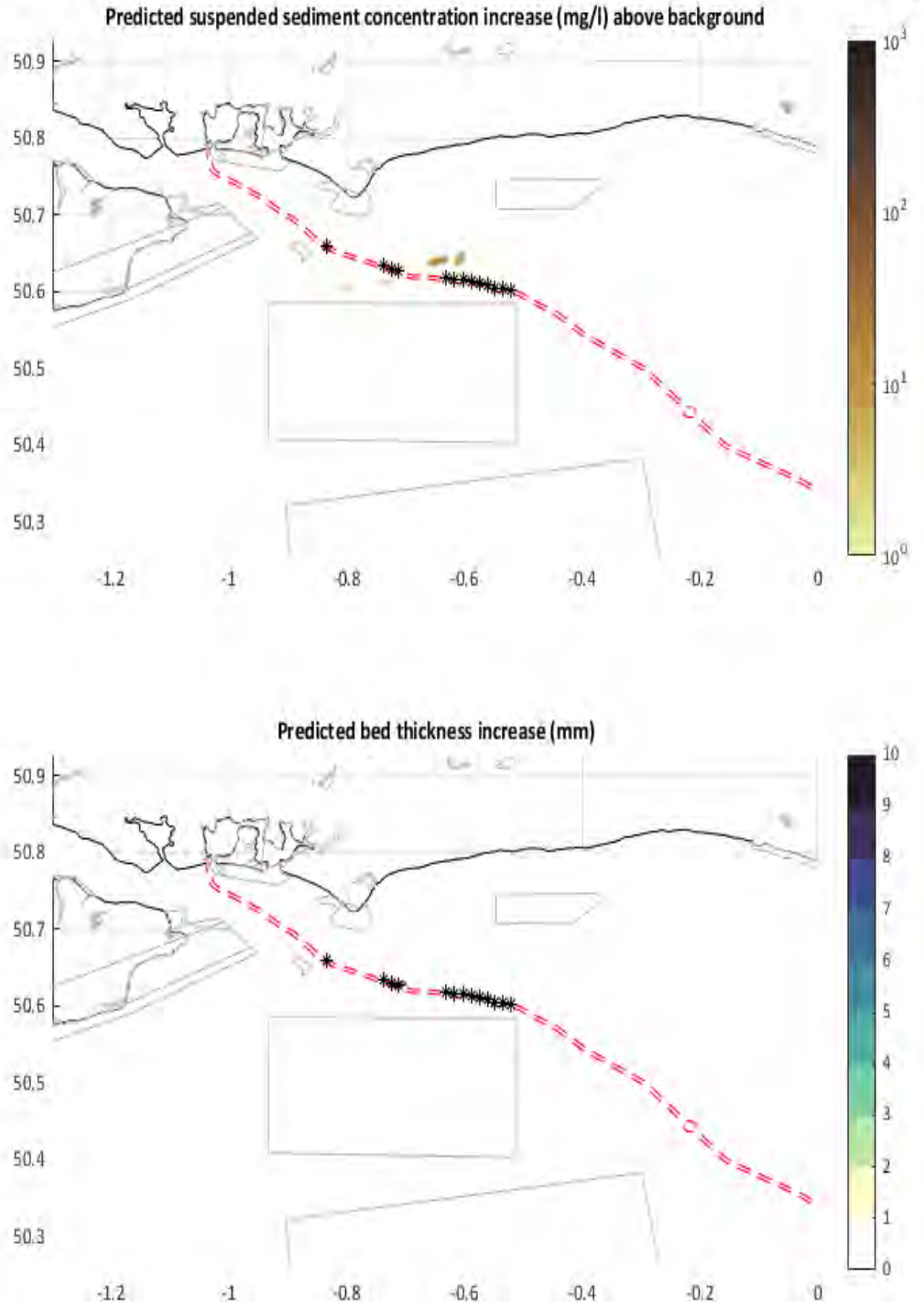

Figure 71 - Time sliced snapshot of the location and associated concentration of suspended sediment plumes and the predicted bed thickness created during disposal of dredge material in UK waters. The snapshot is captured 1 hour after disposal at location 2.

One hour after the end of disposals at disposal location number 3, 1.8 days after start of dredge operations

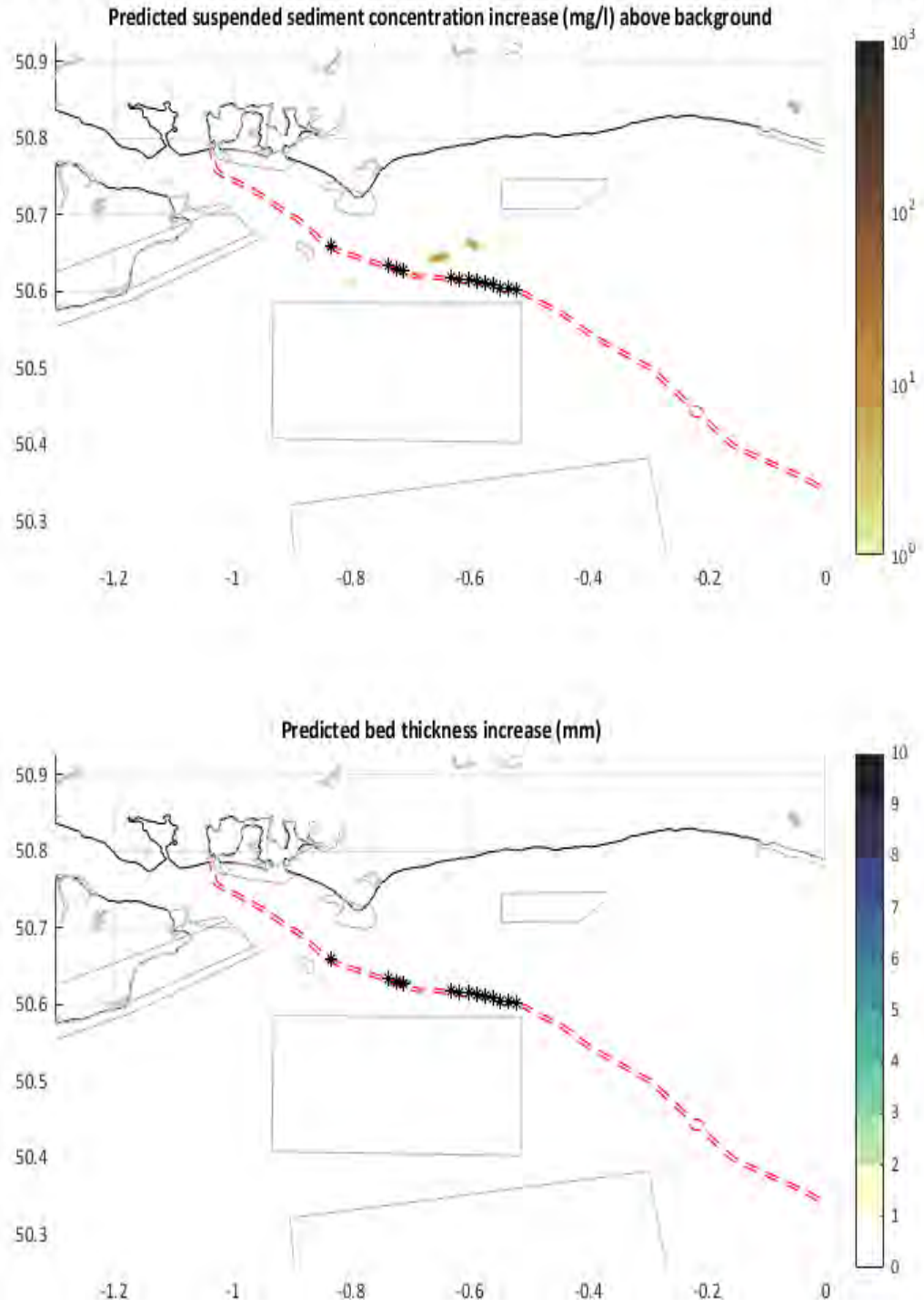

Figure 72 - Time sliced snapshot of the location and associated concentration of suspended sediment plumes and the predicted bed thickness created during disposal of dredge material in UK waters. The snapshot is captured 1 hour after disposal at location 3.

One hour after the end of disposals at disposal location number 4, 2.34 days after start of dredge operations

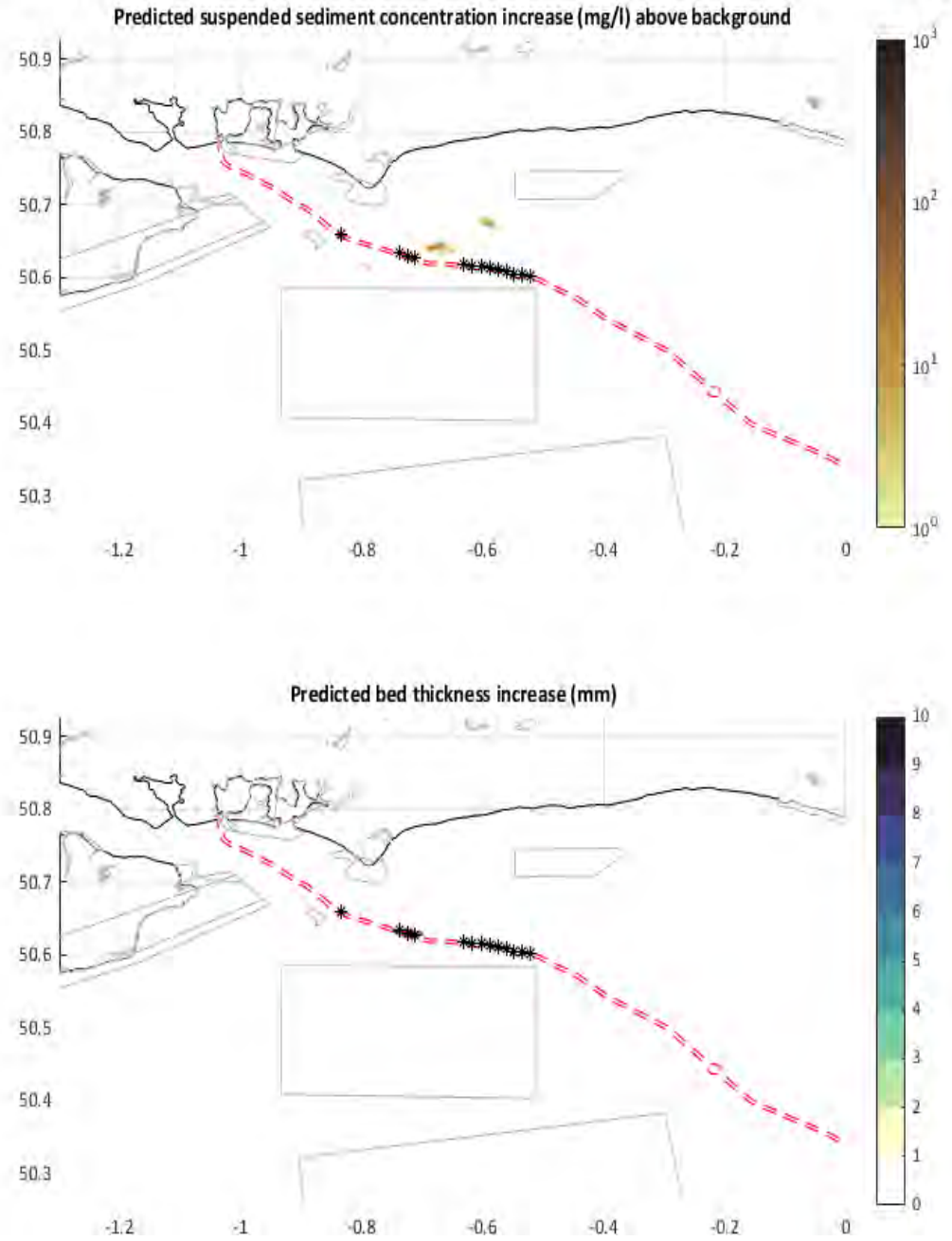

Figure 73 - Time sliced snapshot of the location and associated concentration of suspended sediment plumes and the predicted bed thickness created during disposal of dredge material in UK waters. The snapshot is captured 1 hour after disposal at location 4.

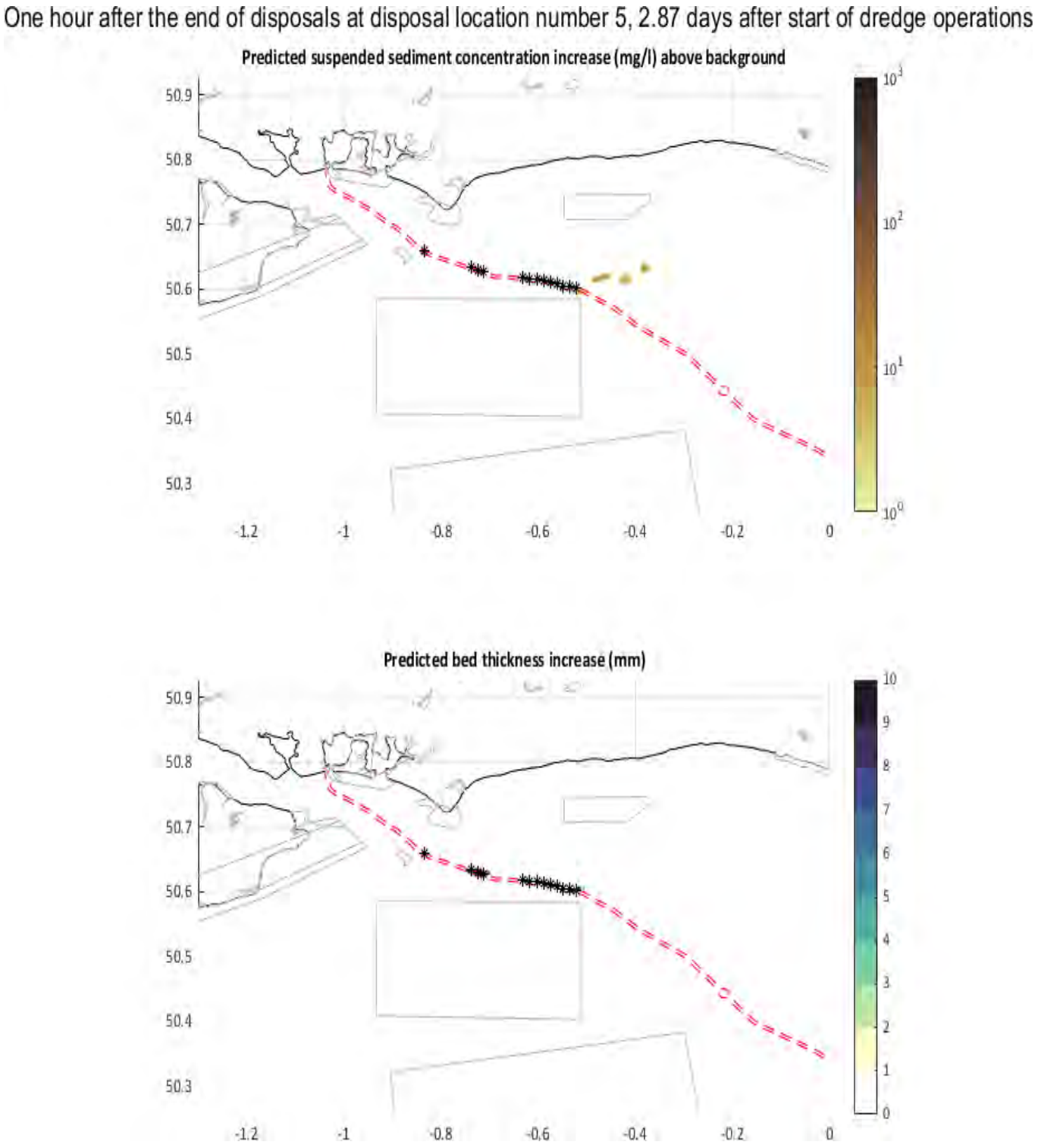

Figure 74 - Time sliced snapshot of the location and associated concentration of suspended sediment plumes and the predicted bed thickness created during disposal of dredge material in UK waters. The snapshot is captured 1 hour after disposal at location 5.

One hour after the end of disposals at disposal location number 6, 3.4 days after start of dredge operations

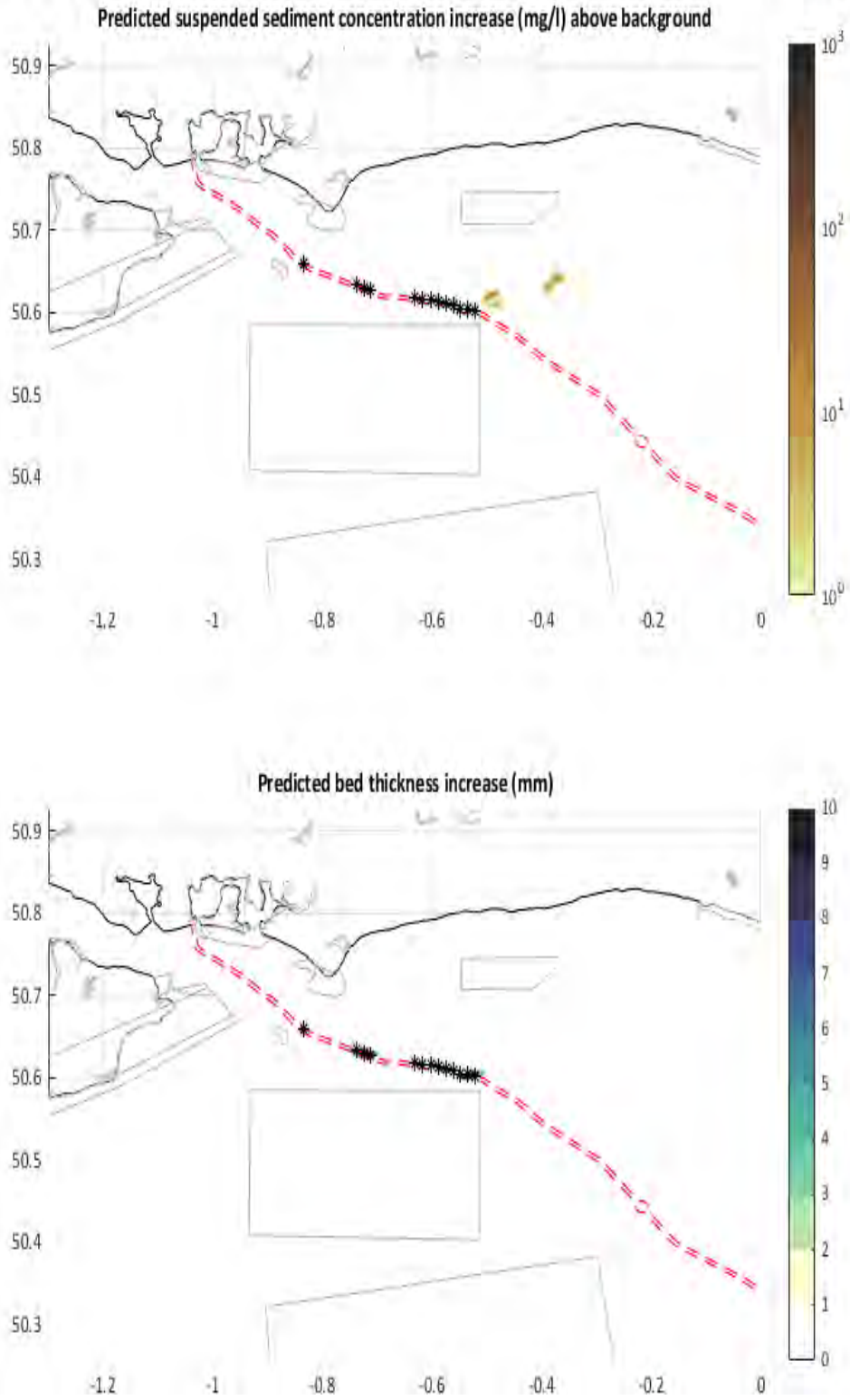

Figure 75 - Time sliced snapshot of the location and associated concentration of suspended sediment plumes and the predicted bed thickness created during disposal of dredge material in UK waters. The snapshot is captured 1 hour after disposal at location 6.

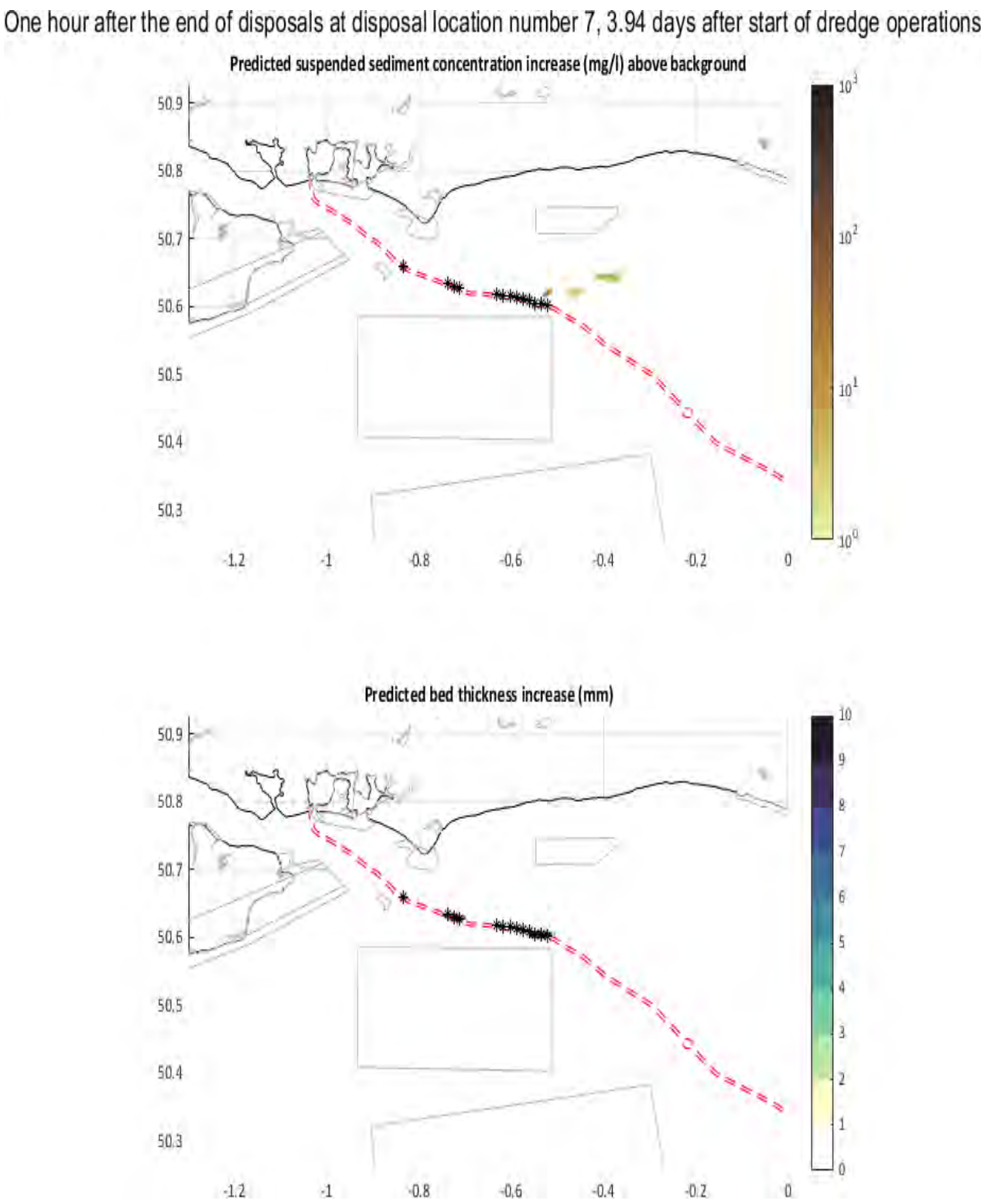

Figure 76 - Time sliced snapshot of the location and associated concentration of suspended sediment plumes and the predicted bed thickness created during disposal of dredge material in UK waters. The snapshot is captured 1 hour after disposal at location 7.

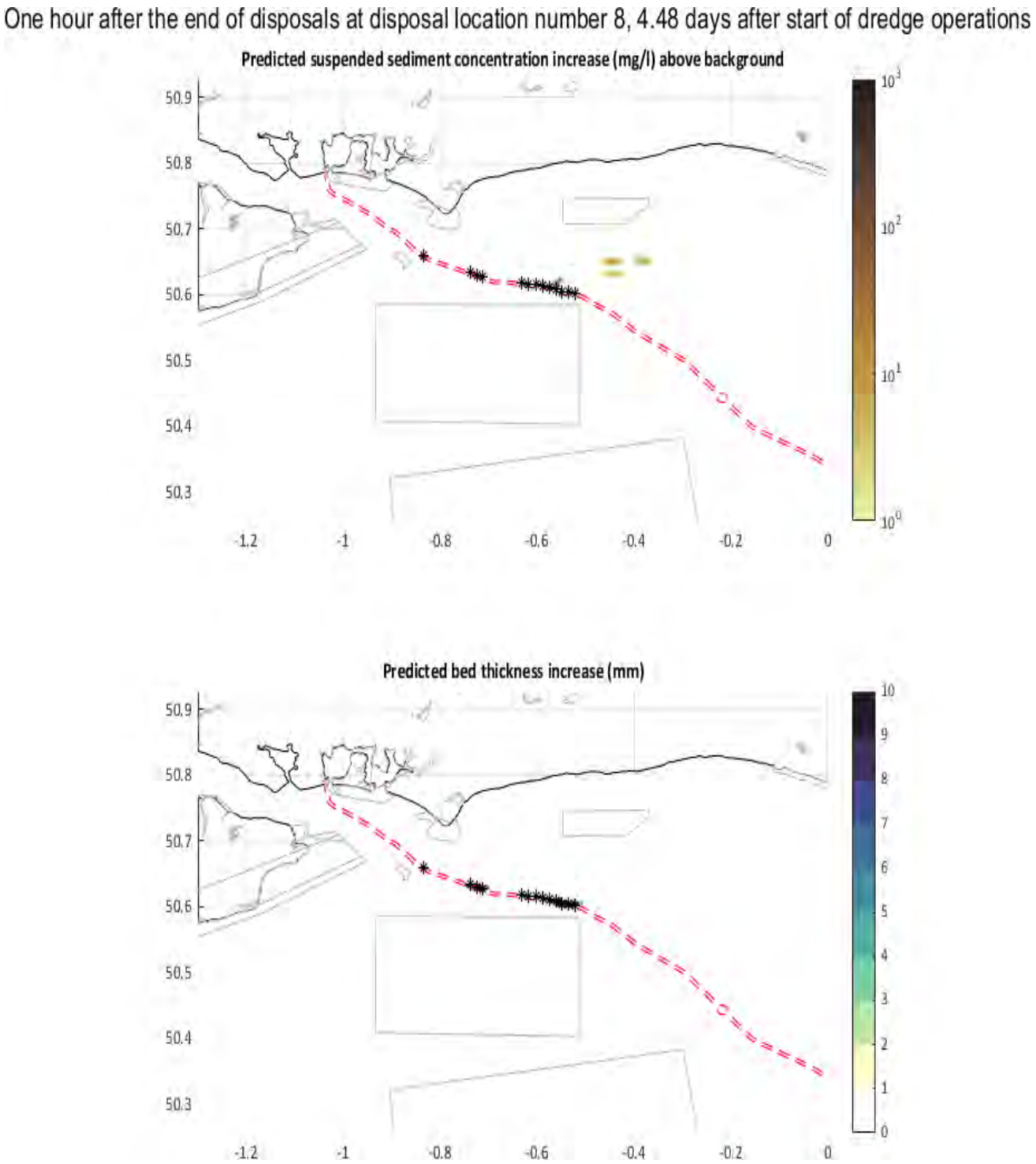

Figure 77 - Time sliced snapshot of the location and associated concentration of suspended sediment plumes and the predicted bed thickness created during disposal of dredge material in UK waters. The snapshot is captured 1 hour after disposal at location 8.

One hour after the end of disposals at disposal location number 9, 5.02 days after start of dredge operations

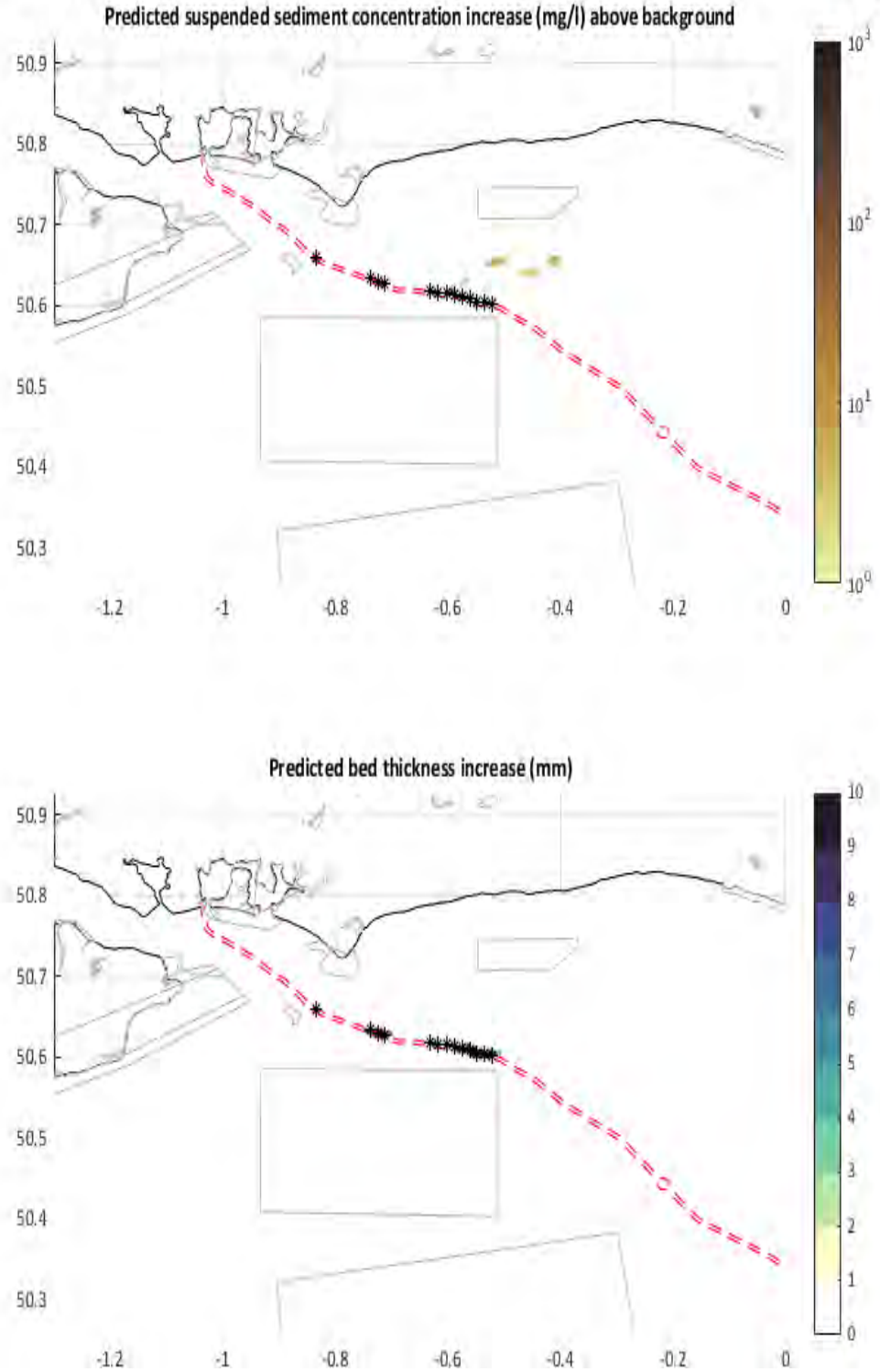

Figure 78 - Time sliced snapshot of the location and associated concentration of suspended sediment plumes and the predicted bed thickness created during disposal of dredge material in UK waters. The snapshot is captured 1 hour after disposal at location 9.

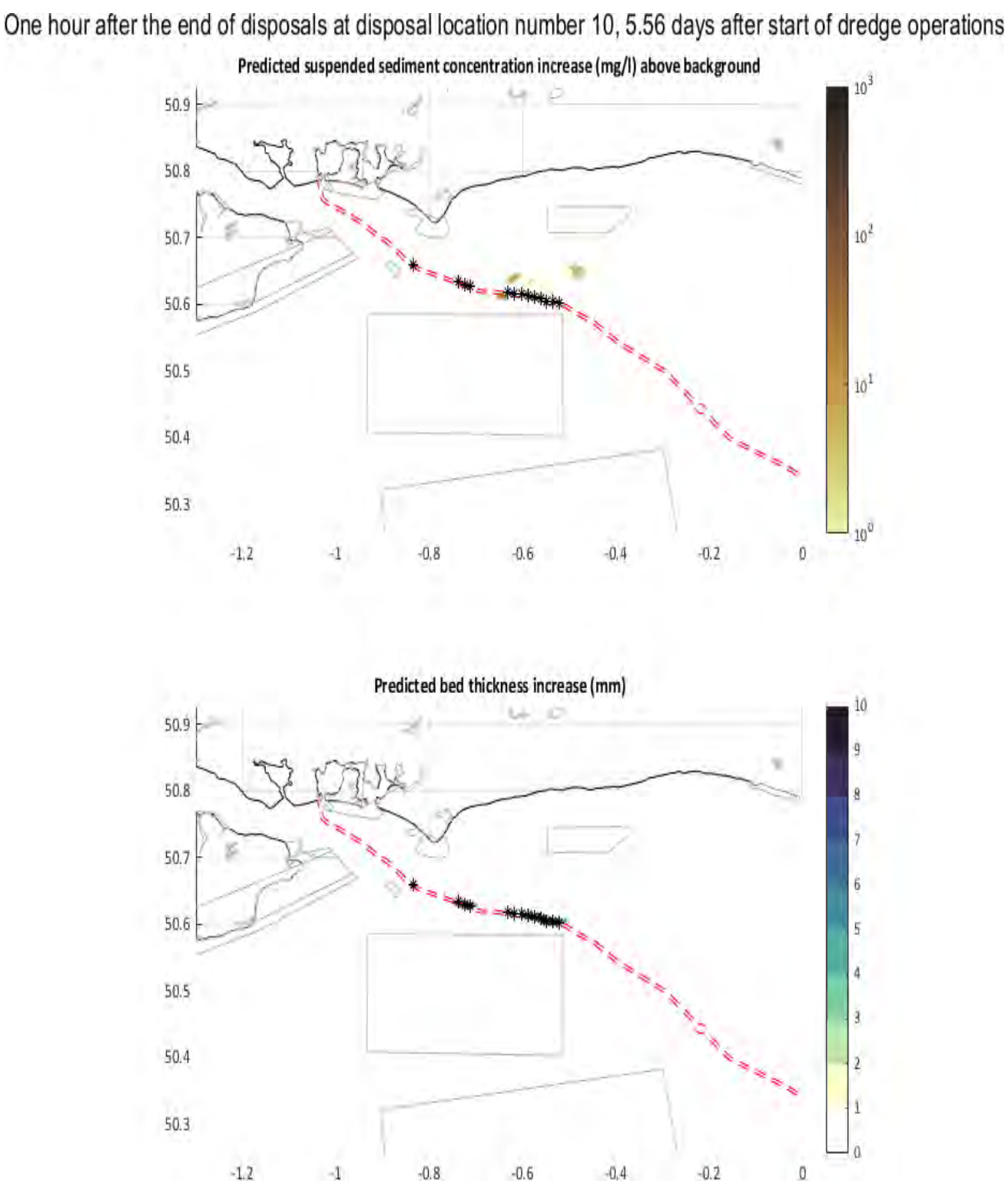

Figure 79 - Time sliced snapshot of the location and associated concentration of suspended sediment plumes and the predicted bed thickness created during disposal of dredge material in UK waters. The snapshot is captured 1 hour after disposal at location 10.

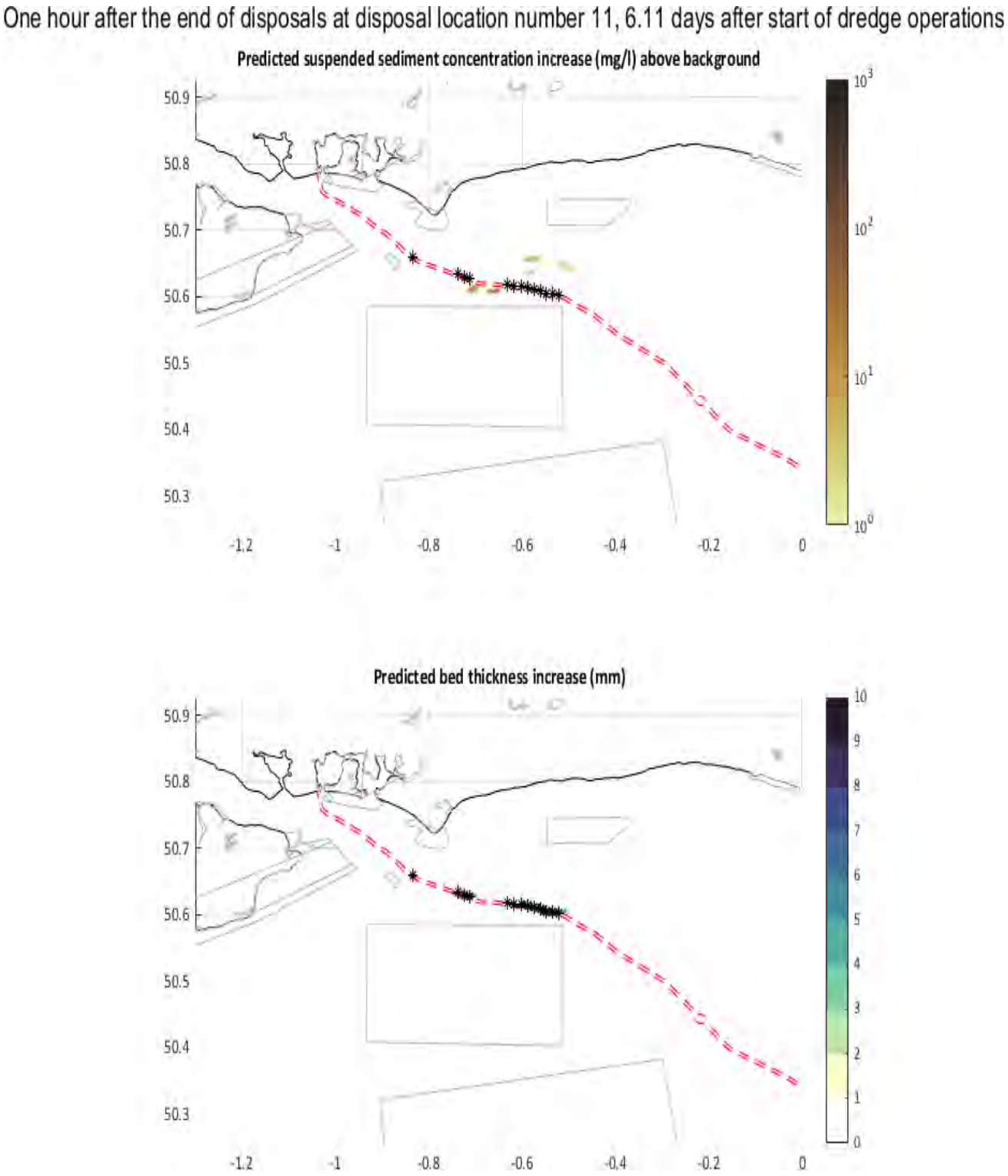

Figure 80 - Time sliced snapshot of the location and associated concentration of suspended sediment plumes and the predicted bed thickness created during disposal of dredge material in UK waters. The snapshot is captured 1 hour after disposal at location 11.

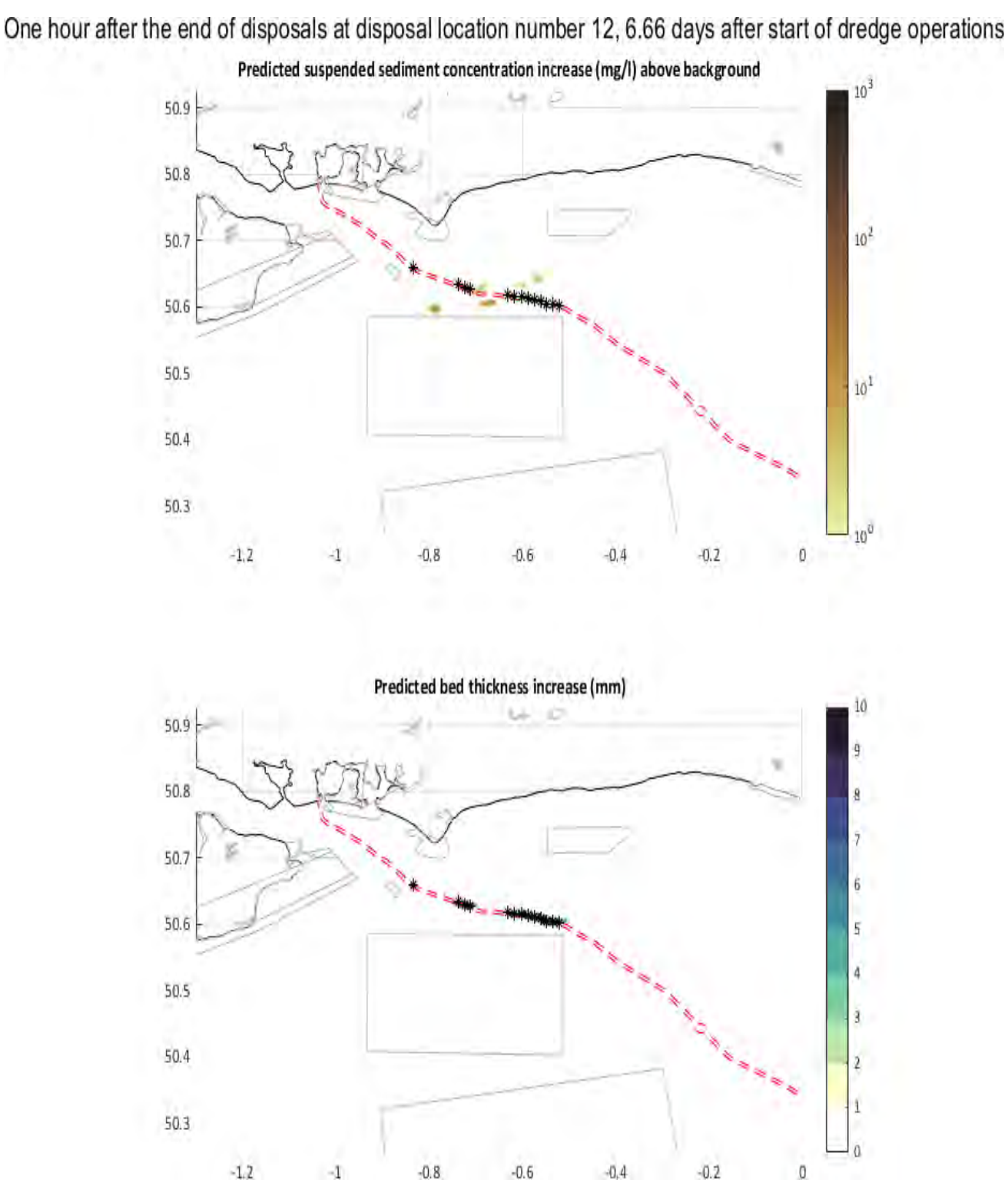

Figure 81 - Time sliced snapshot of the location and associated concentration of suspended sediment plumes and the predicted bed thickness created during disposal of dredge material in UK waters. The snapshot is captured 1 hour after disposal at location 12.

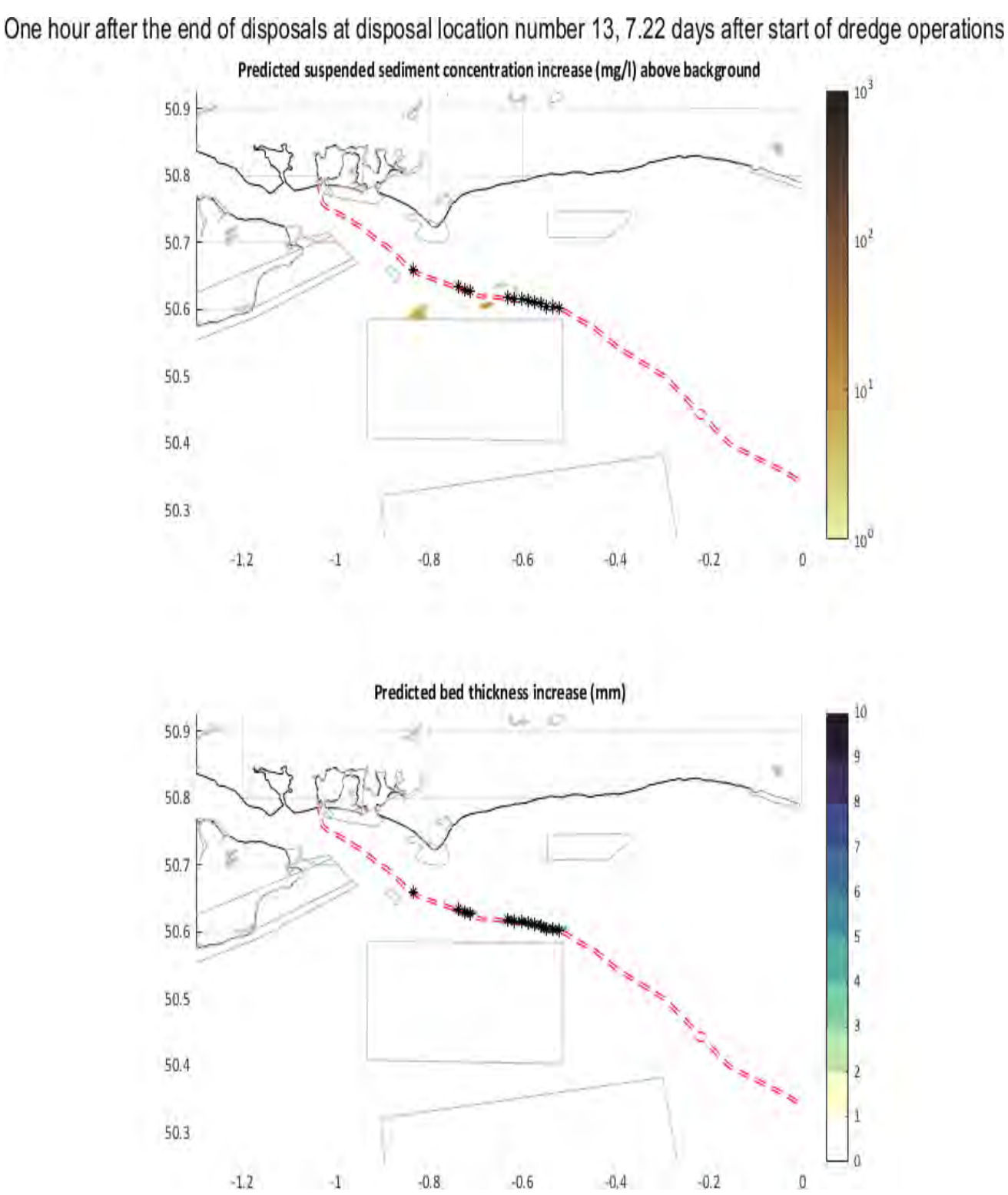

Figure 82 - Time sliced snapshot of the location and associated concentration of suspended sediment plumes and the predicted bed thickness created during disposal of dredge material in UK waters. The snapshot is captured 1 hour after disposal at location 13.

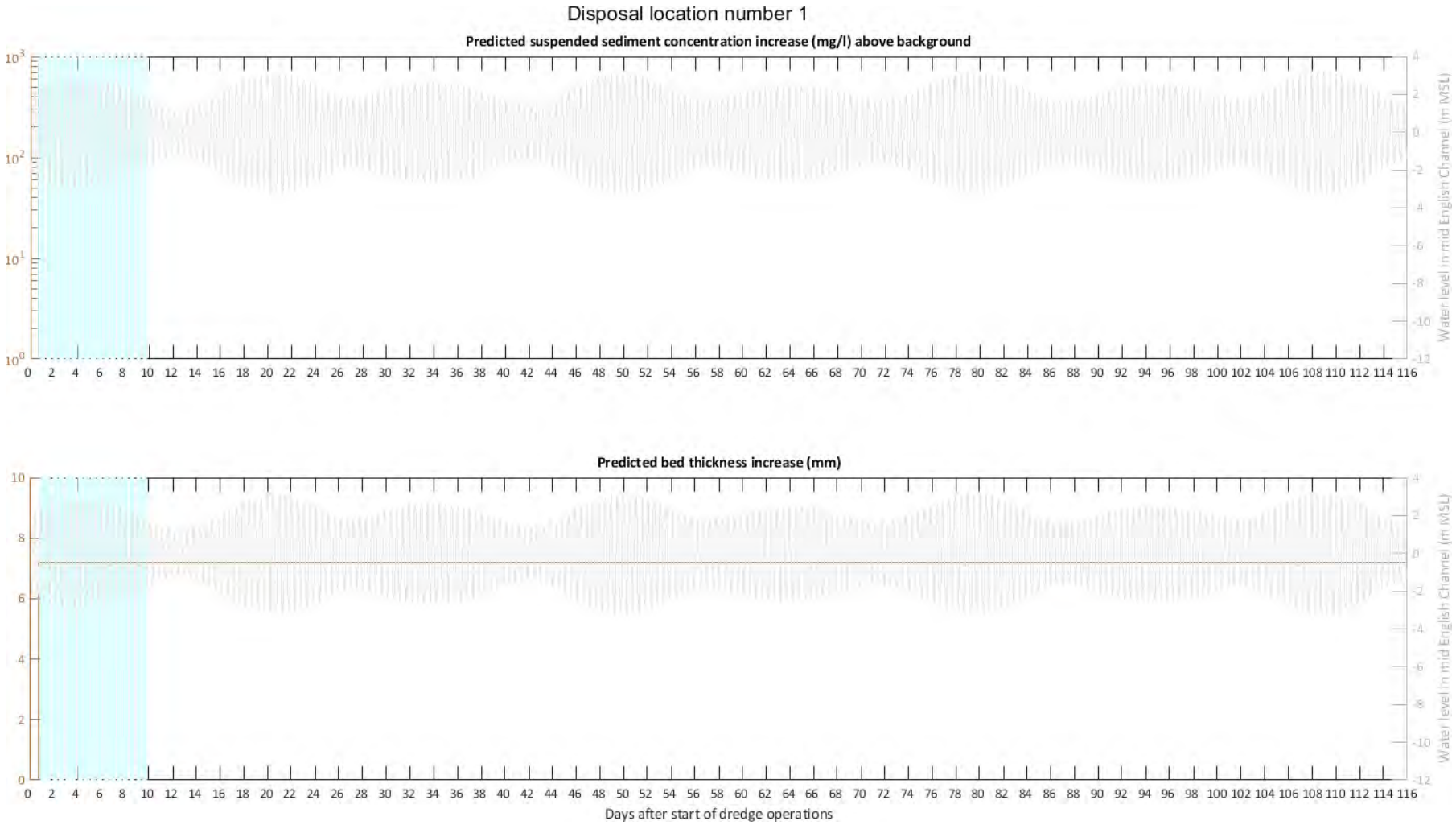

Figure 83 - Time series plots showing predicted suspended sediment concentrations and predicted bed thickness increase at disposal location 1. The light blue shaded area shows the duration of dredge operations, the dark blue shading shows the period of time where disposal activities are occurring at that disposal location within the model.

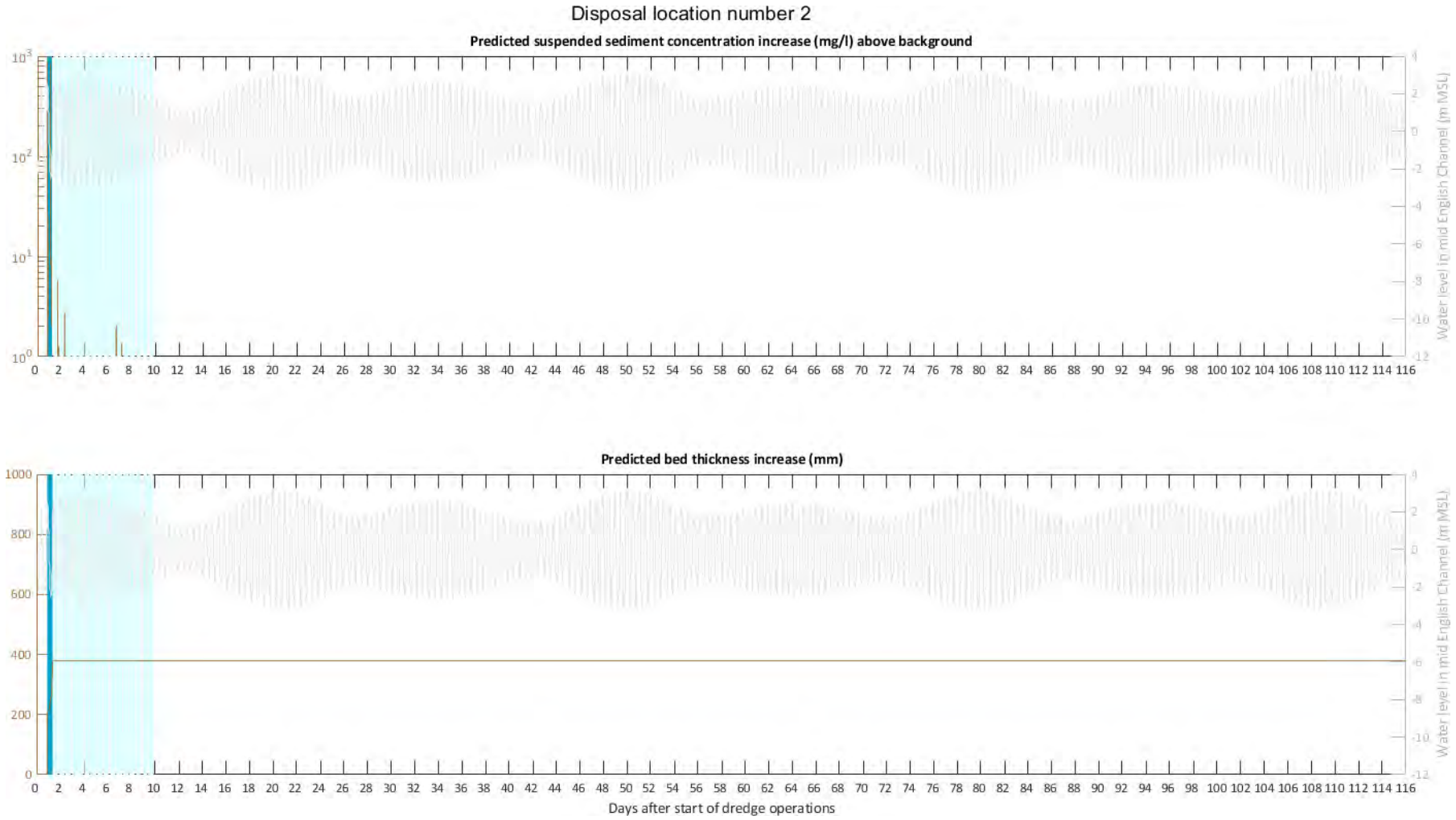

Figure 84 - Time series plots showing predicted suspended sediment concentrations and predicted bed thickness increase at disposal location 2. The light blue shaded area shows the duration of dredge operations, the dark blue shading shows the period of time where disposal activities are occurring at that disposal location within the model.

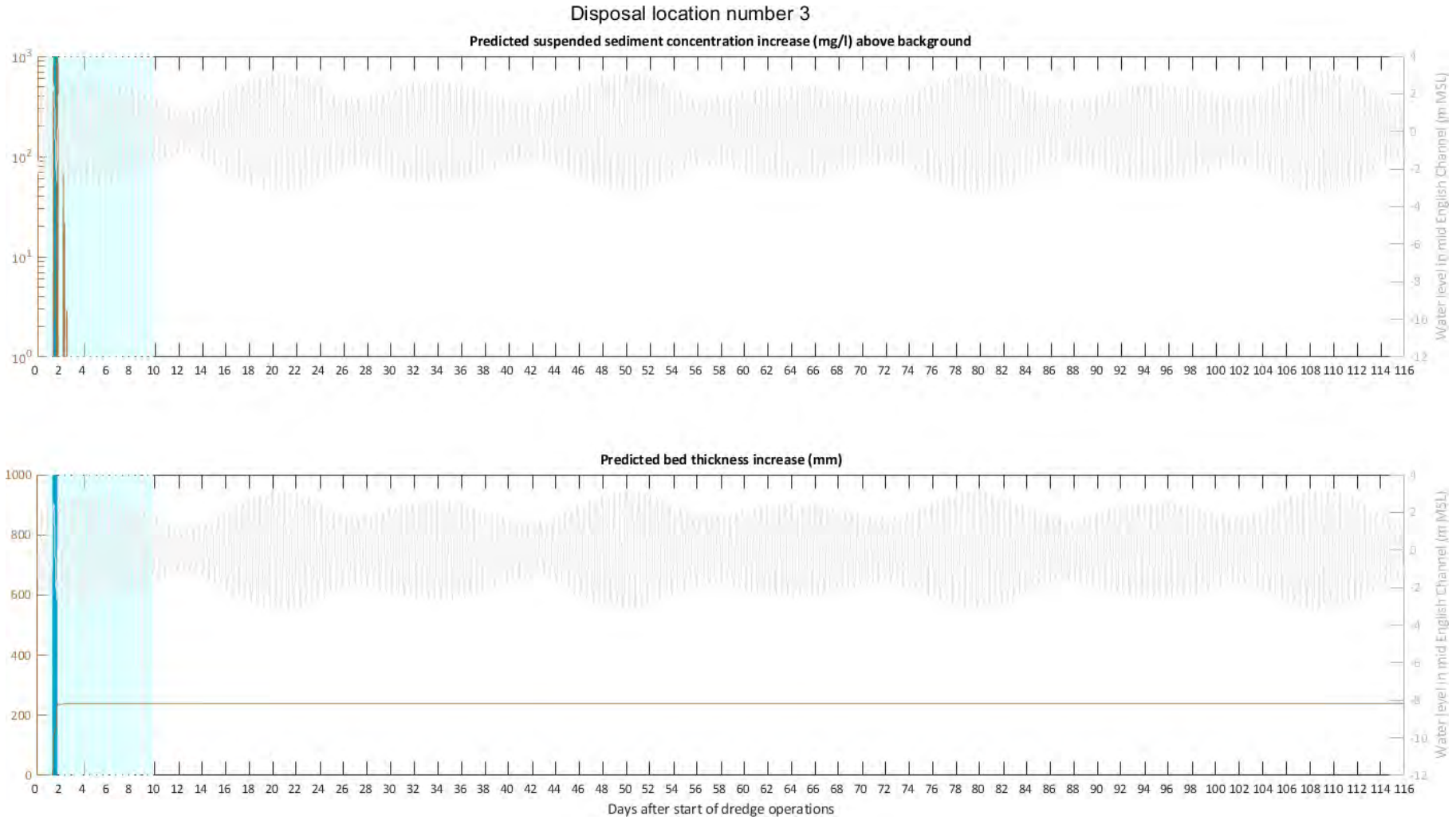

Figure 85 - Time series plots showing predicted suspended sediment concentrations and predicted bed thickness increase at disposal location 3. The light blue shaded area shows the duration of dredge operations, the dark blue shading shows the period of time where disposal activities are occurring at that disposal location within the model.

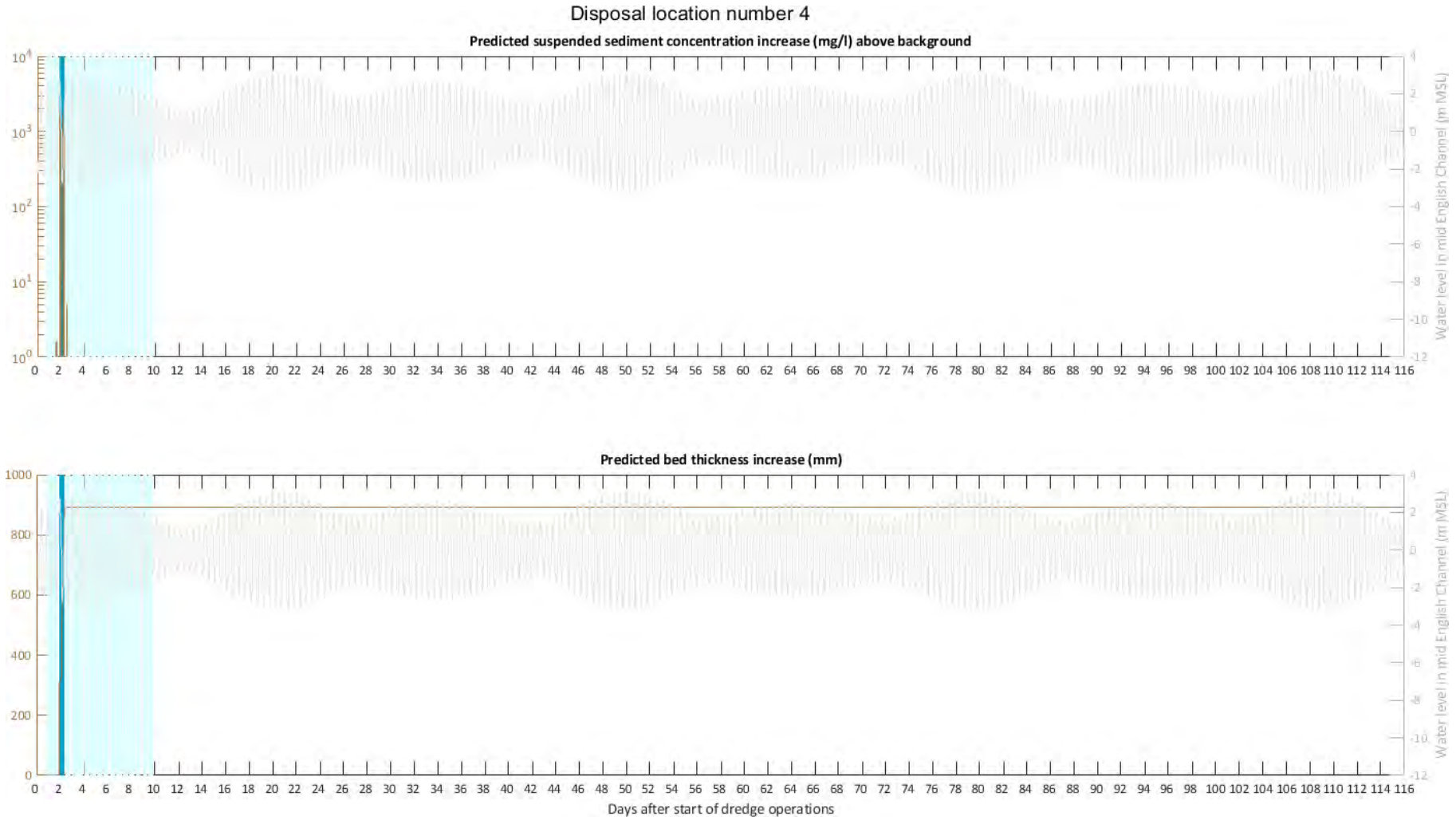

Figure 86 - Time series plots showing predicted suspended sediment concentrations and predicted bed thickness increase at disposal location 4. The light blue shaded area shows the duration of dredge operations, the dark blue shading shows the period of time where disposal activities are occurring at that disposal location within the model.

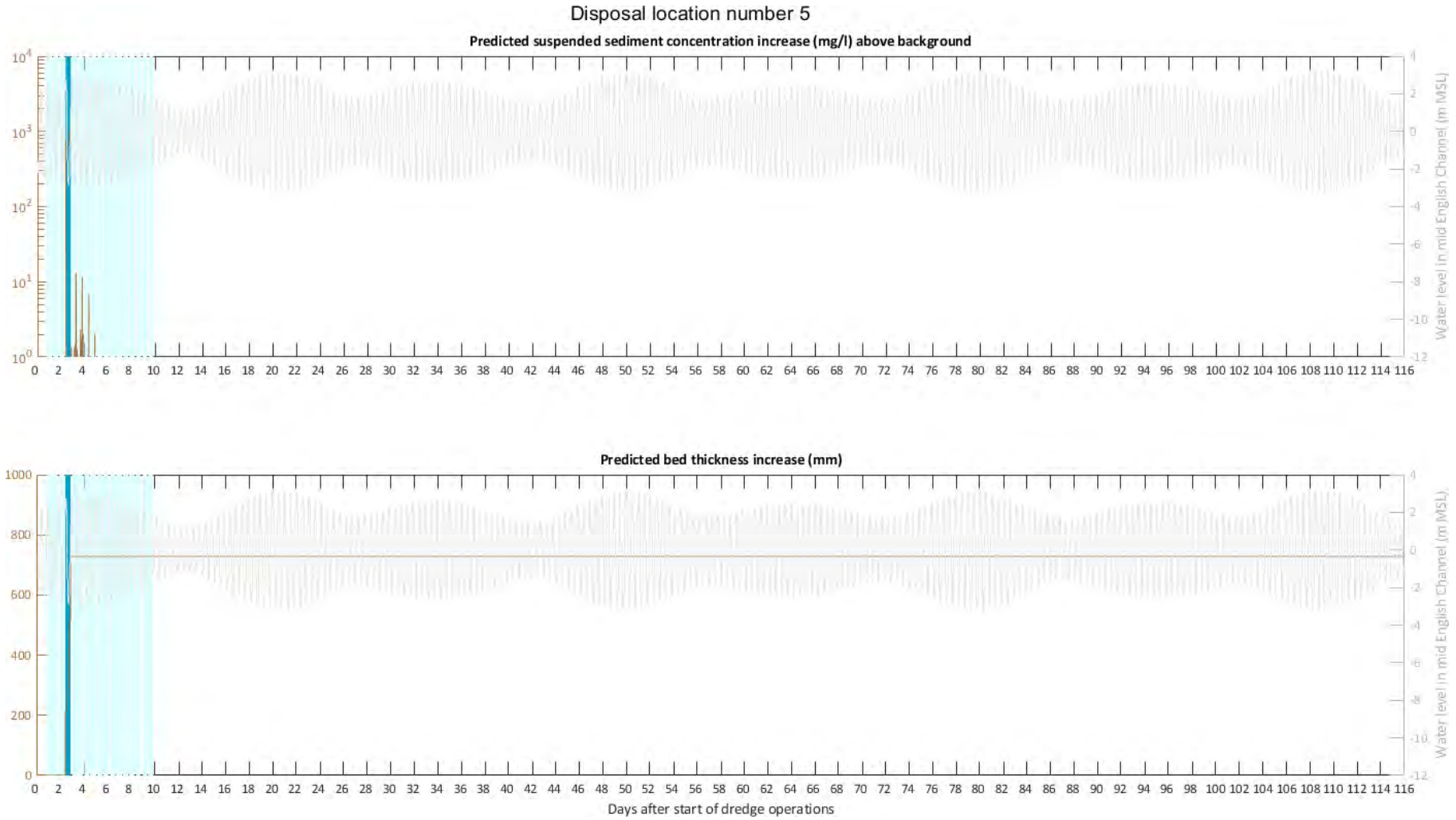

Figure 87 - Time series plots showing predicted suspended sediment concentrations and predicted bed thickness increase at disposal location 5. The light blue shaded area shows the duration of dredge operations, the dark blue shading shows the period of time where disposal activities are occurring at that disposal location within the model.

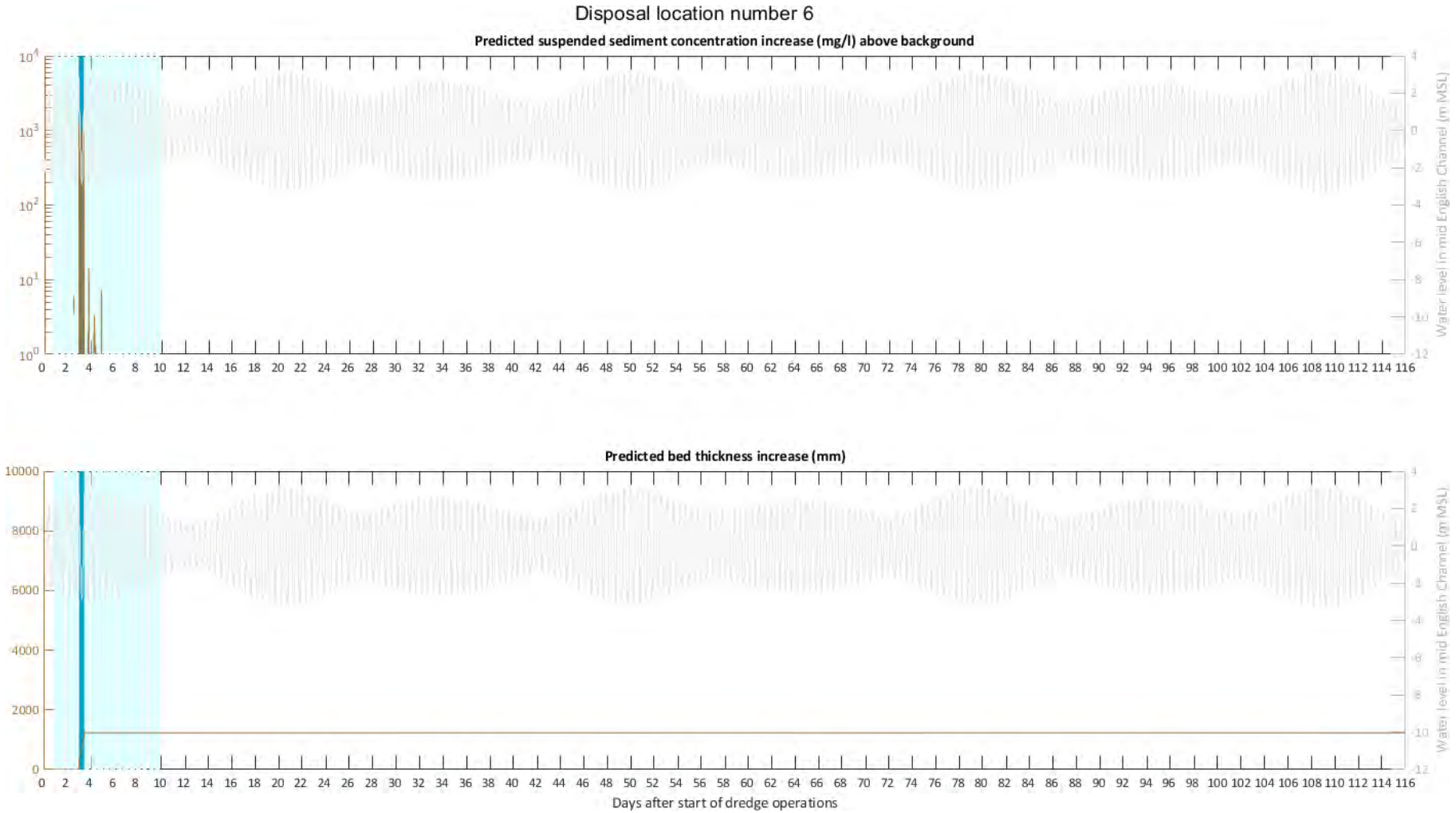

Figure 88 - Time series plots showing predicted suspended sediment concentrations and predicted bed thickness increase at disposal location 6. The light blue shaded area shows the duration of dredge operations, the dark blue shading shows the period of time where disposal activities are occurring at that disposal location within the model.

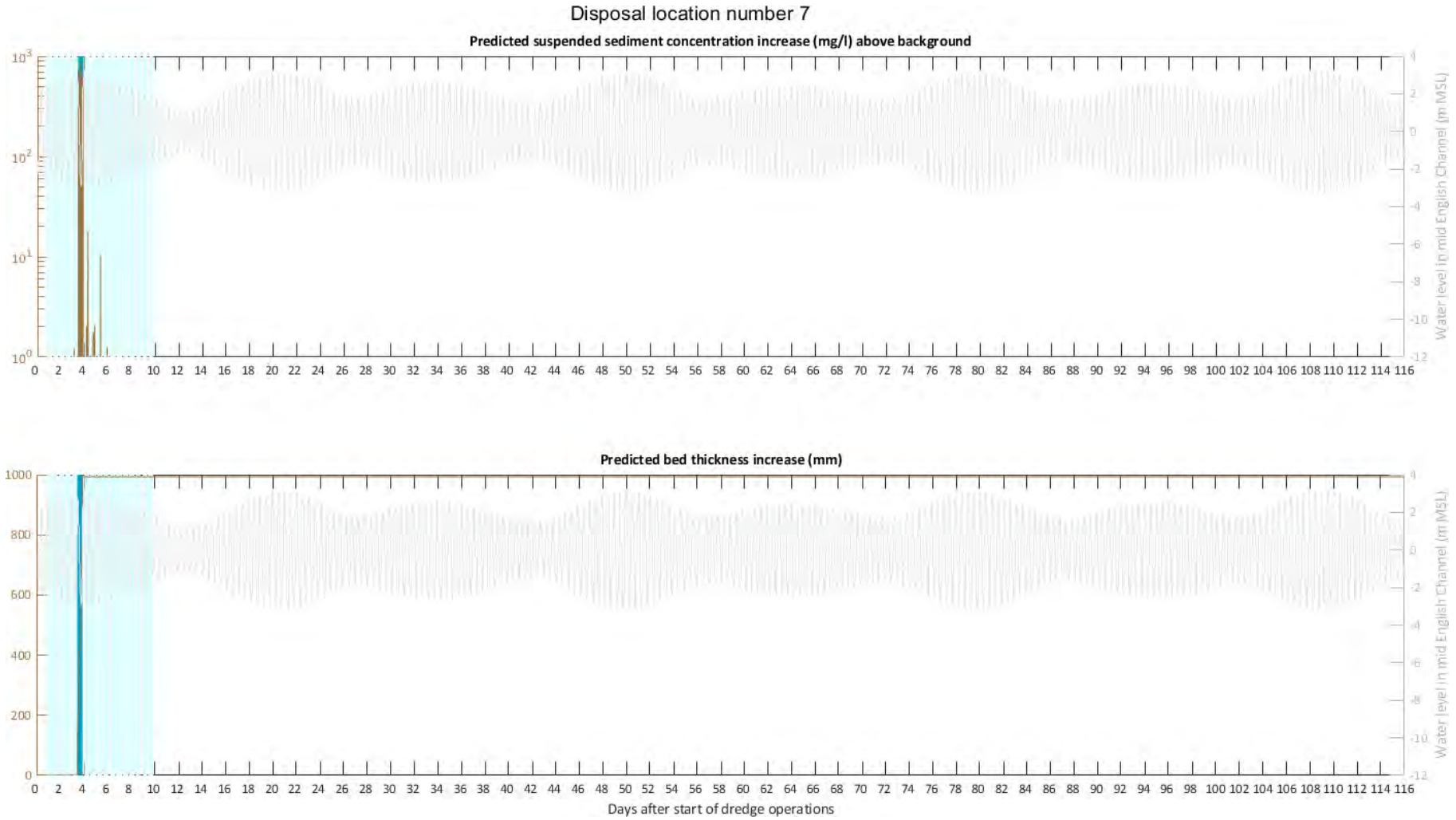

Figure 89- Time series plots showing predicted suspended sediment concentrations and predicted bed thickness increase at disposal location 7. The light blue shaded area shows the duration of dredge operations, the dark blue shading shows the period of time where disposal activities are occurring at that disposal location within the model.

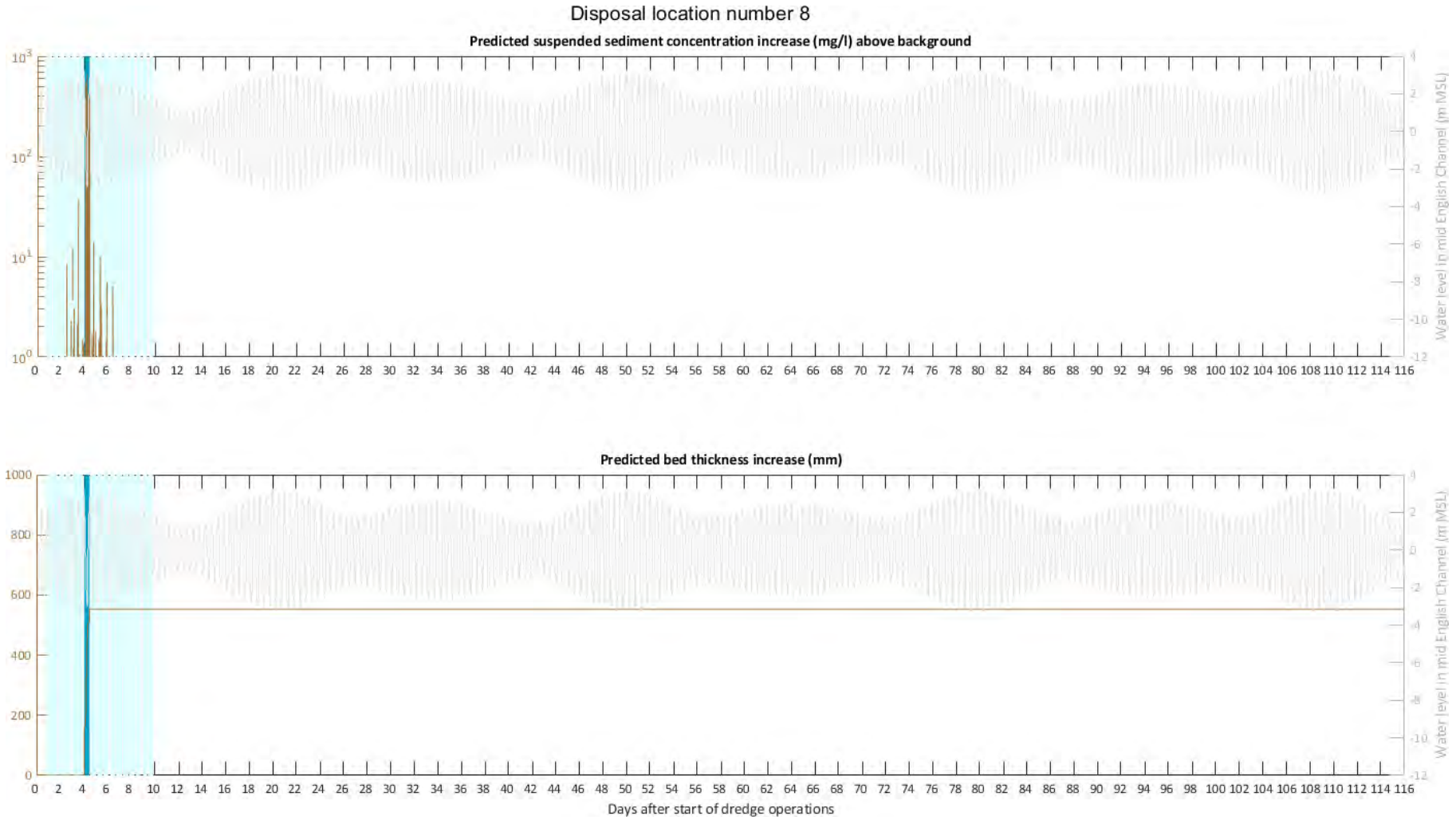

Figure 90 - Time series plots showing predicted suspended sediment concentrations and predicted bed thickness increase at disposal location 8. The light blue shaded area shows the duration of dredge operations, the dark blue shading shows the period of time where disposal activities are occurring at that disposal location within the model.

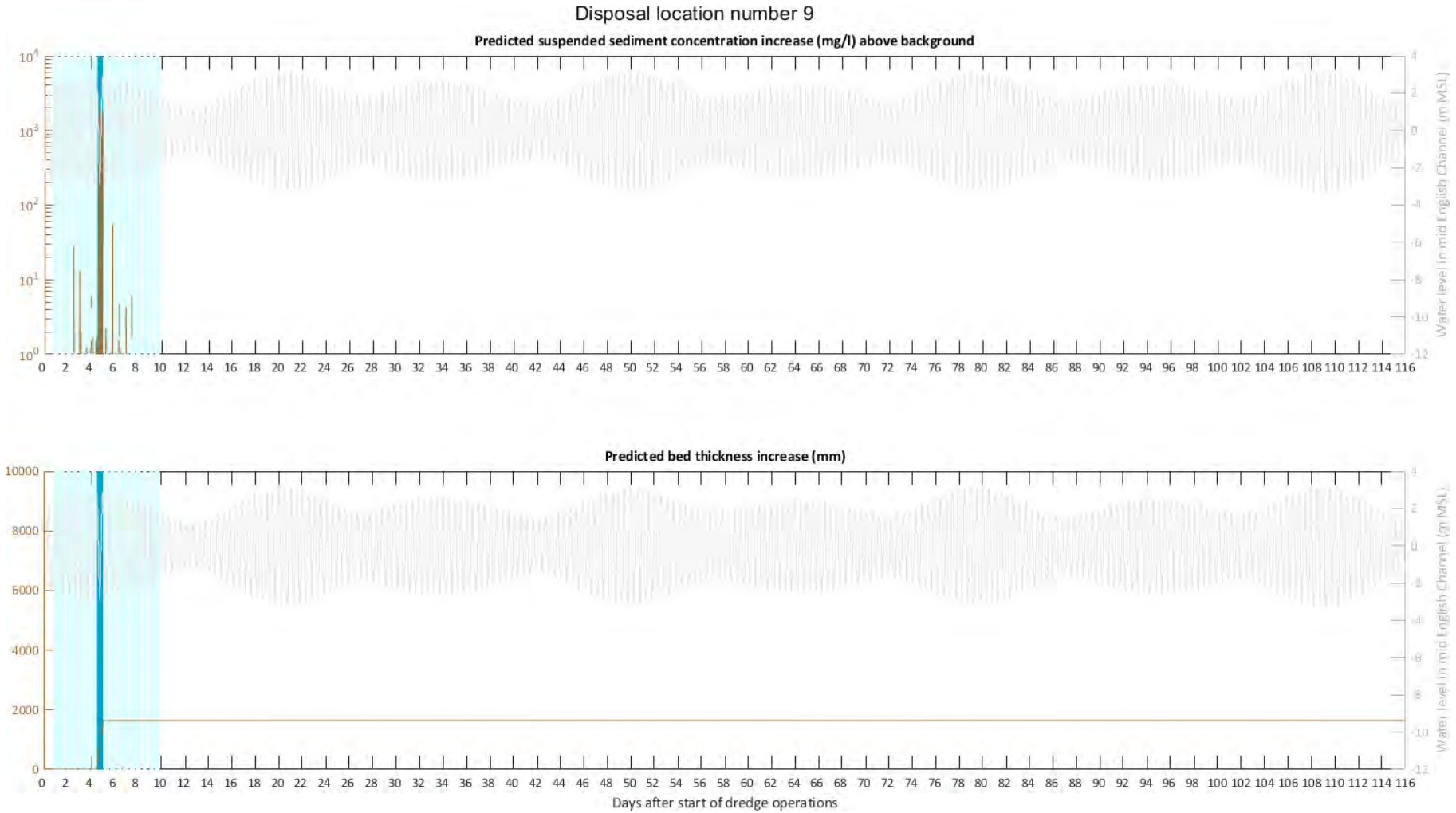

Figure 91 - Time series plots showing predicted suspended sediment concentrations and predicted bed thickness increase at disposal location 9. The light blue shaded area shows the duration of dredge operations, the dark blue shading shows the period of time where disposal activities are occurring at that disposal location within the model.

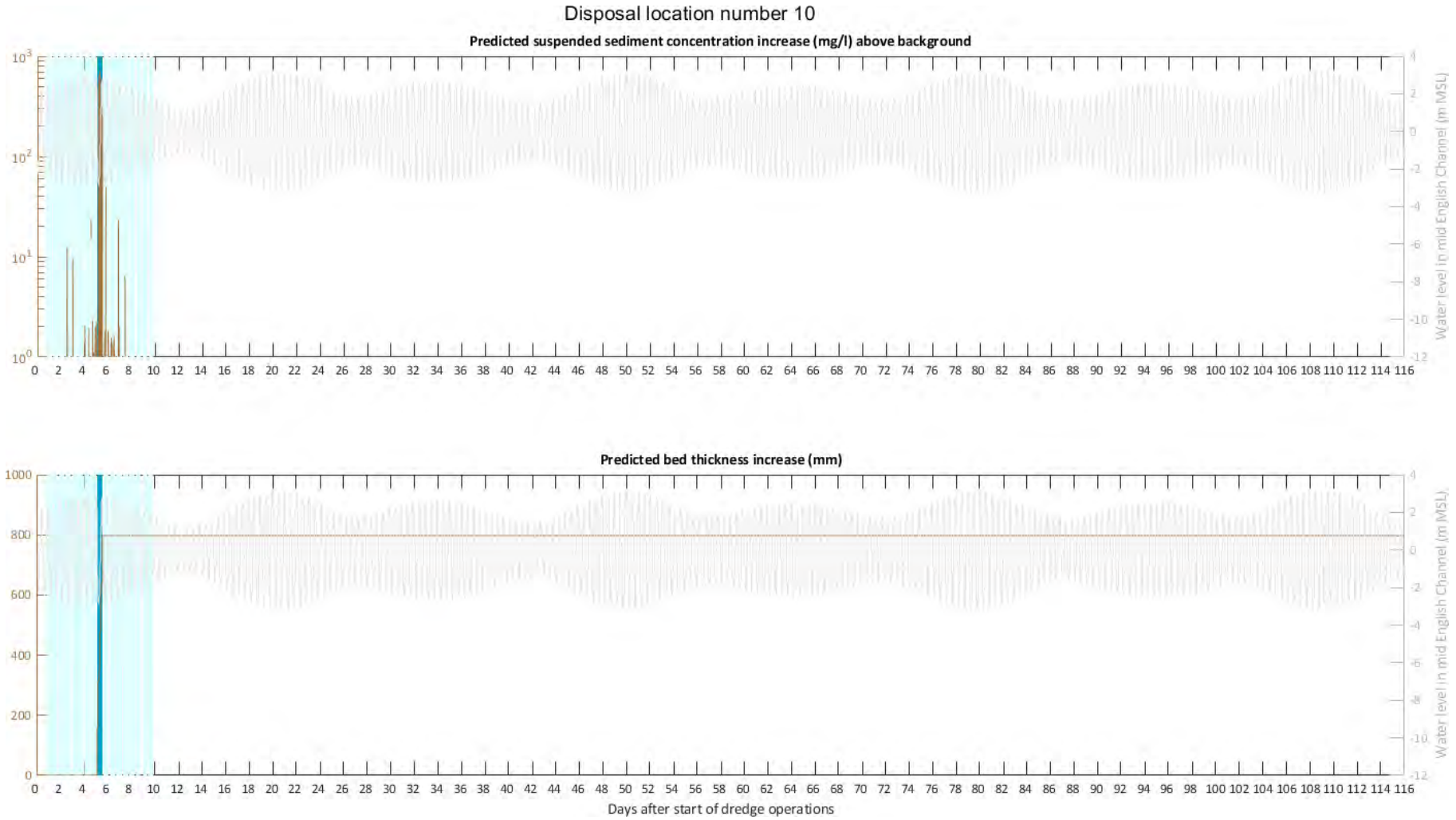

Figure 92 - Time series plots showing predicted suspended sediment concentrations and predicted bed thickness increase at disposal location 10. The light blue shaded area shows the duration of dredge operations, the dark blue shading shows the period of time where disposal activities are occurring at that disposal location within the model.

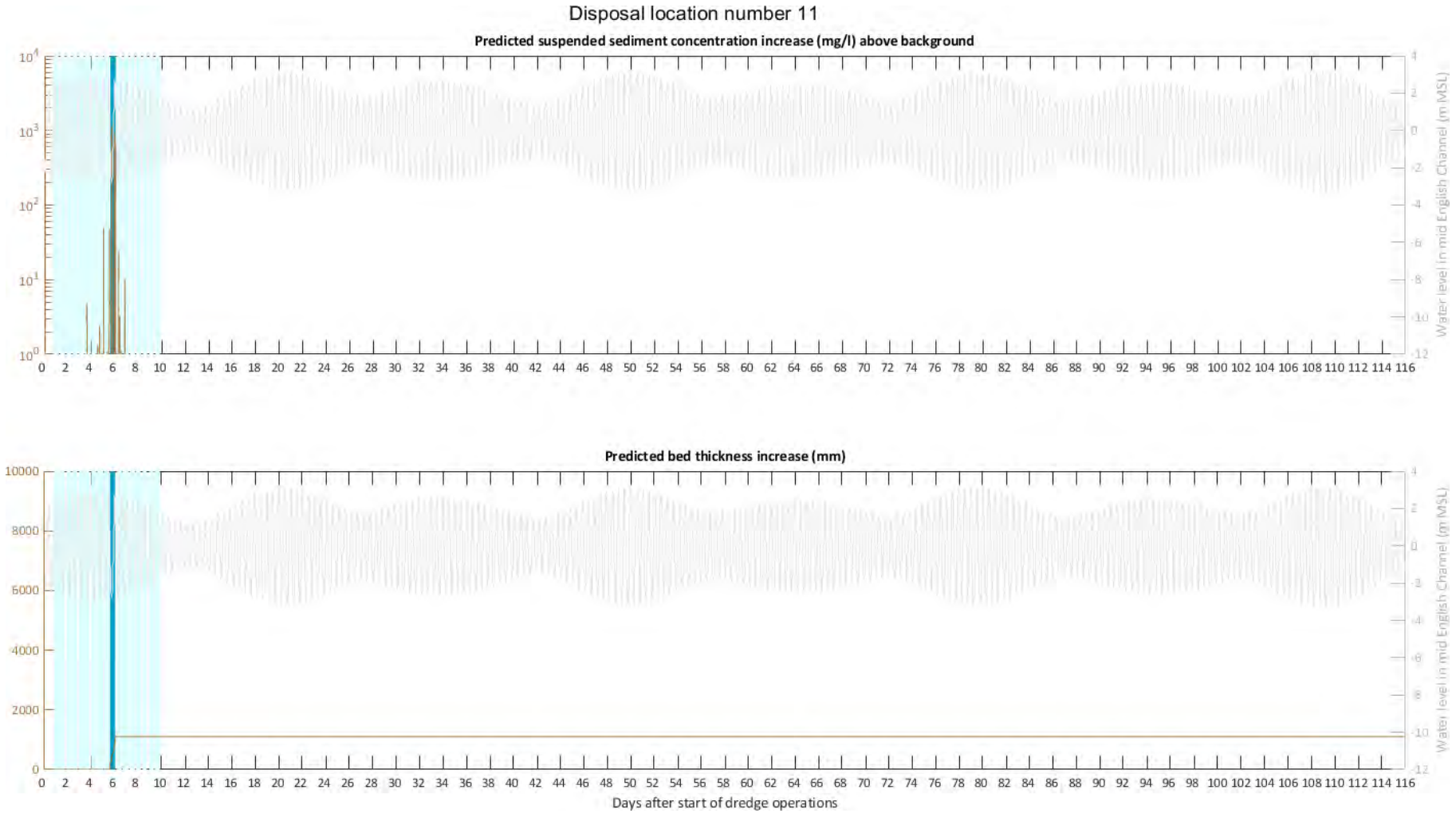

Figure 93 - Time series plots showing predicted suspended sediment concentrations and predicted bed thickness increase at disposal location 11. The light blue shaded area shows the duration of dredge operations, the dark blue shading shows the period of time where disposal activities are occurring at that disposal location within the model.

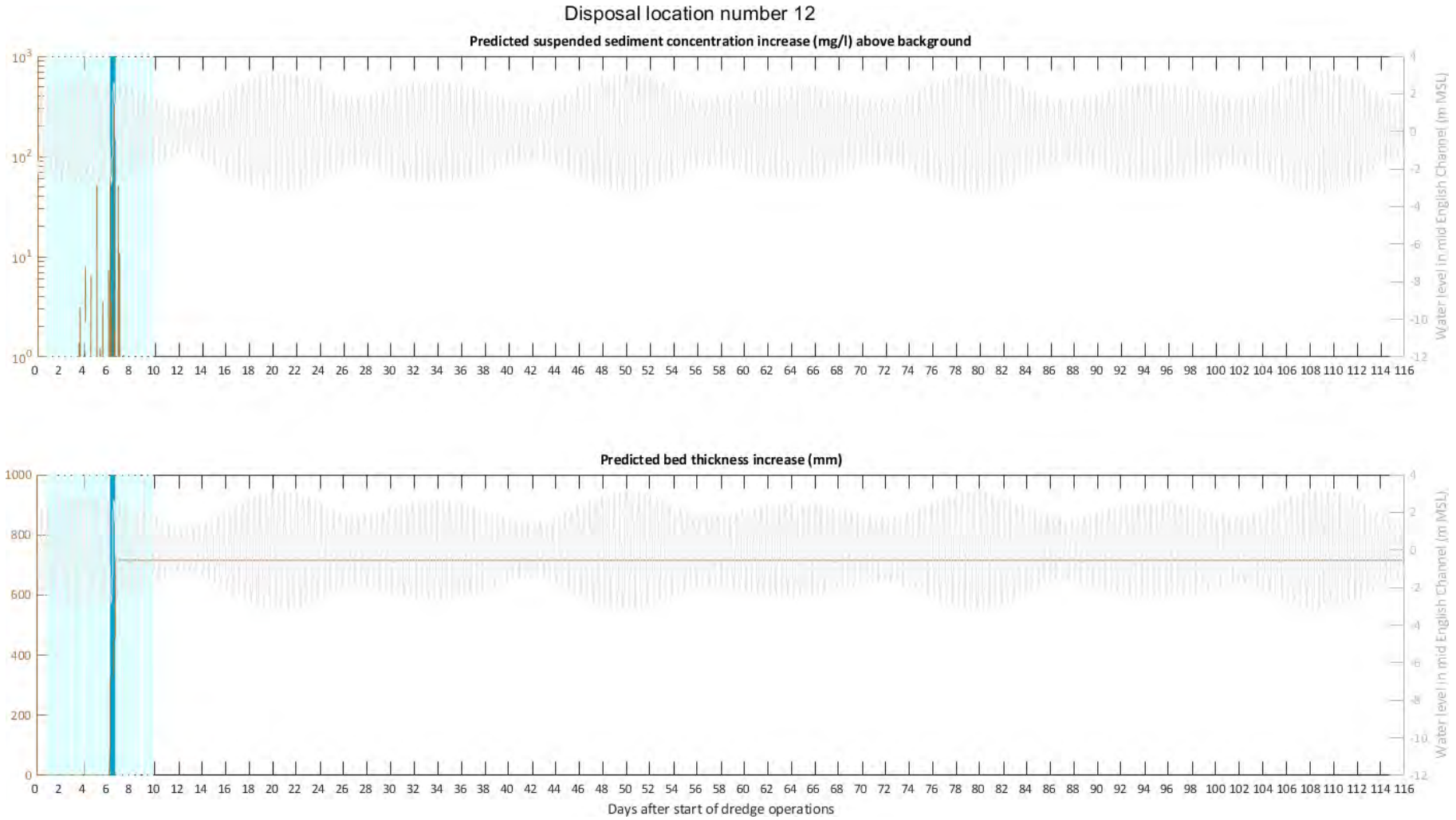

Figure 94 - Time series plots showing predicted suspended sediment concentrations and predicted bed thickness increase at disposal location 12. The light blue shaded area shows the duration of dredge operations, the dark blue shading shows the period of time where disposal activities are occurring at that disposal location within the model.

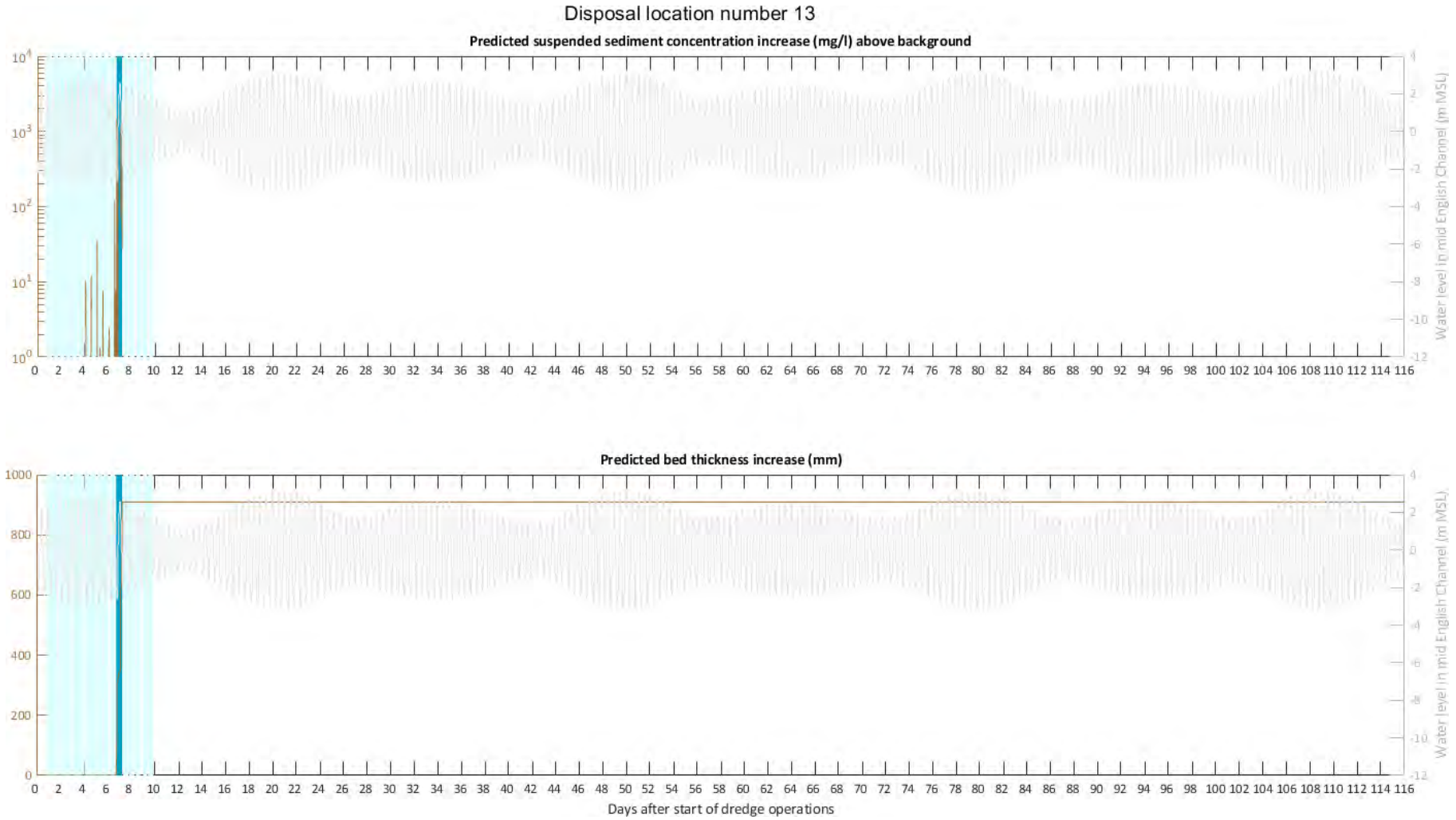

Figure 95 - Time series plots showing predicted suspended sediment concentrations and predicted bed thickness increase at disposal location 13. The light blue shaded area shows the duration of dredge operations, the dark blue shading shows the period of time where disposal activities are occurring at that disposal location within the model.

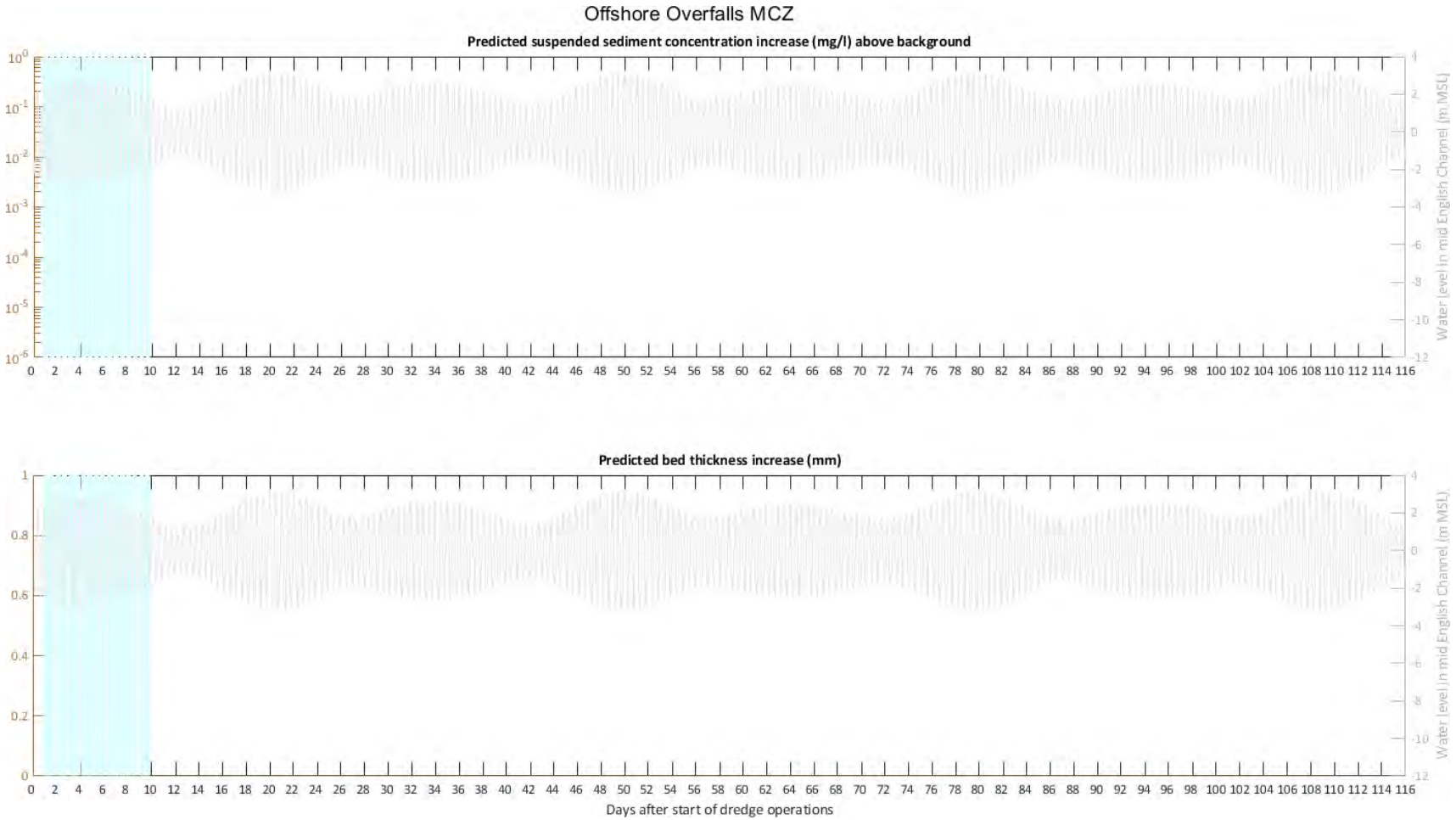

Figure 96 - Time series plots showing predicted suspended sediment concentrations and predicted bed thickness increase at the centroid of Offshore Overfalls MCZ. The light blue shaded area shows the duration of dredge operations, the dark blue shading shows the period of time where disposal activities are occurring at that disposal location within the model. These data are presented as it is the closest designated MCZ to the disposal operations.

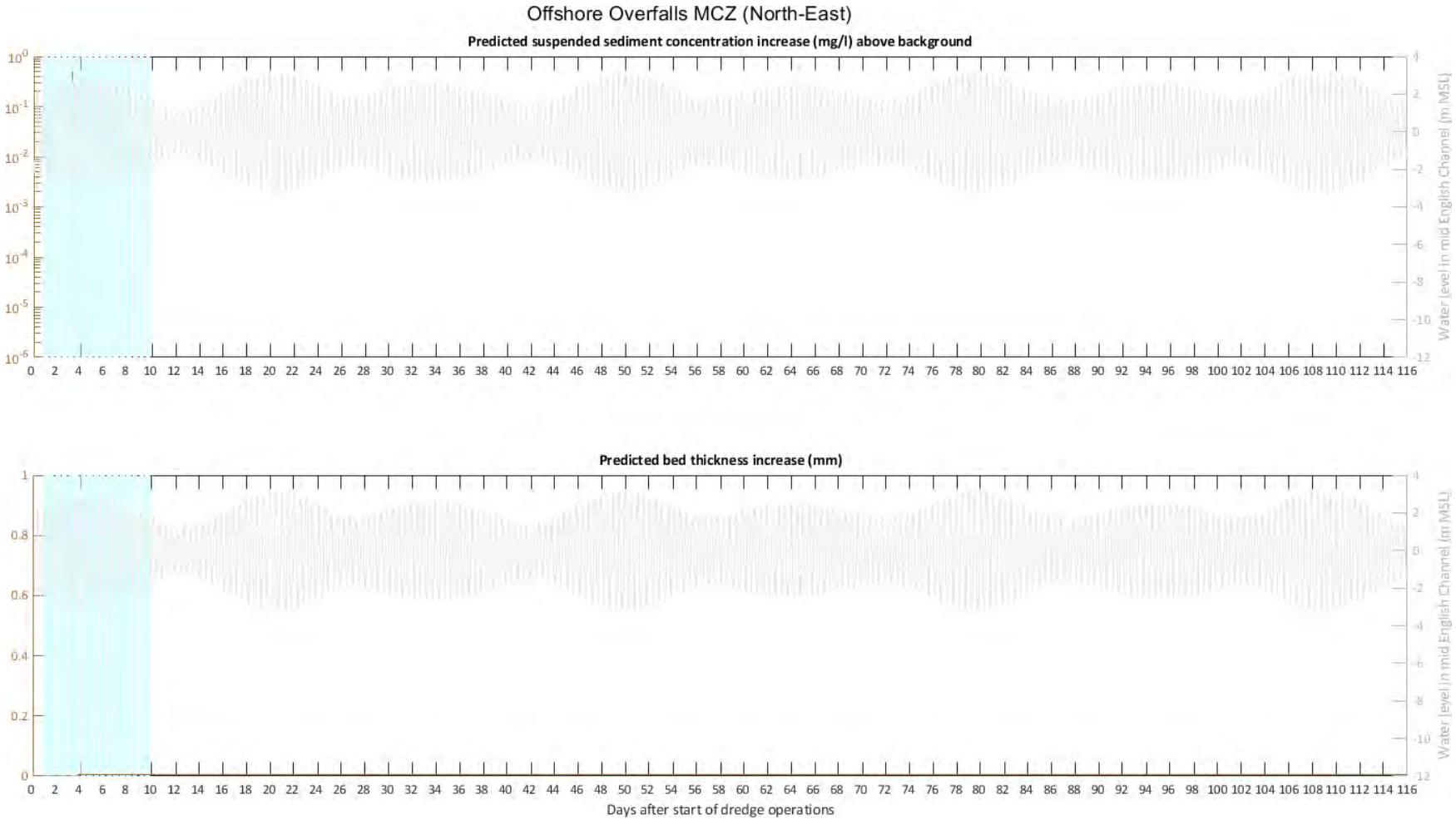

Figure 97 - Time series plots showing predicted suspended sediment concentrations and predicted bed thickness increase at the NE of Offshore Overfalls MCZ. The light blue shaded area shows the duration of dredge operations, the dark blue shading shows the period of time where disposal activities are occurring at that disposal location within the model. These data are presented as it is the closest designated MCZ to the disposal operations.

4.5. CONCLUSIONS

4.5.1.1. Significant points to note from the outputs of the modelling regarding plume dispersion are:

- That the plume disperses broadly eastward on a flooding tide and broadly westward on an ebbing tide.
- Where disposals are conducted on a neap tidal phase, suspended sediment concentrations would be slightly increased local to the release site due to the reduced flow velocity magnitude; the plumes, following a similar path and direction, would disperse but across a reduced spatial extent. The opposite would be true if disposals were conducted during the spring tidal phase.
- As the plume disperses, material will encroach beyond the boundary of the Offshore Overfalls MCZ (Figure 69). Suspended sediment concentrations would be further enhanced within the MCZ where disposals are conducted locally, on an ebbing tide.
- Although peak suspended sediment concentrations can approach 1000 mg l^{-1} over background levels during disposal, these are transient, and suspended sediment concentrations are predicted to return to background levels within 1 hour of the final release of material during the model scenario (see Figures 70 to 82).
- Similarly, depositional thickness is predicted to approach 1.5 m in disposal areas along the Marine Cable Corridor (see Figures 83 to 97). While this deposited sediment will likely remain in place in the short-term, bedload transport processes will act to disperse this sediment through time. The wider deposition of fine sediment following dispersion is predicted to be negligible, and again transient, with fine sediments transported and redistributed under tidal forcing quickly reducing to background levels.
- No transboundary effects from disposal activities on either side of the Channel are predicted within the model scenario.

REFERENCES

Aarninkhof, S. G. J, Luijendij, A. P. (2010). *Safe Disposal of Dredged Material In A Sensitive Environment Based On Innovative Plume Predictions*. Available: https://www.iadc-dredging.com/ul/cms/terraetaqua/document/2/7/8/278/278/1/article-safe-disposal-of-dredged-material-in-a-sensitive-environment-based-on-innovative-plume-predictions-terra-et-aqua-119-3.pdf. Last accessed 03/10/2019.

Battjes, J.A. and J.P.F.M. Janssen (1978). Energy loss and set-up due to breaking of random waves, Proc. 16th Int. Conf. Coastal Engineering, ASCE, 569-587

CIA World Data Bank II (WDBII) (2018) https://www.evl.uic.edu/pape/data/WDB/. Last accessed: 03/10/2019.

Becker, J., van Eekelen, E., van Wiechen, J., de Lange, W., Damsma, T., Smolders, T. and van Koningsveld, M. (2015) Estimating source terms for far field dredge plume modelling. *Journal of Environmental Management*. 14, 282-293.

Channel Coastal Observatory (CCO) (2018) Channel Coastal Observatory under Open Government Licence.https://www.channelcoast.org/data_management/online_data_catalogue/. Last accessed: 03/10/2019.

Dee DP et al. 2011. The ERA- Interim reanalysis: configuration and performance of the data assimilation system. Q. J. R. Meteorol. Soc.137: 553 – 597. DOI:10.1002/qj.828.

Egbert, Gary D., and Svetlana Y. Erofeeva. "Efficient inverse modeling of barotropic ocean tides." Journal of Atmospheric and Oceanic Technology 19.2 (2002): 183-204.

Golder Associates Ltd. (2015). Permitting of Dredged Material Disposal at Sea - Rio Tinto. Alcan: Modelling Dredged Material Deep Water Placement In Upper Kitimat Arm, BC. Report Number: 1314360089-101-R-RevA.

Hasselmann, Klaus & Hasselmann, Klaus. (1985). Computations and Parametrizations of the nonlinear energy transfer on a gravity-wave spectrum. part II: Parametrizations of the nonlinear energy transfer for applications in wave models. J. Phys. Ocean.. 15. 1378-1391.

HR Wallingford. (2008). Falmouth Cruise Terminal Hydrodynamic and Sedimentary studies. Report Number: EX 5809.

K.Hasselmann & al., "Measurements of Wind-Wave Growth and Swell Decay during the Joint North Sea Wave Project (JONSWAP)" Deutsche Hydrographische Zeitschrift, Reihe A (8 sup 0), No.12, 1973.

Komen, G & Hasselmann, Klaus. (1984). On the Existence of a Fully Developed Wind-Sea Spectrum. Journal of Physical Oceanography - J PHYS OCEANOGR. 14. 1271-1285. 10.1175/1520-0485(1984)014<1271: OTEOAF>2.0.CO;2.

Land J and Bray R N, 1998, Acoustic measurement of suspended solids for monitoring of dredging and dredged material disposal, Proceedings of the 15th World Dredging Congress (WODCON XV), June 28 to July 2, Las Vegas, USA, Volume 1, pp105-120

Laplace, Pierre Simon, marquis de, 1749-1827, Louis Courcier, J. B. M Duprat, and Charles Crapelet. Traité De Mécanique Céleste. A Paris: De L'Imprimerie de Crapelet , 7179817991825.

OceanWise (2018) https://www.oceanwise.eu/data/raster-charts-xl/. Last accessed: 03/10/2019

UK National Tide Gauge Network (NTGN) (2018), owned and operated by the Environment Agency, hosted by the British Oceanographic Data Centre, at https://www.bodc.ac.uk/data/hosted_data_systems/sea_level/uk_tide_gauge_network/. Last accessed: 03/10/2019.

URS Australia Pty Ltd. (2011). Technical Report Darwin Port Expansion EIS Dredge Dispersion and Spoil Disposal Modelling. Report Number: 42214000.

Royal Haskoning DHV. (2015). York Potash Harbour facilities Order - Environmental Statement. Available: https://infrastructure.planninginspectorate.gov.uk/projects/north-east/york-potash-harbour-facilities-order/?ipcsection=docs&stage=app&filter1=Environmental+Statement. Last accessed: 03/10/2019.

Saha, S., et al 2010: The NCEP Climate Forecast System Reanalysis. Bull. Amer. Meteor. Soc., 91, 1015–1058, https://doi.org/10.1175/2010BAMS3001.1. Last accessed: 03/10/2019

Soulsby, R. (1997) Dynamics of marine sands. London: Thomas Telford Publications.

The European Marine Observation and Data Network (EMODnet) (2018) http://www.emodnet.eu/bathymetry. Last accessed: 03/10/2019.

Wessel, P., and Smith, W. H. F., A Global Self-consistent, Hierarchical, High-resolution Shoreline Database, Journal of Geophysical Research, Vol. 101, No. B4, pp. 8741–8743, 1996.

World Vector Shoreline (WVS) (2018) https://shoreline.noaa.gov/data/datasheets/wvs.html. Last accessed: 03/10/2019.

WSP Ltd (2018). Technical Note on requirement for sand wave clearance and dredging for the purposes of cable installation.

WSP Ltd (2019). Aquind – Revised Dredging Volumes – UK and France. Memo. Date: 20/05/2019.